Vacuum-UV negative photoion spectroscopy of gas-phase polyatomic molecules

Simpson, Matthew J.; Tuckett, Richard P.

DOI:
10.1080/0144235X.2011.581000

Document Version
Early version, also known as pre-print

Citation for published version (Harvard):
Simpson, MJ & Tuckett, RP 2011, 'Vacuum-UV negative photoion spectroscopy of gas-phase polyatomic molecules', *International Reviews in Physical Chemistry*, vol. 30, no. 2, pp. 197-273. https://doi.org/10.1080/0144235X.2011.581000

Vacuum-UV negative photoion spectroscopy of polyatomic molecules

M.J. Simpson and R.P. Tuckett

Int. Rev. Phys. Chem., (2011) **30(2)**, 197-273.

DOI : 10.1080/0144235X.2011.581000

Professor Richard Tuckett (University of Birmingham) / July 2011

Vacuum-UV negative photoion spectroscopy of gas-phase polyatomic molecules

(revised version following referee's comments, submitted 11.4.11) : adapted 12.5.11

Matthew J Simpson and Richard P Tuckett *

School of Chemistry, University of Birmingham, Birmingham B15 2TT, UK.

Number of pages : 62 (number of words : *ca.* 32000, including abstract, references, tables and figure captions)

Number of tables : 11

Number of figures : 34

* Author for correspondence : E r.p.tuckett@bham.ac.uk ; F 0044 121 414 4403 ; T 0044 121 414 4425

This Review describes recent experiments to detect anions following vacuum-UV photoexcitation of gas-phase polyatomic molecules. Using synchrotron radiation in the range 10–35 eV at a resolution down to 0.02 eV, negative ions formed are detected by mass spectrometry. The molecules studied in detail include CF_4, SF_6 and CH_4; the CF_3X series where X = Cl,Br,I; the CH_3Y series where Y = F,Cl,Br; and SF_5Z where Z = CF_3,Cl. Spectra and raw data only are reported for other members of the CH_xF_y, CH_xCl_y including CCl_4, and CF_xCl_y series where $(x+y) = 4$; and saturated and unsaturated members of the C_mH_n and C_mF_n series up to $m = 3$. Anions detected range from atomic species such as H^-, F^- and Cl^- through to heavier polyatomics such as SF_5^-, CF_3^- and CH_2Cl^-. The majority of anions display a linear dependence of signal with pressure, showing that they arise from unimolecular ion-pair dissociation, generically written as ABC + hν → D^- + E^+ + neutral(s). In a few cases, the anion signal increases much more rapidly than a linear dependence with pressure, suggesting that anions now form *via* a multi-step process such as dissociative electron attachment. Cross sections for ion-pair formation can be put on to an absolute scale by calibrating the signal strength with those of F^- from SF_6 and CF_4, although there are difficulties associated with the determination of H^- cross sections from hydrogen-containing molecules unless this anion is dominant. Following normalisation to total vacuum-UV absorption cross sections

(where data are available), quantum yields for anion production are obtained. Cross sections in the range *ca.* 10^{-23} to 10^{-19} cm^2, and quantum yields in the range *ca.* 10^{-6} to 10^{-3} are reported. The Review describes the two ion-pair mechanisms of *indirect* and *direct* formation and their differing characteristics, and the properties needed for anion formation by dissociative electron attachment. From this huge quantity of data, attempts are made to rationalise the circumstances needed for favourable formation of anions, and which anions have the largest cross section for their formation. Since most anions form indirectly *via* predissociation of an initially-excited Rydberg state of the parent molecule by an ion-pair continuum, it appears that the dynamics of this curve crossing is the dominant process which determines which anions are formed preferentially. The thermochemistry of the different exit channels and the microscopic properties of the anion formed do not appear to be especially significant. Finally, for the reaction $ABC + h\nu \rightarrow A^- + BC^+$, the appearance energy of A^- can be used to determine an upper limit to the bond dissociation energy of AB (to A + BC), or an upper limit to that of ABC^+ (to $A + BC^+$). Where known, the data are in excellent agreement with literature values.

Keywords: ion-pair formation, anion, electron attachment, synchrotron, bond dissociation energy.

CONTENTS

1. Introduction

The production of an anion-cation pair of fragments following unimolecular dissociation of an isolated gas-phase molecule is often called 'ion-pair formation'. For a diatomic molecule, AB, this reaction can generally be described as:

$$AB + h\nu \rightarrow A^- + B^+ \qquad (1)$$

For a polyatomic molecule, ABC, the ion-pair reaction may also produce neutral fragments,

$$ABC + h\nu \rightarrow A^- + BC^+ \qquad (2)$$

or $$ABC + h\nu \rightarrow A^- + B^+ + C \qquad (3)$$

This Review is concerned exclusively with polyatomic molecules, so from henceforth we will use reactions (2) or (3) to describe a generic ion-pair reaction. In these studies, it is usually the anion, A^-, that is detected as a function of the photon energy. Anions formed in this way can either form *directly* or *indirectly*, described fully in Section 2. An anion-cation pair may be formed by direct excitation to the ion-pair state, or indirectly *via* predissociation of an initially-excited neutral state of ABC. Indirect formation is by far the more common mechanism, the excited neutral states are nearly always Rydberg in character, and so our experiments relate closely to the vacuum-UV absorption spectroscopy of Rydberg states of polyatomic molecules.

A^- can also be produced above the ionisation energy of the parent molecule by the alternative mechanism of dissociative electron attachment:

$$ABC + h\nu \rightarrow ABC^+ + e^-$$

followed by $$ABC + e^- \rightarrow A^- + BC \;\; or \;\; A^- + B + C \qquad (4)$$

A more accurate description of this type of study is therefore 'negative photoion spectroscopy', this explains the title of this Review, and one should regard ion-pair formation in a polyatomic molecule, (2) or (3), as a special case of negative photoion spectroscopy in which a cation is produced simultaneously. Furthermore,

with ion-pair formation the signal of A^- increases *linearly* with the concentration or pressure of ABC, as only one molecule of parent is needed to produce one anion. By contrast, if A^- is produced by dissociative electron attachment, (4), then the A^- signal should increase *quadratically* with the concentration of ABC since two molecules of ABC are needed to produce one anion; at the very least, the rate of change of A^- signal will increase as the concentration of parent molecule increases. Whilst the formation of A^- by reaction (4) is also a multi-step indirect process, we will always describe this method of anion production as two-step dissociative electron attachment. This will avoid confusion with the indirect ion-pair reaction described above for production of an anion-cation pair by predissociation of a Rydberg state of ABC.

Typically, these reactions are endothermic by at least 8 eV, corresponding to a photon wavelength less than *ca.* 150 nm, with this energy increasing as the extent of fragmentation of the polyatomic molecule increases. Therefore, a photon in the vacuum-ultraviolet (VUV) region of the electromagnetic spectrum must be absorbed by the molecule, and it is no surprise that the majority of negative photoion studies of polyatomic molecules use tunable VUV radiation from a synchrotron as the source of electromagnetic radiation. For spectroscopic studies, the relatively poor resolution of such sources, compared to other sources such as VUV lasers, is more than compensated by the ease which which the photon energy can be tuned. For dynamical studies, radiation from a synchrotron can operate either as a source of linearly- *or* circularly-polarised radiation, but such properties have received little attention to date in negative photoion or ion-pair studies.

For reaction (2), the appearance energy of the anion, $AE(A^-)$ is constrained to the energetic relationship:

$$AE(A^-) \geq D^o(A–BC) + IE(BC) - EA(A) \qquad (I)$$

where D^o is a dissociation energy, IE an ionisation energy and EA an electron affinity. If experiments are performed at 298 K, then we can write:

$$AE_{298}(A^-) \geq D^o_{298}(A–BC) + IE(BC) - EA(A) \qquad (II)$$

To avoid confusion about signs, we note that whilst the *IE* of a molecule is always positive (*i.e.* the reaction $ABC \rightarrow ABC^+ + e^-$ is always endothermic), we use the convention used by most chemical physicists that a positive *EA* corresponds to the energy of A^- lying below that of A (*i.e.* the reaction $A + e^- \rightarrow A^-$ is exothermic). As stated earlier, ion-pair production can either occur directly into the ion-pair continuum, or indirectly following predissociation of an initially-excited Rydberg electronic state into the continuum. On Franck-Condon grounds the latter process is more common [1], so the detection of ion pairs provides information on the electronic structure of a molecule and the decay dynamics of its excited states.

An alternative way to express the inequality of eq. (I) is to write:

$$AE(A^-) \geq IE(ABC) + D^o(A\text{–}BC^+) - EA(A)$$

or $$AE_{298}(A^-) \geq IE(ABC) + D^o_{298}(A\text{–}BC^+) - EA(A) \qquad \text{(III)}$$

Thus, ion-pair formation may occur at energies below the adiabatic *IE* of ABC if the electron affinity of A exceeds the dissociation energy of $A\text{–}BC^+$. Anions are then being detected in the absence of photoelectrons, facilitating the experiment. This condition is met for all the thallium halide diatomic molecules [2]. Furthermore, for TlBr and TlI the threshold for ion-pair formation occurs above the VUV onset of 200 nm, or below *ca.* 6 eV, making the detection of anions with conventional UV lamp sources relatively easy. Thus the study of the negative photoion spectroscopy of these molecules started as early as the 1930s. The halogen and inter-halogen diatomic molecules provide a rich source of ion-pair states, due to the relatively high *EA* value of all the halogen atoms. These molecules, reviewed in [3], could be studied by VUV and UV lasers operating in the wavelength range of *ca.* 150–250 nm (or 5–8 eV), and were complemented by synchrotron studies using VUV radiation from the second generation of these sources.

The first studies on *polyatomic* molecules in the 1960s, mostly from the National Bureau of Standards in Washington DC, USA, used the continuum sources from discharge lamps coupled with mass spectrometric detection of the anion, but these studies rarely accessed wavelengths below 100 nm, or photon energies above 12.4 eV [4,5]. The first set of dedicated experiments on polyatomic molecules using VUV radiation from a synchrotron were made in the early 1990s by Mitsuke *et al.* at the Institute of Molecular

Sciences in Okasaki, Japan, and a range of molecules were studied including CH_4 and larger hydrocarbons, CF_4, SF_6 and CH_3X (X = F,Cl,Br) [6-10]. The state of knowledge of ion-pair states in diatomic and polyatomic molecules up to 1996 was reviewed by Berkowitz [1]. A more recent project using a pulsed time-of-flight reflectron mass spectrometer to detect anions has been initiated by Tian *et al.* at the National Synchrotron Radiation Laboratory in Hefei, China [11]. Starting in the 1990s, the development of imaging techniques opened a new window into ion-pair spectroscopy. Coupled with linearly-polarised VUV lasers, the dynamics of ion-pair dissociation *via* molecular Rydberg states started to be investigated, with detailed studies on CH_3Cl and CH_3Br being reported [12,13]. Simultaneously, the development of threshold ion pair production spectroscopy [14,15] applied to diatomic and some hydride triatomic molecules meant that the full potential of laser-based coherent VUV sources at high resolution could be applied to ion-pair formation. These studies up to 2006 were reviewed by Suits and Hepburn [16].

In a series of experiments performed over the last five years, we have exploited the increased sensitivity of modern mass spectrometers and the wide tunability and availability of synchrotron sources over the energy range 10–30 eV to study anion formation from a wide range of polyatomic molecules. The systems studied include CH_4, CF_4, SF_6, CH_3X (X = F,Cl,Br), CF_3Y (Y = Cl,Br,I), SF_5Z (Z = Cl,CF_3), CH_xF_y ($x+y = 4$), CH_aCl_b ($a+b = 4$), CF_cCl_d ($c+d = 4$), C_mH_n and C_mF_n (m = 1,2,3) [17-22]. For common molecules studied, a much wider range of anions are observed than those observed by Mitsuke *et al.*, and we have developed a generic methodology to determine ***absolute*** cross sections and quantum yields for anion formation; this has never been done before for such a wide range of molecules. Our data form the most comprehensive collection of information on ion-pair formation in polyatomic molecules since the Berkowitz review [1]. Perhaps more than other reviews on ion-pair formation, here we attempt to explain ***why*** some anions form in preference to others. Since many of our studies involve fluorinated molecules, it is perhaps not surprising that phenomena such as the electronegativity of the departing anion and the perfluoro effect [23] can explain some of the observations. However, certainly for indirect ion-pair formation, it is the ***dynamics*** of the crossing between the Rydberg and the ion-pair state which determine predominantly the product anions that are formed.

2. Direct and indirect ion-pair formation, Rydberg states

In their review on halogen diatomic molecules, Lawley and Donovan [3] suggest a model for the potential energy function of an ion-pair state, incorporating an exponential repulsion term with a long-range Coulombic attractive interation,

$$V(r) = A\exp(-\alpha r) - \frac{e^2}{4\pi\varepsilon_0 r} + E_{\text{ip}} \qquad \text{(IV)}$$

$V(r)$ is the potential energy, r the bond distance along the reaction coordinate, A and α are constants, and E_{ip} is the energy needed to place $V(r)$ onto an absolute scale. For reaction (1), $E_{ip} = D^o(\text{A–B}) + IE(\text{B}) - EA(\text{A})$. This model assumes both pure ionic behaviour and the equilibrium bond distance of the ion-pair state at equilibrium being large.

As stated in Section 1, anion-cation pair may be formed by direct excitation to the ion-pair state, or indirectly *via* predissociation of an initially-excited neutral state. Figure 1 shows these two processes for the generic polyatomic molecule ABC dissociating into $A^- + BC^+$. Direct ion-pair formation involves excitation to the repulsive inner wall of the potential energy surface above the asymptotic dissociation energy. Consequently, the transition may have very small Franck-Condon factor at threshold, and vibrational states of the ion-pair potential curve cannot be probed. However, given the necessary sensitivity in the experiment, unless the Franck-Condon factor is truly zero at threshold one would expect the signal of A^- to turn on at its thermochemical energy. By contrast, for the indirect process the restricting factor is not this Franck-Condon overlap, but rather the degree of coupling between the initially-excited neutral state and the ion-pair state. In addition, vibrational levels within the neutral excited state can be probed. Although it is not shown as such in Figure 1(b), there is now no reason why the signal of A^- should turn on at its thermochemical threshold, because the initially-excited neutral state may lie higher in energy than the $A^- + BC^+$ threshold. This explains the inequality in the energetics of equations (I) – (III). Nevertheless, regardless of which process leads to the formation of ion pairs, competing processes can result in products

other than $A^- + BC^+$ being formed. These processes include neutral dissociation, molecular ionisation, or fluorescence. The measurement of quantum yields for these different exit channels is notoriously difficult, especially in the VUV region of the spectrum where absolute standards can be difficult to obtain. However, the general acceptance is that the quantum yield for ion-pair formation in polyatomic molecules is small, typically 10^{-3} or less, with the value decreasing as the size of the molecule increases [1,16,24].

Rydberg states are commonly identified as the initially-excited intermediate involved in indirect ion-pair formation [*i.e.* ABC* in Figure 1(b)] [1,24]. A molecular Rydberg state is a high-lying electronic state of the neutral molecule where an electron is excited such that it observes the molecule as a distant positively-charged core. The Rydberg electron resides in an atomic-like orbital which is very large compared to the size of the molecule. Series of Rydberg states converge to ionisation limits and generally obey the Rydberg formula [24,25]:

$$E_n = IE - \left[\frac{R_\infty}{(n-\delta)^2}\right] \qquad \text{(V)}$$

where E_n is the energy of the nth Rydberg state, IE is the ionisation energy to which the Rydberg series converges, R_∞ is the Rydberg constant (109737.32 cm^{-1} *or* 13.6059 eV, the IE of atomic hydrogen), n is the principal quantum number of the Rydberg orbital, and δ is the quantum defect. $(E_n - IE)$ is called the *term value*. The angular momentum quantum number, l, of the Rydberg orbital is identified by δ. For example, the value of δ will be the same for each member of an *ns* (or *np* or *nd*… *etc*.) Rydberg series. Typical values of δ for period 1 and 2 elements of the periodic table are: for *ns* series, 0.9–1.2; for *np* series, 0.3–0.6; for *nd* series, < 0.1 [25]. In addition, δ values increase with increasing period number. Thus, an *np* Rydberg orbital in Cl will have a larger quantum defect than an *np* Rydberg orbital in F. δ therefore represents an arbitrary, dimensionless number, the magnitude of which reflects the degree of orbital-core penetration, including the shielding effects of 'core' electrons on the Rydberg electron. The Rydberg formula originated from the analysis of the spectrum of atomic hydrogen, a single-electron system with no requirement to define δ; in equation (V), for atomic H $\delta = 0$. The quantum defect is introduced for many-electron systems

to account for electron-electron interactions. Thus, the smaller the value of δ, the more the system behaves like a hydrogen atom and the more diffuse the Rydberg orbital becomes.

Peaks in a spectrum (providing a value for E_n) may be assigned to a Rydberg orbital using the Rydberg formula if the value for the *IE* is known. In practice, it is common that several assignments exist for the same value of E_n because of many possible combinations for *IE*, n and δ. Assignments presented later are therefore given with a degree of uncertainty, reflecting the moderate resolution at which the negative photoion spectra are recorded. One particular difficulty in assigning *molecular* Rydberg orbitals is that only quantum defect values for atomic systems are well known. In this work the tabulations by Theodosiou *et al*. were used as a guide to identify appropriate quantum defect values [26]. More confident assignments require E_n to be known more accurately from higher-resolution spectra, or several peaks to be fitted to the same Rydberg series; the latter is more likely to be possible from total photoabsorption or atomic spectroscopy.

3. Thermochemical aspects of negative photoion or ion-pair spectroscopy

The standard enthalpy of a unimolecular reaction, $\Delta_r H°$, can be calculated if the standard enthalpies of formation ($\Delta_f H°$) for each individual reactant and product species are known. All our experiments are performed at 298 K, and thus the following relationship can be used:

$$\Delta_r H^\circ_{298} = \sum \Delta_f H^\circ_{298}\,(products) - \sum \Delta_f H^\circ_{298}\,(reactnts) \qquad \text{(VI)}$$

The $\Delta_f H°_{298}$ values used to calculate these enthalpies of reaction are taken from standard sources [27,28], although more recent and accurate data may be available for some of the ion-pair products we observe. In reality, however, it is the change in standard Gibbs energy of the reaction, $\Delta_r G°$, and not the change in standard enthalpy, which determines the thermodynamic feasibility of a reaction. The relationship between $\Delta_r G°$ and $\Delta_r H°$ is given by:

$$\Delta_r G° = \Delta_r H° - T\Delta_r S° \qquad \text{(VII)}$$

where T is the temperature in K and $\Delta_r S°$ is the standard entropy of reaction. Thus, the effects of entropy in a reaction are ignored when using enthalpy, and not free energy, values. For most ion-pair reactions needing the input of a vacuum-UV photon (*e.g.* 10 eV ≡ *ca.* 965 kJ mol^{-1}), the $T\Delta_r S°$ term is small compared to the magnitude of $\Delta_r G°$ or $\Delta_r H°$, even though Δn, the number of product minus the number of reactant species, for reactions (1)–(3) is always positive and never zero. We therefore believe that the use of $\Delta_r H°$, the endothermicity of the reaction, instead of $\Delta_r G°$ is justified, provided this fact is acknowledged. However, in the very few cases where $\Delta_r H°$ is very small and $\Delta_r S°$ is very large, this approximation may not be applicable. Note that for *bimolecular* reactions involving cations or anions, which are not considered in this Review, $\Delta_r H°$ values can be much smaller, and the magnitude of $T\Delta_r S°$ may sometimes lie within the uncertainty of the calculated $\Delta_r H°$ value. Then entropic effects may be significant.

We have seen already that the asymptotic ion-pair formation energy, E_{ip}, from a generic polyatomic molecule ABC can be expressed using either of the two equations:

$$E_{ip}(A^- + BC^+) = D^o(A–BC) + IE(BC) – EA(A)$$

or
$$E_{ip}(A^- + BC^+) = IE(ABC) + D^o(A–BC^+) – EA(A) \qquad \text{(VIII)}$$

As seen earlier, one advantage of using the second of these two equations is to identify that ion-pair formation can occur at an energy below the onset to ionisation: $E_{ip} < IE$ when $EA(A) > D^o(A–BC^+)$. This is often the case when A is a halogen atom because their EA values are relatively large. Below the *IE, any* ion formed must arise as a result of an ion-pair reaction, and positive or negative species can be detected with relative ease. Above the *IE*, however, in addition to anions, cations and free electrons are produced often in huge excess, which provide additional experimental challenges.

In practice, the value of E_{ip} is often not known or cannot be measured, and it is more convenient to use the experimental appearance energy instead. Although there are several definitions of the appearance energy in the literature, at the relatively modest resolution of our experiments, *ca.* 0.05–0.20 eV (see Section 4), we believe it most appropriate to define the AE_T at the temperature of the experiment, T (which is usually

298 K), as the lowest energy at which ion-pair formation is detected; that is, the photon energy at which an anion signal is first observed above the background noise. This can be considered as the value for *hv* shown earlier in Figure 1(a) and 1(b). The two equations (VIII) may then be re-written as the inequalities shown earlier in equations (I), (II) and (III). These inequalities can be used to calculate an upper limit to the value of either a bond dissociation energy or an ionisation energy, or a lower limit to the value of an electron affinity whichever has the least well-known value [1,29].

We shall see that the anion detected is identified by its mass (Section 4). However, the positive ion and any neutral fragments produced by the ion-pair reaction are not known. The enthalpy change for a unimolecular ion-pair reaction may be calculated using equation (VI) and compared with onsets to features in a spectrum. Previous experimental results from Mitsuke *et al.* showed that an experimental AE_T value commonly occurs at, or slightly higher in energy than the calculated thermochemical threshold (*i.e.* the value for E_{ip} calculated from equation (VIII). Assigning an AE_T value to a particular reaction is often straightforward, because usually only one ion-pair dissociation is energetically possible; for the lowest-energy ion-pair process only one bond is broken and no neutral fragments are produced. Assigning a reaction to features in a spectrum at higher energy is often more difficult because many different ion-pair dissociation channels become energetically open.

The values calculated from the right-hand side of equation (VI) are *enthalpy* changes. Before proceeding further, *energy* and *enthalpy* must be distinguished. We consider one molecule of an ideal gas interacting with a photon to produce a negative–positive pair of ions. The enthalpy change, $\Delta_r H^o$, does not allow for the fact that some internal energy is transferred to the surroundings as an increase in volume and/or pressure; the number of gaseous species increases due to the unimolecular dissociation reaction, $\Delta n > 0$, and the products are produced with translational momentum. The enthalpy change of a gas-phase reaction where all the species behave as ideal gases is defined by:

$$\Delta_r H^o = \Delta_r U^o + RT\Delta n \qquad \text{(IX)}$$

where U is the internal energy and R the universal gas constant. Energy and enthalpy are only equivalent quantities when $T = 0$ or $\Delta n = 0$. Corrections to AE_T values, so that they may be compared to those for $\Delta_r H^o_T$, have been outlined by Traeger and McLoughlin for photoionisation reactions [30]. For the generic ion-pair reaction ABC + hν $\rightarrow$ $A^- + BC^+$ at 298 K, their methods can be modified to show that

$$\Delta_r H^o_{298} \leq AE_{298}(A^-) + \int_0^{298} c_{p,m}\,(A^-).dT + \int_0^{298} c_{p,m}\,(BC^+).dT - \frac{5}{2}RT \qquad \text{(X)}$$

where $c_{p,m}$ is a molar specific heat capacity at constant pressure. The upper limit for $\Delta_r H^o_{298}$ arises because the appearance energy of A^- defines an upper limit to the thermochemical energy of $A^- + BC^+$. The inequality arises in the presence of a kinetic shift and/or a barrier in the exit channel, the equality holds if both effects are insignificant. Considering the second and third terms in the right-hand side of Eqn. (X),

$$\int_0^{298} c_{p,m}\,(A^- \text{ or } BC^+).dT = H^o_{298} - H^o_0 \qquad \text{(XI)}$$

For both anion and cation, this term may contain contributions from translational (2.5RT), rotational (up to 1.5RT) and vibrational ($N_A h\nu / [\exp(h\nu / k_B T) - 1]$ per mode) motion evaluated at $T = 298$ K. For many neutral molecules where all its vibrational frequencies are known, values of $(H^o_{298} - H^o_0)$ are tabulated [27]. For some anions and cations, *ab initio* calculations of vibrational frequencies may be necessary. In practice, however, unless the products of the reaction are large polyatomic species with many low-frequency vibrational modes contributing to their vibrational partition functions, the difference between $\Delta_r H^o_{298}$ and AE_{298} is relatively small, typically < 0.1 eV or 10 kJ mol^{-1}. This correction falls within the combination of uncertainties in the calculated $\Delta_r H^\circ_T$ and AE_T values determined in our work. In this work, the thermal correction is therefore ignored: experimental *energy* values are compared like-for-like with calculated *enthalpy* changes.

4. Experimental aspects

Data were collected at the second-generation Synchrotron Radiation Source (SRS), Daresbury, in the two years before its closure in the autumn of 2008. All experiments used the 1 m focal length Wadsworth monochromator on beamline 3.1 which was commissioned in 2004. This beamline has been described in detail elsewhere [31]. It was designed as a high-flux beamline operating at fairly moderate resolution for use in flux-limited experiments, with ease of tunability a high priority. Since vacuum-UV negative photoion spectroscopy is a flux-limited experiment, it might seem a strange choice of source to use for such experiments when superior beamlines, *e.g.* based on a VUV undulator¸ are available elsewhere in Europe. However, many of the VUV beamlines on third-generation European sources, *e.g.* Soleil in France, are based on undulators where tunability over a wide range of the VUV/XUV is not facile, *or* they operate at a much higher resolution, *e.g.* the Swiss Light Source VUV beamline, than is ideal for these experiments and their resolution cannot be degraded sufficiently to enhance the flux. In retrospect, therefore, we believe that the Daresbury source, despite its age, combined with a newly-commissioned VUV monochromator designed for maximum flux at modest resolution was the ideal combination for these experiments. This beamline could operate over the range 8–35 eV, this energy range being provided by two gratings mounted back-to-back and interchangeable under vacuum. If there was sufficient flux to operate an experiment at high resolution, the best resolution attainable, determined by the size of the horizontal electron beam in the storange ring, was *ca.* 0.05 nm, corresponding to 0.004 eV at 10 eV or 0.016 eV at 20 eV. In practice, the monochromator was usually operated at an inferior resolution to enhance flux. The maximum flux output at the peak of the two lamellar gratings, *ca.* 60 and 120 nm or 20 and 10 eV, was approximately 4×10^{11} photons per second per 100 mA of stored beam current when operating at a bandwidth of 0.1% of the excitation wavelength [31]. All experiments were conducted using the pseudo-continuous-wave nature of the synchrotron beam.

The apparatus used for these negative photoion spectroscopic studies is shown in Figure 2. Before our experiments, it had been used to detect anions at higher photon energies above *ca.* 25 eV, and its operation

in this mode is described elsewhere [32]. A 2 mm diameter, 300 mm long capillary light guide connected the beamline to the apparatus, focussing the monochromatised light directly into the interaction region. The light guide also provided the necessary differential pumping, *ca.* three orders of magnitude in pressure, between the beamline and the experiment. The gas under study is injected *via* a needle generating an effusive directed jet (with no internal cooling) which bisects orthogonally the incident photon beam. The crossing point, which dictates the centre of the interaction region, is positioned in the middle of two grids on the third orthogonal axis. A potential difference across the grids sweeps negative ions along this axis towards a three-element electrostatic lens for focussing, and into a Hiden Analytical HAL IV triple quadrupole mass spectrometer (QMS) for mass selection. Detection is achieved by a channeltron electron multiplier. Sensitivity is considerably enhanced by differential pumping which reduces the number of free electrons and secondary collisions in the QMS. Spectra recorded where the monochromator is scanned are flux normalised using a sodium salicylate (NaSal) window and visible photomultiplier tube (PMT) combination, which has a constant response over the energy range of the experiments. The apparatus and QMS, connected *via* a 1 mm diameter aperture, are pumped by separate turbo pumps which are backed by a common rotary pump, and the base pressure of the apparatus is approximately 10^{-7} mbar. With sample gas running, the typical pressure in the chamber is *ca.* 10^{-5} mbar. The pressure inside the chamber is measured using an ionisation gauge, the sensitivity of which to the sample under study is calibrated in a separate experiment relative to N_2 gas using a capacitance manometer (Table 1) [33,34].

Mass spectra are recorded to observe *all* the anions produced from photoabsorption of the sample gas by exposure to white light (*i.e.* using the monochromator set to zero order). The mass-to-charge ratio (*m/z*) of each peak in the mass spectrum is then fixed and the signal recorded as a function of photon energy, typically over the range 8–35 eV. In addition, for each anion, its signal is recorded at a fixed photon energy (usually the energy of a peak observed in the spectrum) as a function of sample gas pressure over the typical range $(0.5 – 5.0) \times 10^{-5}$ mbar. As described in Section 1, anions which show a non-linear dependence with pressure cannot be assigned as ion-pair products, and their signal is most likely due to a two-step process such as dissociative electron attachment. Anions which show a linear dependence of signal with pressure

can be attributed to ion-pair formation; being a unimolecular process, the rate of formation of ion pairs will then obey first-order kinetics.

4.1 Determination of absolute cross sections and quantum yields for anion formation

Anion spectra resulting from ion-pair formation are presented as cross sections, σ, in absolute units of cm^2. The value of σ at a given photon energy hv is calculated by:

$$\sigma(hv) = k\left(\frac{SM}{frp}\right) \qquad \text{(XII)}$$

where S is the detected signal in counts s^{-1}, M is the relative mass sensitivity of the QMS, f is the relative photon flux (effectively a measure of the grating efficiency), r is the storage ring current, p is the sample gas pressure corrected for ionisation gauge sensitivity, and k is a constant of proportionality. Correction to f, r and p is straightforward, although this procedure cannot be used for anions produced by dissociative electron attachment because the anion signal is not a linear function of gas pressure. Correction to M, however, is not trivial, and often seems to be ignored by others working in this field. An extensive set of experiments was therefore performed to determine M as a function of m/z. All quadrupole mass spectrometers exhibit an element of mass discrimination, with a tendency to transmit heavier ions less efficiently [35]. To allow for this effect the mass factor, M, has been determined by comparing the cation mass spectra of many polyatomic molecules in the QMS, following 70 eV electron impact ionisation, to 'true' mass spectra published in the electronic NIST database [36]. The values for M used in Eqn (XII) are taken from the plot shown in Figure 3. It can be seen that as m/z increases, the detection efficiency of the QMS decreases and a higher value of M is required to allow for this effect.

The zero-blast effect is a phrase commonly used by mass spectrometrists. It arises because *all* ions entering the QMS may be transmitted when the lens potentials are set to detect m/z values close to zero [35]. This effect therefore becomes especially important when studying hydrogen-containing molecules since the

tail of the zero-blast peak in the mass spectrum may overlap with *m/z* 1. Therefore, H^- spectra can only be trusted where there is no resemblance to other anion spectra recorded from the same molecule. Examples where this has caused severe problems include the weak H^- signal detected from CH_3Y molecules (Y = F, Cl, Br), which mimic the much stronger X^- spectra [20]. By contrast, H^- detected from CH_4 is an example where this is not an issue because the H^- signal is dominant [19].

To determine absolute cross sections, the signal corrected to *f*, *r*, *p* and *M* for F^- from SF_6 is normalised to the known cross section at 14.3 eV of $(7 \pm 2) \times 10^{-21}$ cm^2 [9]. Likewise, the corrected signal for F^- from CF_4 is normalised to its value at 13.9 eV of $(1.25 \pm 0.25) \times 10^{-21}$ cm^2 [8]. It should be noted, however, that these cross section values from Mitsuke *et al.* are strictly not absolute, but are obtained from calibrated measurements of O^- yields from O_2 [37]. Thus, normalisation factors $k(SF_6)$ and $k(CF_4)$ are determined. In theory, these two values should be the same. In practice, they vary by a factor ranging from 1.2 to 1.7. An average of the values is therefore used in Eqn (XII) to determine cross section values for anions from the sample under study. These measurements were made at every visit to the SRS, occurring typically every three months, and the appropriate value of *k* was used for each set of data collection. Overall, we believe that our values for anion cross sections are accurate to an error no better than ± 50–100 %. Whilst this might seem disappointing, absolute measurements of this kind are notoriously difficult to make, and are prone to errors which have often, in our opinion, been underestimated in the literature.

At any photon energy, the quantum yield for anion production is determined by dividing the anion cross section by the total photoabsorption cross section at that energy. It represents the probability for anion formation, where this process is competing with other decay channels such as neutral dissociation, molecular ionisation and fluorescence. In terms of unimolecular rate constants, *k*, the quantum yield can be written:

$$\Phi_{\text{anion}} = \frac{k_{anion}}{\sum_i k_i} = \frac{k_{anion}}{k_{anion} + k_{dissociation} + k_{ionisation} + k_{fluorescence} + \ldots\ldots\ldots} \qquad \text{(XIII)}$$

Thus, total cross-section data from VUV photoabsorption spectroscopy are needed to determine Φ_{anion}. With the wide availability of tunable synchrotron radiation, whilst there has been a huge increase in the last twenty years in measurements of absorption cross sections up to the lithium fluoride window edge of 11.8 eV (or 105 nm), often driven by the needs of atmospheric chemists [38], data for energies in the range 12–30 eV remain sparse except for the most stable of molecules such as CF_4, SF_6 and CH_4. Furthermore, the Berkowitz review showed that anion formation is a very minor channel where other decay channels are energetically open, with quantum yields in the range *ca.* 10^{-7} – 10^{-2} [1]. A very high sensitivity of the apparatus is therefore necessary to observe the weak channels for anion production.

5. Results for SF_6, CF_4, and SF_5CF_3

The first molecule studied at Daresbury by negative photoion spectroscopy was the greenhouse gas trifluoromethyl sulphur pentafluoride, SF_5CF_3, and full details are given in ref. [17]. The atmospheric significance of this work is described in Section 5.3. This molecule can be regarded either as a perturbed SF_6 molecule in which one F atom is replaced by a CF_3 radical, or a perturbed CF_4 molecule in which one F is replaced by an SF_5 radical. VUV absorption studies suggest the former is closer to the truth [39]. It therefore seemed sensible to study initially SF_6 and CF_4 by anion spectroscopy. With enhanced sensitivity in our experiment we were able to extend the earlier studies of Mitsuke *et al.* [8,9]. Thus the results presented here report a larger number of anions observed, Mitsuke *et al.* only observing formation of F^- from these two molecules. As explained in Section 4, these studies also allowed us to develop a method of calibration so that *absolute* cross sections and quantum yields for anion production from unknown molecules could be determined. Full details are given in ref. [17].

5.1 SF_6

The white light negative ion mass spectrum for SF_6 shows eight peaks corresponding to the anions F^- (100%), F_2^- (1%), SF^- (<1%), SF_2^- (<1%), SF_3^- (<1%), SF_4^- (<1%), SF_5^- (2%), and SF_6^- (67%). The

relative signal strengths are shown in parentheses. Where sensitivity allowed, anion signals from SF_6 were recorded as a function of photon energy and are presented in Figure 4. Table 2 shows appearance energies of the anions, their cross sections and quantum yields. For comparative purposes, Figure 4 includes the threshold photoelectron spectrum (TPES) of SF_6 [40]. Poor signal strengths prevented the ion yields of SF^-, SF_2^-, SF_3^- and SF_4^- from being recorded. SF_6 has O_h symmetry, and the electronic configuration of the outer-valence molecular orbitals can be written ….. $(1t_{1g})^6\ (3e_g)^4\ (1t_{2u})^6\ (5t_{1u})^6\ (1t_{1g})^6$. The F^- and F_2^- signals increase linearly with pressure, those of SF_5^- and SF_6^- non-linearly with the rate of change increasing as pressure increases. Figure 5 shows the plot of anion signal *vs.* SF_6 pressure, with the behaviour of F^- compared with SF_5^-. The linear pressure dependence of the F^- and F_2^- anion signals suggest that they result from unimolecular ion-pair formation, whereas the SF_5^- and SF_6^- signals are formed by a secondary process. The cross sections for F^- and F_2^- can therefore be determined absolutely, whereas those for SF_5^- and SF_6^- cannot and only relative values are given.

The following ion-pair reactions are suggested as responsible for formation of F^- and F_2^-:

$$SF_6 \rightarrow F^- + SF_x^+ + (5 - x)\ F \qquad (x \leq 5) \qquad (5)$$

$$SF_6 \rightarrow F_2^- + SF_x^+ + (4 - x)\ F \qquad (x \leq 4) \qquad (6)$$

The calculated enthalpy changes for reaction (5) are 10.4, 14.9, 15.5, 19.7 and 23.7 eV for $x = 5$, 4, 3, 2 and 1, respectively. For reaction (6) they are 13.6, 14.1, 18.4 and 22.4 eV for $x = 4$, 3, 2 and 1, respectively. F^- produced from reaction (5) has been observed before by Mitsuke *et al.* in the photon energy range 11–31 eV and a detailed analysis performed [9]. Below 14.9 eV the associated cation can only be SF_5^+, and the present spectrum is in very good agreement with this earlier study. Scully *et al.* have also observed the ion-pair products F^- and F_2^- from SF_6 in the higher photon energy range 20–205 eV [45], and both anions showed broad bands centred at 35.5 eV. Although not photoexciting SF_6 above 35 eV, our study clearly shows the onsets to these features. The F_2^- spectrum in Figure 4 shows features in the energy range 16–21 eV not observed before. Below 18.4 eV it is not possible to say whether the associated cation is SF_4^+ or

SF_3^+. The low F_2^- cross section is reflected in a poor signal-to-noise ratio. Three peaks are identified at 17.2, 18.2 and 19.7 eV. They most likely reflect the presence of Rydberg states which couple effectively to the ion-pair state, the peak energies therefore representing Rydberg transitions. Mitsuke *et al.* found that the most prominent features in the F^- ion yield at 13.2 and 14.3 eV were due to the $(1t_{1g})^{-1}4p$ and $(5t_{1u})^{-1}4s$ Rydberg transitions, respectively [9]. The peaks in the F_2^- ion yield at 17.2, 18.2, and 19.7 eV approximately match with peaks in the TPES of SF_6 at 17.1, 18.5, and 19.9 eV, respectively. A similar observation is made for the yield of F_2^- from SF_5CF_3 (Section 5.3).

Previous ion-pair experiments have also observed SF_5^- and SF_6^- from SF_6, their formation being attributed to the electron attachment process [9,45]:

$$SF_6 + h\nu \rightarrow SF_6^+ + e^- \quad (7)$$

$$SF_6 + e^- \rightarrow SF_6^- \quad (8)$$

$$SF_6 + e^- \rightarrow SF_5^- + F \quad (9)$$

SF_6 is a well-known electron scavenger, the rate coefficient at 300 K being $(2.38 \pm 0.15) \times 10^{-7}$ cm^3 s^{-1} [46]. It attaches zero-energy electrons with a very large cross section [47], and only reaction (8) can be responsible for the appearance of SF_6^-. Furthermore, Figure 4 highlights the striking similarities between the ion yield of SF_6^- and the SF_6 TPES. This is a common effect for molecules with a very high rate coefficient for electron attachment, and is considered in more detail in Section 8.5.

5.2 CF_4

The white light negative ion mass spectrum for CF_4 shows three peaks corresponding to the anions F^- (100%), CF^- (1%) and F_2^- (3%). The F^- and F_2^- signals were recorded as a function of photon energy and are shown in Figure 5(i), along with the TPES of CF_4 [41]. The corresponding data is shown in Table 2. The ion yield of CF^- could not be measured due to poor signal strength. CF_4 has T_d symmetry, and the

electronic configuration of the outer-valence molecular orbitals can be written …….. $(4a_1)^2\,(3t_2)^6\,(1e)^4\,(4t_2)^6\,(1t_1)^6$.

The F^- and F_2^- signals both increase linearly with pressure, the cross sections reported are therefore absolute values, and the following ion-pair reactions are suggested for their formation:

$$CF_4 \rightarrow F^- + CF_x^+ + (3-x)\,F \qquad (x \leq 3) \qquad (10)$$

$$CF_4 \rightarrow F_2^- + CF_x^+ + (2-x)\,F \qquad (x \leq 2) \qquad (11)$$

The calculated enthalpy changes for reaction (10) are 11.3, 17.7 and 20.7 eV for x = 3, 2 and 1, respectively; for (11) they are 16.3 and 19.3 eV for x = 2 and 1, respectively. The F^- ion yield recorded here is in good agreement with the previous study of Mitsuke *et al.* in the energy range 12–31 eV [8]. The F^- and F_2^- yields are also in good agreement with those reported by Scully at higher resolution in the photon range 20–35 eV (Figure 6c and 6d) [34], but absolute cross sections were not determined in their work. It is immediately obvious from Figure 6 that the F^- and F_2^- yields share a similar feature between 20 and 23 eV. Mitsuke *et al*. assigned this feature in the F^- yield to three Rydberg transitions $(3t_2)^{-1}np$ (n = 4, 5 or 6) at energies 20.96, 21.16 and 21.45 eV, respectively, converging on the third excited valence state of CF_4^+ ($\tilde{C}\,^2T_2$) [8]. The Rydberg states excited at these energies then couple to an ion-pair state which dissociates to F^-, the corresponding cation, and any neutral fragments. The presence of Rydberg states in this energy region has also been observed in a high resolution threshold photoelectron study of CF_4 by Yencha *et al*. [48]. Autoionising structure is observed from 20.3 to 21.6 eV, preceding the onset of the $\tilde{C}\,^2T_2$ state of CF_4^+ at 21.68±0.01 eV [49]. This can be observed in the TPES in Figure 6 as a slight rise above the baseline in the same energy range. It is therefore proposed that Rydberg states converging to CF_4^+ $C\,^2T_2$ couple to ion-pair states which dissociate to both F^- *and* F_2^-. At 21.8 eV the F^- cross section is *ca.* 16 times larger than that of F_2^-. This may reflect the degree of coupling between states and/or the steric disadvantage of the formation of an extra bond to produce F_2^-.

The feature between 20 and 23.5 eV in the F^- ion yield has been recorded with better resolution, and is shown in Figure 7. It shows the CF_4^* $(3t_2)^{-1}4p$, $5p$, and $6p$ overlapping Rydberg states converging on the CF_4^+ $C\,^2T_2$ state. Structure is also observed in the spectrum, showing the $\nu_1(a_1)$ totally-symmetric stretching mode in CF_4^*. These progressions have been observed before in the ion-pair study by Mitsuke *et al.* [8], and Table 3 compares the two sets of data, listing energy positions, energy spacings, and the vibrational quantum number assignments. The vibrational spacing of the progressions observed in these *np* Rydberg states in the F^- ion yield average to 90 ± 5 meV. The assignments are taken directly from Mitsuke *et al.* Their quantum defect analysis yielded a δ value which is almost exactly the same for all three Rydberg states, *ca.* 0.60. This analysis also agrees with the photoabsorption study of Lee *et al.* [50]. Photoelectron spectroscopy shows a vibrational progression in the band representing ionisation to the $C\,^2T_2$ state of CF_4^+ with a spacing of *ca.* 90 meV and assigned to the ν_1 C–F breathing mode [48], and a higher-resolution optical emission spectrum of the $\tilde{D}\,^2A_1 - C\,^2T_2$ transition in CF_4^+ gave ν_1 $(C\,^2T_2) = 729\pm1$ cm^{-1} or 90.386 meV [51]. Since all these studies only involve excitation of the one totally-symmetric vibrational mode in T_d symmetry, the Jahn-Teller distortion in the triply-degenerate $C\,^2T_2$ state of CF_4^+ is minimal.

Figure 7 shows an additional feature at 22.82 eV which was not observed in the previous studies. It is assigned to the $(4a_1)^{-1}3p$ Rydberg transition. This assignment uses a value for the vertical ionisation energy of 25.11 eV for the fourth excited state of CF_4^+ with term symbol $\tilde{D}\,^2A_1$ [51]. The resulting term value of 2.29 leads to a quantum defect value of 0.56. This assignment is consistent with the observation of features in the F^- ion yield at 24.00 and 24.45 eV by Mitsuke *et al.*, and assigned by them to the $(4a_1)^{-1}4p$ and $(4a_1)^{-1}5p$ Rydberg transitions, the next two members of this *p* Rydberg series, with δ values of 0.50 and 0.46, respectively [8]. The next discrete state in the photoelectron spectrum, corresponding to ionisation of the $2t_2$ inner-valence electron, is the $E\,^2T_2$ state at 40.3 eV [52]. Both the F^- and F_2^- yields increase above 25 eV, and the spectral features at higher energies are more clearly observed in the work of Scully which extends to 110 eV [34].

5.3 SF_5CF_3

It is important to put the work to be reported into an atmospheric context. The presence of SF_5CF_3 in the atmosphere was first reported eleven years ago by Sturges *et al.* [53]. Although the atmospheric concentrations of SF_5CF_3 are still very low, its lifetime is very long, *ca.* 800–1000 years [44], it has the highest molecular radiative forcing of anthropogenic greenhouse gases through absorption of infrared radiation in the wavelength range of 5–30 μm and has a global warming potential 18,000 times greater than that of CO_2 [54]. Since its discovery, SF_5CF_3 has been the focus of numerous studies aimed to understand better its spectroscopic properties and reactivity, and also its atmospheric sources and sinks. Of anthropogenic origin, SF_5CF_3 has been linked to SF_6 production and the manufacture of fluorochemicals [53], but the main source of this potent greenhouse gas has not yet unambiguously been identified. Having no hydrogen atoms, SF_5CF_3 is not oxidised *via* reaction with the OH radical in the troposphere, and UV photolysis in the stratopshere is unlikely to contribute significantly to a sink mechanism due to the absence of photoabsorption by SF_5CF_3 below 8 eV [44,55] and the high value of the SF_5–CF_3 bond dissociation energy, 3.86 ± 0.45 eV [56]. We note here that *ab initio* calculations obtain a significantly lower value for the bond dissociation energy [57].

The microscopic physical and chemical processes that remove SF_5CF_3 from the atmosphere therefore occur at higher altitude in the mesosphere. One process could be ion-pair formation following VUV absorption due to the high intensity of this radiation, especially Lyman-α radiation at 10.2 eV, that exists in this region of the atmosphere [44]. Other processes include ion-molecule reactions and electron attachment. Ion-molecule reaction studies have shown that both cations and anions react rapidly with SF_5CF_3 [58,59], and may therefore remove it from the upper atmosphere. However, the concentration of atmospherically-relevant ions (*e.g.* O^+, O_2^+, N^+, N_2^+) is so low that the pseudo-first-order rate constant for ion-molecule reactions, $\sum k_{ion}[\text{ion}]$, is too small for this channel to contribute to any significant extent [56]. Low-energy electron attachment to SF_5CF_3 is relatively fast, 7.7×10^{-8} cm^3 molecule^{-1} s^{-1} at 298 K [60], and the absorption cross section at the Lyman-α wavelength of 121.6 nm is surprisingly high, 1.3×10^{-17} cm^2

[39,44,55]. With certain assumptions, we showed that the electron attachment process is responsible for *ca.* 99 % of the removal of SF_5CF_3 in the mesosphere, VUV photodissociation is responsible for the remaining *ca.* 1 % [44,56]. One of the possible products which is energetically allowed following VUV photoexcitation of SF_5CF_3 at 121.6 nm is ion-pair formation to $CF_3^+ + SF_5^-$. It was for this rationale that we performed a complete negative photoion spectroscopic study of SF_5CF_3 over the full range of the vacuum-UV, and absolute cross sections and quantum yields were evaluated for all anions observed [17]. These results are described below. However, the long lifetime of SF_5CF_3 in the earth's atmosphere, 800–1000 years, ultimately is not determined by such *microscopic* chemical processes that occur in the mesosphere, but by much slower *macroscopic* meteorology that transports the pollutant from the earth's surface up into the mesosphere [44,56].

The white light negative ion mass spectrum for SF_5CF_3 shows eight peaks corresponding to the anions F^- (100%), CF^- (1%), F_2^- (2%), SF^- (1%), SF_2^- (1%), SF_3^- (1%), SF_4^- (2%) and SF_5^- (14%). With the exception of SF_5^-, all anion signals show a linear dependence with the pressure of SF_5CF_3. SF_5^- shows a similar pressure behaviour to its formation from SF_6, discussed in Section 5.1. Absolute cross sections and quantum yields for the anions resulting from ion-pair formation are presented in Figure 8, the data in Table 2. The quantum yields all fall in the range 10^{-6} to 10^{-4}, consistent with expectations for a large polyatomic molecule [1,24]. The ion yield of F^- below 12 eV was recorded with a LiF window in the beamline, transmitting only $h\nu < 11.8$ eV, to display the threshold region more clearly. An appearance energy (AE_{298}) value of 11.05 ± 0.05 eV was determined.

The following reactions are suggested as the main sources for six of the anions:

$$SF_5CF_3 \rightarrow F^- + CF_3^+ + SF_4 \qquad (12)$$

$$SF_5CF_3 \rightarrow SF_4^- + CF_3^+ + F \qquad (13)$$

$$SF_5CF_3 \rightarrow SF_3^- + CF_3^+ + F + F \qquad (14)$$

$$SF_5CF_3 \rightarrow F_2^- + CF_3^+ + SF_3 \qquad (15)$$

$$SF_5CF_3 \rightarrow SF_2^- + CF_3^+ + 3F \qquad (16)$$

$$SF_5CF_3 \rightarrow SF^- + CF_3^+ + 4F \qquad (17)$$

In all cases the cation formed is CF_3^+, the associated anion therefore resulting from the SF_5 part of the SF_5CF_3 molecule. An alternative mechanism to reaction (12) for production of F^- might be from dissociative electron attachment,

$$\textit{e.g.} \qquad SF_5CF_3 + e^- \rightarrow F^- + SF_4 + CF_3 \qquad (18)$$

This possibility is rejected because the only product of low-energy electron attachment to SF_5CF_3 is SF_5^- (reaction (20) below) [60], and we note the much stronger signal of F^- compared to that of SF_5^- (Figures 8 and 9).

The S–C bond is most likely to be the weakest in the molecule, the dissociation energy at 0 K measured to be 3.86 ± 0.45 eV [56]. In addition, Xu *et al.* have calculated bond dissociation energies at 298 K in SF_5CF_3, resulting in D^o_{298} (SF_5CF_2–F) > D^o_{298} (F–SF_4CF_3) > D^o_{298} (SF_5–CF_3) [57]. One cannot say conclusively that reactions (12)–(17) are responsible for *all* of the signal from these six anions across the complete energy range studied. Certainly, more channels become energetically accessible at higher energies. It is, however, interesting that the thermochemical thresholds for reactions (12)–(17), 11.5, 13.4, 16.0, 14.3, 20.0 and 23.0 eV respectively, approximately reflect the observed *AE* values for the corresponding anion (Table 2). The only apparent exception is reaction (15), production of F_2^-, where steric constraints on forming a new F–F bond could be responsible. This trend can be visualised in Figure 8 by vertical arrows representing the enthalpies of the calculated thermochemical thresholds. No errors are given, but there is significant uncertainty in some of the $\Delta_f H°_{298}$ values used which probably explains why the calculated *AE* value is sometimes greater than the experimental value (*e.g.* F^- and SF_4^- in Figure 8). The formation of F^- and F_2^- over the complete energy range 11–35 eV is unlikely to result exclusively from reactions (12) and (15), respectively, whereas the channels available to form the sulphur-containing anions

are fewer. Indeed, the ion yields of F^- and F_2^- do show structure over a much wider energy range than those of SF_x^- (x = 1–4).

The ion yields for F^-, F_2^- and SF_5^- are presented in Figure 9 and compared to the TPES of SF_5CF_3 [42]. SF_5^- is the only anion detected which is *not* associated with ion-pair formation, and therefore only its relative yield can be determined. Three comparisons can be made between the behaviour of SF_5^- formed from SF_5CF_3 and SF_5^- formed from SF_6 (Section 5.1). First, for both molecules the SF_5^- signal increases non-linearly with pressure, with the rate of change of signal increasing as the pressure increases. Second, electron attachment to SF_5CF_3 is dissociative, forming $SF_5^- + CF_3$ as the only significant channel [60]. Third, the yield of SF_5^- from SF_5CF_3 shows many similarities to the TPES of SF_5CF_3. The dominant mechanism for the production of SF_5^- from SF_5CF_3 is likely, therefore, to be dissociative electron attachment following photoionisation of the parent molecule as the source of low-energy electrons:

$$SF_5CF_3 + h\nu \rightarrow SF_5CF_3^+ + e^- \qquad (19)$$

$$SF_5CF_3 + e^- \rightarrow SF_5^- + CF_3 \qquad (20)$$

As shown in Figure 9, the F^- and F_2^- ion yields also show similarities to the TPES of SF_5CF_3. Due to its higher signal-to-noise ratio, it is the F^- spectrum where these similarities are most obvious. In the photon energy range 13–23 eV the agreement between peak positions is good and the relative signal strengths show only small differences. The resemblance of the F^- ion yield to the TPES could be explained by a process involving electron attachment being significant in F^- formation. However, the F^- signal rises *linearly* with increasing gas pressure, suggesting strongly that a primary process, *i.e.* ion-pair formation to $F^- + SF_4CF_3^+$ (or $F^- + CF_3^+ + SF_4$), is dominant. The features in the F^- yield are labelled 1 to 11 in Figure 8. The experimental AE_{298} (F^-) is 11.05±0.05 eV, and this anion gives rise to peak 1 centred at 11.7 eV. This peak occurs below the onset of ionisation for SF_5CF_3, 12.9 eV [42], so the presence of photoelectrons from reaction (19) is not relevant. The energy of peak 1 is close to peaks observed in the SF_5CF_3 photoabsorption and total fluorescence yield spectra at 11.4 eV [39,61]. These two studies give different assignments to this

transition. Holland *et al*. [39] assign it to a blend of several valence-valence transitions, whilst Ruiz *et al*. [61] assign it to the $(29a')^{-1}4s$ Rydberg transition, where 29a' is the highest-occupied molecular orbital. Following dissociation of $SF_5CF_3^*$, fluorescence at this energy was reported to originate from the CF_3 fragment, In addition, this was the most intense band observed within the photon energy range studied of 10–28 eV [61]. It must represent a transition to the same intermediate state which predissociates along two different reaction coordinates to yield CF_3^* and F^- anions. The ion-pair quantum yield at this maximum in the F^- ion yield at 11.7 eV is $\Phi = 1.5 \times 10^{-4}$. This small value, coupled with the fact that fluorescence from $SF_5CF_3^*$ is unlikely to have a large quantum yield, suggests strongly that predissociation into *neutral* fragments is the favoured process at this energy, not ion-pair formation. The agreement of peak positions in SF_5CF_3 between the photoabsorption spectrum, the total fluorescence yield and the F^- ion yield extends up to 17 eV. Above this energy, similarities between the spectra are less clear.

It is interesting that the F^- ion-pair quantum yield does not decrease above the onset of ionisation of SF_5CF_3 at 12.9 eV. Features 1 and 4 at 11.7 and 16.9 eV, for example, have $\Phi = 1.5 \times 10^{-4}$ and 3.4×10^{-4}, respectively (Table 4). As a result of significant photoabsorption leading to ionisation, one would expect the ion-pair quantum yield to decrease, as observed for both SF_6 and CF_4 (Table 4). However, the opposite occurs for SF_5CF_3. In fact, features 2–11 of Figure 8 occur at, or just below, vertical ionisation energies in the TPES of SF_5CF_3 [42]. Only feature 1 does not follow this trend. It seems unlikely that valence states of SF_5CF_3 which predissociate into ion pairs coincidentally lie very close to the ionisation thresholds, certainly across this large energy range. It is much more likely that Rydberg states play an important role. Certainly the F^- ion yield could be explained if coupling to ion-pair states was more significant from Rydberg states close to the ionisation thresholds than from those lower in energy. Contributions to the F^- ion yield from low-lying Rydberg states would then be the dominant cause of peak 1, and very likely a weak background across the spectrum. F^- ions produced *via* high-lying Rydberg states would be dominant at higher energy, and hence responsible for features 2–11 in the ion yield. If this is true, it negates the generally accepted rule that it is low-*n*, and not high-*n*, Rydberg states which interact most strongly with ion-pair states. However, most of the ion-pair experiments on polyatomics to date have studied halogenated molecules where the

lowest ion-pair threshold lies *below* the first ionisation energy [1], so by definition it is the low-*n* states which have been the most widely studied.

This analysis also extends to the yields of SF_4^-, SF_3^-, F_2^-, SF_2^- and SF^-; their peak positions and observed structure can be explained in the same way as for F^-. The SF_4^-, SF_3^- and SF_2^- yields show less structure than is seen from F^-. In the energy regions where peaks are observed, their energies agree with those in the F^- ion yield, and hence with vertical ionisation energies of SF_5CF_3. It is likely that the number of available ion-pair states reflects the structure seen in the ion yields. SF_4^-, for example, is likely to arise from reaction (13) only. It is certainly the channel that is most sterically unhindered. Coupling of high-lying Rydberg states to this ion-pair state will give rise to the peaks in the SF_4^- yield at 14.0 and 15.0 eV (Figure 8). The absence of structure above 16 eV represents the energy where this ion-pair state no longer couples significantly to Rydberg states. SF_3^- and SF_2^- may also arise through coupling of high-lying Rydberg states to an appropriate ion-pair state, and only over a limited energy range above onset. By contrast, many more dissociation channels will be available to yield the F^- and F_2^- anions. As a result, extensive structure in both ion yields extends from onset to 25 eV. Finally, we observe that shape resonances have been observed in the yields of many anions in both SF_6 and CF_4 above 25 eV [45,34]. There is no obvious evidence for such peaks in the anion yields from SF_5CF_3, but it would be surprising if they were not present.

The difficulties in assigning peaks in the total fluorescence yield spectrum of SF_5CF_3 have already been noted by Ruiz *et al*. [61], and at our modest resolution there are several Rydberg transitions which could be assigned to peaks 2–11 in Figure 8a. Indeed, there is even disagreement whether transitions observed in the VUV absorption spectrum of SF_5CF_3 and the CF_3^* fluorescence excitation spectrum are due to valence or Rydberg transitions. Peaks in the absorption and electron energy loss spectra of SF_5CF_3 have been assigned by Limao-Vieira *et al*. to Rydberg transitions, and quantum defects determined [62]. Ruiz *et al*. also assign peaks in the absorption spectrum leading to CF_3^* fluorescence to Rydberg transitions [61]. Holland *et al*., however, assign the main peaks in the absorption spectrum to valence transitions [39]. The spectra presented here observe a different exit channel, *i.e.* photodissociation of excited states of SF_5CF_3 leading to

production of *anions*. However, the primary excitation process in all these experiments is the same, and their assignment to Rydberg transitions is favoured for two reasons. First, all previous work on ion-pair production from polyatomic molecules has preferred the process of Rydberg state photoexcitation, followed by predissociation into an ion-pair state [1,16]. Second, apart from the low-energy peak in the F^- yield at 11.7 eV below the ionisation energy of SF_5CF_3, all F^- peaks have energies very close to peaks in the TPES of this molecule. Since it is Rydberg states that have energies converging on ground and excited electronic states of $SF_5CF_3^+$, it seems very likely that these F^- peaks correspond to photoexcitation of Rydberg states.

The dominant VUV radiation in the mesosphere is Lyman-α radiation with a photon wavelength of 121.59 nm or energy of 10.20 eV. If production of anion(s) or ion-pair dissociation are important sink routes for SF_5CF_3 in the mesosphere, it is the processes occurring at this energy that will be the most important. Ion-pair dissociation of SF_5CF_3 to both $CF_3^- + SF_5^+$ and $SF_5^- + CF_3^+$ are energetically open channels at this energy, these two reactions having small $\Delta_r H^o_{298}$ values of only +1.82 and –0.90 eV, respectively [44]. The enthalpy of reaction to produce $F^- + SF_4CF_3^+$ is not known due to the enthalpy of formation of $SF_4CF_3^+$ being unknown. However, since anion formation appears to occur indirectly in SF_5CF_3 *via* initial excitation of Rydberg states, no anions can be observed until the lowest Rydberg states are accessed. The VUV absorption spectrum shows that this does not happen until energies exceed 8 eV [39,44,55], the appearance energies of F^- and SF_5^- are 11.05 ± 0.05 and 12.9 ± 0.2 eV (see earlier), and CF_3^- is not observed. No anions are observed at 10.20 eV. Thus it appears that anion or ion-pair formation does not contribute to the processes removing SF_5CF_3 from the earth's atmosphere in the mesosphere, and the only two significant microscopic processes are dissociative electron attachment and photodissociation at 10.20 eV to neutral species [44,56].

6. Results for SF_5Cl, CF_3X (X = Cl, Br, I) and CH_3Y (Y = F, Cl, Br)

One obvious question to ask about the formation of anions from a polyatomic molecule is whether the anions which are formed from a *non*-symmetrical molecule and their cross sections bear any relation to the

strength of the breaking bond. In both SF_6 and CF_4, all the six and four bonds in the parent molecule, respectively, have equal strength. However, if the symmetry of either molecule is reduced by replacing one fluorine by a chlorine atom, for example, one may ask whether F^- or Cl^- are more likely to form following VUV photoexcitation, and whether their appearance energies relate in any way to the relative strength of the S(C)–F and S(C)–Cl bonds. In polyatomic *cations* of this size, *e.g.* $CF_2H_2^+$, when two different bonds can break, assuming the ground state of the cation is bound for at least some of its vibrational levels, the first fragment cation is that produced by cleavage of the weakest bond. The second cation is formed by cleavage of the second-weakest bond *etc.* Thus, in unpublished work from the high-resolution VUV beamline of the Swiss Light Source, using imaging photoelectron photoion coincidence spectroscopy we have measured the $AE_{0\,K}$ of CF_2H^+ from CF_2H_2 to be 13.060 ± 0.002 eV, whilst the $AE_{0\,K}$ of CFH_2^+ is *ca.* 1 eV higher at 14.00 ± 0.03 eV [63]. These data correlate with bond strengths in the neutral molecule, with D^o_{298}(H– CHF_2), 4.48 ± 0.04 eV, being weaker than D^o_{298}(F–CH_2F), 5.14 ± 0.09 eV [64]. The same ordering is maintained in the cationic species, with D^o_{298}(H–CHF_2^+), ≤ 0.1 ± 0.1 eV, now being much weaker than D^o_{298}(F–CH_2F^+), ≤ 2.5 ± 0.1 eV (Table 11) [22]. These upper limits for D^o_{298}(A–BC^+) were obtained from eqn (III) using experimental values for the appearance energies of H^- and F^- following VUV photoexcitation of CF_2H_2. This forms the rationale to study molecules related to SF_6 and CF_4, *e.g.* SF_5Cl and CF_3X (X = Cl, Br, I) in which one fluorine atom is replaced by a different halogen atom, by anion spectroscopy [21,18]. We then investigate whether the presence of fluorine atoms is significant by studying the CH_3Y (Y = F, Cl, Br) series [20]. This section summarises the results.

6.1 SF_5Cl

The structure of SF_5Cl, C_{4v} symmetry in the gas phase, has been established by microwave spectroscopy and electron diffraction [65,66]. Four equitorial S–F bonds have a slightly shorter length, 0.157 nm, than the S–F axial bond, 0.159 nm, whilst that of S–Cl is significantly longer, 0.204 nm. The relative ordering of the valence molecular orbitals (MO) of the molecule has been calculated using self-

consistent discrete variational Xα methods [67], and there have been two photoelectron studies by He I / He II and threshold electron spectroscopy [68,69]. The fragmentation dynamics of the electronic states of SF_5Cl^+ has been studied by threshold photoelectron photoion coincidence spectroscopy [69]. Chim *et al.* [69] also reported results from a Gaussian 03 calculation [70] which supported the MO assignments made by Klyagina *et al* [67]. Figure 10 summarises the combined findings of these investigations, and correlates the MOs for SF_5Cl with those of SF_6 of O_h symmetry. The studies of anion formation following excitation of SF_5Cl are even more limited. There have been two measurements of the thermal electron attachment rate coefficient to SF_5Cl: $(4.8\pm1.2) \times 10^{-8}$ cm^3 s^{-1} by van Doren *et al*. [71] and $(2.0\pm0.3) \times 10^{-8}$ cm^3 s^{-1} by Mayhew *et al*. [46], a factor of *ca.* 5–12 slower than the value for SF_6, $(2.38\pm0.15) \times 10^{-7}$ cm^3 s^{-1}. Under thermal electron conditions, electron attachment to SF_5Cl is dissociative, producing SF_5^- (92%), Cl^- (5%) and FCl^- (3%), whereas that to SF_6 is predominantly non-dissociative. A recent crossed beam study of SF_5Cl with low-energy electrons in the range 0–14 eV [72] has clarified inconsistencies arising from an earlier study [73]. As in the thermal experiment, electron attachment to SF_5Cl is dissociative with SF_5^- being the dominant anion at low electron energies, but resonances forming F^-, Cl^- and FCl^- are now observed at $E > 3$ eV.

Only three anions, F^-, Cl^- and SF_5^- were detected following VUV photoexcitation of SF_5Cl in the photon energy range 10–25 eV. The F^- signal was by far the strongest, followed by Cl^- whilst SF_5^- was detected only just above the sensitivity limit of the apparatus. The signals of F^- and Cl^- show a linear dependence with pressure, showing that these ions form by an ion-pair process. As with SF_6 and SF_5CF_3, the SF_5^- signal from SF_5Cl shows a non-linear dependence with pressure, with the signal rising more rapidly with pressure than from a linear relationship. As before, this suggests that SF_5^- most likely results from the two-step process of dissociative electron attachment: $SF_5Cl + h\nu \rightarrow SF_5Cl^+ + e^-$, followed by $SF_5Cl + e^- \rightarrow SF_5^- + Cl$, where a quadratic dependence of SF_5^- signal with pressure is predicted. It is noted immediately that the strength of the F^- signal is somewhat surprising, given that the F–SF_4Cl bond dissociation energy, 3.70 eV, is significantly stronger than that of Cl–SF_5, 2.54 eV [69].

The cross section for F^- formation is shown in Figure 11a over the range 12–30 eV. Its onset is 12.7 ± 0.2 eV (Figure 11b) which lies *above* the adiabatic ionisation energy for SF_5Cl of 12.3 eV. The onset is gradual, with an enhanced gradient for hν > *ca.* 13.6 eV (labelled shoulder '1' in Figure 11b). The maximum cross section, 6.1×10^{-20} cm^2, occurs at an energy of 14.06 eV, labelled '2' in the figure. The shoulder between 12.7 and 13.6 eV may arise from

$$SF_5Cl \rightarrow F^- + SF_4Cl^+ \qquad \Delta_r H^o_{298} \leq 11.58 \text{ eV} \qquad (21)$$

$$SF_5Cl \rightarrow F^- + SF_3^+ + FCl \qquad \Delta_r H^o_{298} = 11.41 \text{ eV} \qquad (22)$$

$$SF_5Cl \rightarrow F^- + SF_3Cl^+ + F \qquad \Delta_r H^o_{298} \text{ unknown} \qquad (23)$$

SF_3Cl^+ has not been observed in any photon or electron-induced dissociative ionisation experiment, suggesting that production of F^- from reaction (23) is unlikely. The increase in gradient of the σ *vs.* hν spectrum at 13.6 eV may correlate to production of F^- from

$$SF_5Cl \rightarrow F^- + SF_4^+ + Cl \qquad \Delta_r H^o_{298} = 13.47 \text{ eV} \qquad (24)$$

At higher energies it becomes even more difficult to assign features in ion-pair spectra to specific dissociation reactions with any confidence because, with the lower symmetry of the molecule compared to SF_6, the number of accessible ion-pair products increases dramatically,

$$\textit{e.g.} \quad SF_5Cl \rightarrow F^- + Cl^+ + SF_3 + F \qquad \Delta_r H^o_{298} = 18.64 \text{ eV} \qquad (25)$$

Feature 1 of the F^- ion yield exhibits the characteristics associated with direct ion-pair formation; a gradual onset and a broad structureless spectrum. Features 2–9 show the characteristics associated with indirect formation (see Section 2), and have been assigned to Rydberg states of SF_5Cl (Table 5). These data assume that, in most cases, the given Rydberg state converges towards the excited state of SF_5Cl^+ closest in energy to that of the resonance. For example, it is assumed that feature 2 at 14.06 eV converges to SF_5Cl^+ ($A\ ^2A_1$) at 14.79 eV, and not to SF_5Cl^+ ($B\ ^2A_2$) at 15.35 eV. These higher-energy peaks, 3–9, are much weaker with cross sections approximately one order of magnitude weaker than the cross section of peak 2; thus the cross

section at 23.2 eV, corresponding to feature 6, is only 5.9×10^{-21} cm^2. This large difference may be due to the nature of the Rydberg state assigned to feature 2. Gaussian 03 calculations have shown that the $A\,^2A_1$ state of SF_5Cl^+ involves the removal of an electron from the $15a_1$ molecular orbital which has both S–F_{eq} and S–Cl bonding character [70]; the Rydberg state represented by feature 2 is thought to converge to the first excited state of SF_5Cl^+, and has been identified to come from reaction (24) where a S–F and S–Cl bond in the molecule are both broken. Of course, it is not known whether the F^- signal comes from one of the four equivalent equitorial S–F bonds, or from the longer and weaker axial S–F bond.

The ion yield of Cl^- is shown in Figure 12, only one peak at 10.9 eV was detected in the range 8–35 eV, and its onset is 10.6 ± 0.2 eV. This energy lies below the ionisation energy of SF_5Cl, and therefore Cl^- can only be formed from an ion-pair reaction. The only energetically-allowed reaction is

$$SF_5Cl \rightarrow Cl^- + SF_5^+ \qquad \Delta_r H°_{298} = 8.72 \text{ eV} \qquad (26)$$

with the onset occurring 1.9 eV above the thermochemical threshold. The sharp onset implies that this ion-pair product forms indirectly. This feature can be assigned to a resonant transition from the highest-occupied MO of SF_5Cl to the *4p* Rydberg state converging on SF_5Cl^+ $X\,^2E$ which then predissociates into the $Cl^- + SF_5^+$ ion-pair state. The quantum defect of this $(9e)^{-1}4p$ Rydberg state is then calculated to be 1.47, consistent with data for high-lying Rydberg states (Table 5). The Cl^- ion yield in Figure 12 could not be put accurately onto an absolute scale because the signal level was so weak. However, by comparison of the signal-to-noise ratio of the Cl^- spectrum with that of weak anions observed in other studies of non-symmetric molecules where different bonds can break [18,20], it is estimated that the maximum cross section for Cl^- production is less than *ca.* 10^{-22} cm^2. From eq. (II) an upper limit for the S–F and S–Cl bond dissociation energy in SF_5Cl at 298 K can be determined. Using $AE(F^-) = 12.7 \pm 0.2$ eV, an upper limit for $D^o_{298}(F–SF_4Cl)$ of 4.8 ± 0.3 eV is obtained. Likewise, using $AE(Cl^-) = 10.6 \pm 0.2$ eV, an upper limit for $D^o_{298}(Cl–SF_5)$ of 4.4 ± 0.3 eV is obtained. These upper-limit values are consistent with the thermochemically-determined bond dissociation energies of 3.70 and 2.54 eV for cleavage of the S–F and S–Cl bonds, respectively, in SF_5Cl [69].

The apparent absence of ion-pair reactions producing Cl^- with any significant yield is not easily explained. The quantum yield for production of either F^- or Cl^- cannot be quantified because absolute VUV absorption cross sections in the range 10–20 eV are not known for SF_5Cl. However, the yield of F^- is orders of magnitude higher, despite the S–F bond being *ca.* 50% stronger than the S–Cl bond. Furthermore, the thermochemical energy of the lowest channel producing F^-, *i.e.* $F^- + SF_4Cl^+$, is *ca.* 2.8 eV higher than that for production of Cl^-, *i.e.* $Cl^- + SF_5^+$. It would appear that the dynamics of the crossing of Rydberg states with the ion-pair continuum determines the relative intensities of the two atomic anions that can be formed, and not the thermochemistry of the different dissociation channels or the physical properties (*e.g.* electron affinity, electronegativity or polarisability) of the corresponding neutral atom.

6.2 CF_3X (X = Cl, Br, I)

A similar situation is observed with the CF_3X series of molecules [18], in which one F atom in the symmetrical CF_4 molecule is replaced by a different halogen atom; competition can occur between cleavage of the C–F and the C–X bond. In addition to F^- and X^- anions being observed, a large range of other anions are now also observed: F_2^-, FX^-, CF^-, CF_2^- and CF_3^-. With the exception of Br^- and I^-, all the observed anions show a linear dependence of signal with pressure. The dissociative electron attachment process dominates the production of Br^- and I^-. Unlike SF_5Cl, *all* cross sections for anions produced by ion-pair formation can be put on to an absolute scale by calibrating the signal strengths with those of F^- from both SF_6 and CF_4 (Section 4.1). Furthermore, since data for VUV absorption cross sections are available [74-76], quantum yields can be determined. The data are shown in Table 6, with Figures 13 and 14 showing the F^- and X^- ion yields from CF_3X, respectively. (These figures also show, where available, the absorption, threshold photoelectron and fluorescence excitation spectra of these molecules, showing that the Br^- and I^- spectra from CF_3Br and CF_3I show some similarilty with the threshold photoelectron spectra which is not present in the four other anion yields.) Absolute cross sections are reported for F^- from CF_3X and Cl^- from CF_3Cl, but clearly not for Br^- and I^- from CF_3Br and CF_3I. However, there is one exception. The lowest-

energy peak in the I^- yield at 9.0 eV, with a threshold of 8.8 ± 0.2 eV, occurs at an energy *below* the adiabatic ionisation energy of CF_3I, 10.4 eV [78]. It can therefore only arise from ion-pair formation,

$$e.g.\ CF_3I \rightarrow I^- + CF_3^+ \qquad \Delta_r H°_{298} = 8.3\ \text{eV} \qquad (27)$$

For this one peak, we can determine the cross section for I^- formation to be 3.8×10^{-21} cm^2 and, *via* normalisation to the absorption cross section, a quantum yield of *ca.* 8×10^{-5}.

The F^- signal from CF_3X shows an onset at 16.0 ± 0.2, 14.7 ± 0.2 and 9.7 ± 0.2 eV for X = Cl, Br and I, respectively. On thermochemical grounds, it seems likely that the F^- anion from CF_3X (X = Cl and Br) arises in combination, not with CF_2X^+, but with $CF_2^+ + X$, since the enthalpies of reactions (28) – (29) are close to these values,

$$CF_3Cl \rightarrow F^- + CF_2^+ + Cl \qquad \Delta_r H°_{298} = 15.8\ \text{eV} \qquad (28)$$

$$CF_3Br \rightarrow F^- + CF_2^+ + Br \qquad \Delta_r H°_{298} = 14.9\ \text{eV} \qquad (29)$$

The energy of the equivalent channel in CF_3I is 14.2 eV, yet signal is observed at lower energy (Figure 13c). We can predict with confidence that the weak peak in the F^- yield from CF_3I at 9.8 eV can only arise from F^- forming with CF_2I^+, even though the enthalpy of formation of CF_2I^+ is unknown. The energies of the equivalent channels for CF_3Cl and CF_3Br are 10.2 and ≤ 10.1 eV, so it seems unlikely that F^- above *ca.* 15 eV from these molecules forms from this channel.

For CF_3Cl, the quantum yield for production of F^- at the energy of the first maximum at 21 eV, 1.8×10^{-4}, exceeds that for production of Cl^- at the same energy by a factor of *ca.* 6. This comparison cannot be made for CF_3Br and CF_3I. In the former case, Br^- only forms by dissociative electron attachment. In the latter case, the absorption cross section for CF_3I at 20.4 eV has not been measured. Whilst the data is not as conclusive as that for SF_5Cl (Section 6.1), the conclusion from this study of formation of F^- and X^- from CF_3X is that the F^- anion probably forms with a higher quantum yield than X^-, even though the C–F bond is significantly stronger than the C–X bond. The data for these molecules is complicated by the multiple

possibilities of the cation (+ neutral) that are formed with the anion, and by the presence of dissociative electron attachment in CF_3Br and CF_3I being dominant. But the trend that these molecules prefer to form F^- rather than X^- following VUV excitation seems clear. The shape of the peaks in the anion ion yield spectra suggest that these anions form *via* an indirect process. As with SF_5Cl, if this is true it can only mean that the dynamics of the crossing of the initially-excited Rydberg state of CF_3X with the ion-pair continuum is the dominant process in determining the relative quantum yields of the atomic anions that are formed.

Data from ion-pair formation of F^- from SF_6, SF_5X (X = CF_3, Cl), CF_4 and CF_3Cl are collected in Table 7. Two points are striking. First, the relative energy of the $AE(F^-)$ to the adiabatic ionisation energy of the parent molecule may be important. The most significant features in the F^- spectrum from SF_6 appear below its AIE [9,17], yet for SF_5Cl the $AE(F^-)$ and the first F^- peak exceed the AIE [21]. The same comment can be made when comparing F^- from CF_4 with F^- from CF_3Cl [8,17,18,79]; for CF_4 the $AE(F^-)$ is less than the adiabatic IE, whereas for CF_3Cl the $AE(F^-)$ exceeds the adiabatic IE. SF_6 and CF_4 follow the expected trend that the probability for an excited electronic state to predissociate into ion pairs is greater in the absence of a competing autoionization process. It is possible, therefore, that the change in symmetry on substituting a fluorine for a chlorine atom suppresses the formation of ion pairs below the ionization energy, or possibly increases the probability of a competing process such as neutral dissociation (*e.g.* $SF_5Cl \rightarrow SF_5 + Cl$). We note that when comparing data for ion-pair formation from CF_3Cl with photoabsorption and fluorescence excitation spectra [75], the evidence suggests that photoexcitation below the ionization energy almost exclusively results in neutral photodissociation. Second, production of F^- from the molecules of lower symmetry appears to be accompanied by a simultaneous bond cleavage to form an anion plus neutral species. For example, SF_5Cl probably forms $F^- + SF_4^+ + Cl$ and not $F^- + SF_4Cl^+$, CF_3Cl forms $F^- + CF_2^+ + Cl$ and not $F^- + CF_2Cl^+$, SF_5CF_3 forms $F^- + CF_3^+ + SF_4$ and not $F^- + SF_4CF_3^+$. From SF_6 and CF_4, however, F^- appears to form at threshold with SF_5^+ (and not with $SF_4^+ + F$) and CF_3^+ (and not $CF_2^+ + F$). If this is a generic effect, the reason for it is unclear.

6.3 CH_3Y (Y = F, Cl, Br)

The common theme from Sections 6.1 and 6.2 is that F^- forms with the highest cross section from substituted SF_6 and CF_4 molecules when one F atom is replaced by a larger halogen atom X, even though the S(C)–F bond is significantly stronger than the S(C)–X bond. It seems unlikely, but the five- and three-fold statistical weighting in favour of production of F^- from SF_5Cl and CF_3X, respectively, may be one important factor. To investigate this effect further, we have studied the CH_3Y (Y = F, Cl and Br) series of molecules [20] to see if H^- is the dominant anion. For this series of molecules, the bond strength should not be an issue because the H–CH_2Y bond strength is less than, comparable to, or exceeds that of the Y–CH_3 bond; the former have values of 4.39, 4.34 and 4.43, the latter have values of 4.77, 3.63 and 3.05 eV for Y = F, Cl and Br, respectively [64]. We did not study CH_3I because previous work has shown that the cross sections of any anions are too small to produce measurable quantities of ion pairs in the VUV region [1].

Our work reported the observation of Y^-, H^-, CHY^- and CH_2Y^-, significantly extending the work of Suzuki *et al.* in which only the Y^- anion was reported [10]. Unlike the situation with CF_3X (Section 6.2), the signal of *all* these anions shows a linear dependence with pressure, showing that they all arise from ion-pair formation and not from dissociative electron attachment. Unfortunately, the question posed in the previous paragraph cannot easily be addressed *quantitatively* because it is difficult to determine absolute cross sections for H^- formation from these CH_3Y molecules because this anion is not dominant. The H^- ion yields are therefore perturbed by the zero-blast effect (Section 4.1) [35]. However, the significant experimental observation is that the dominant anion from all three molecules is production of Y^-, and the ion yields for production of F^- from CH_3F, Cl^- from CH_3Cl and Br^- from CH_3Br in the range 10–30 eV are shown in Figures 15a, 16a and 17b, respectively. Absolute cross sections and quantum yields (Table 8) are determined in the normal way. H^- is observed from all three molecules, but for CH_3F and CH_3Cl the spectrum mimics that of F^- and Cl^-, respectively; the normalised H^- signal is *ca.* 10 and 40 times weaker than that of F^- or Cl^- from CH_3F or CH_3Cl, respectively. Only for CH_3Br with photon energies in excess of 12 eV, *ca.* 2.5 eV above threshold for production of Br^-, was the H^- spectrum significantly different from

the Br^- spectrum. It was then possible to perform a subtraction procedure, and extract the true H^- ion yield over the energy range of 12–30 eV (Figure 17a), although it was not possible to trust with confidence the absolute cross section values that were obtained. The important result is that production of the halogen anion dominates that of H^-. Furthermore, this fact seems independent of the molecule and the relative strengths of the C–Y and C–H bonds, and the three-fold statistical weighting favouring production of H^-.

Further information on the energetics and mechanism of Y^- formation from CH_3Y can be obtained from higher-resolution studies of the threshold region. Figure 18 shows the three threshold regions recorded with a resolution of *ca.* 0.02 eV. Onsets for Y^- formation at 298 K are determined to be 12.28 ± 0.02, 10.04 ± 0.02 and 9.46 ± 0.02 eV for Y = F, Cl and Br, respectively. These values lie below the respective ionisation energies to the $\tilde{X}\ ^2E_{3/2}$ state of CH_3Y^+ of 12.53, 11.29 and 10.54 eV [85,86], but exceed the respective thermochemical values for the appearance energy, given by $D^o_{298}(Y–CH_3) + IE(CH_3) – EA(Y)$, of 11.21, 9.85 and 9.52 eV for X = F, Cl and Br. The inequality of eq. (II) is therefore obeyed in all three cases. Unlike the CF_3X series (Section 6.2), energetically it is only possible for Y^- to form with CH_3^+ at threshold, and further fragmentation to $CH_2^+ + H$ is endothermic in all three molecules,

$$\textit{e.g.}\ CH_3F \rightarrow F^- + CH_3^+ \qquad \Delta_rH°_{298} = 11.18\ \text{eV} \qquad (30)$$

$$\text{but}\ \ CH_3F \rightarrow F^- + CH_2^+ + H \qquad \Delta_rH°_{298} = 16.47\ \text{eV} \qquad (31)$$

Perhaps most revealing with respect to the mechanism for ion-pair formation, the F^- ion yield shows no structure whereas discrete transitions can be identified in the Cl^- and Br^- yields. The latter yields are indicative of *indirect* ion-pair formation in which Rydberg states of CH_3Cl and CH_3Br are populated, followed by predissociation into the Cl^- (Br^-) + CH_3^+ ion-pair continuum. There are two strong pieces of evidence to support this. First, the ground-state photoelectron band of both CH_3Cl and CH_3Br has only limited vibrational structure, with the strongest transitions occurring to $v^+ = 0$ [85,86]. Thus Rydberg transitions in CH_3Cl and CH_3Br converging on the $\tilde{X}\ ^2E$ state of the parent ion would not be expected to exhibit extensive vibrational progressions, and the structure in Figures 18b and 18c can only be Rydberg in

nature. Second, there is an *exact* similarity of the CH_3^+ ion yield from photoionisation mass spectrometric studies to these Y^- ion yields [86,87]; this is as expected, since $Y^- + CH_3^+$ is the only ion-pair channel that is energetically open. It is noted, however, that earlier photoabsorption studies by the same group of Locht *et al.* at a resolution of *ca.* 0.01 eV suggest that there is generally good, but not perfect agreement between the absorption spectrum and the Cl^- (Br^-) ion yield spectrum below the ionisation energy of CH_3Cl and CH_3Br [82,83]. This suggests that competing dissociation channels, such as neutral photodissociation, are operative with a finite quantum yield. By contrast, the ground-state photoelectron band of CH_3F has extended vibrational structure [85]. The origin of the F^- signal from CH_3F is more uncertain, as its first maximum just exceeds the adiabatic ionisation energy, and thus cannot correspond to Rydberg states converging on $v^+ = 0$ of CH_3F^+ $\tilde{X}\ ^2E$. Given the large width of the peak and its lack of structure, it is most likely that it corresponds to a *direct* ion-pair transition. Alternatively, Suzuki *et al.* have suggested that this peak consists of unresolved Rydberg states converging to a number of vibrationally-excited levels of CH_3F^+ $\tilde{X}\ ^2E$ [10].

The Y^- signal from CH_3Y also shows discrete structure at higher energies above 15 eV (Figure 19). The broad, vibrationally-unresolved bands are assigned to Rydberg states converging on the $\tilde{C}\ ^2A_1$ state of CH_3Y^+, and partially-resolved vibrational structure is observed in the $(2a_1)^{-1}4s$ Rydberg state of CH_3Cl which mimics structure in the absorption spectrum [88]. The onsets of the Cl^- and Br^- signals around 15 eV suggest that these ions are now forming with a cation that has resulted from fragmentation of CH_3^+,

i.e. $CH_3Cl \rightarrow Cl^- + CH_2^+ + H$ $\quad \Delta_r H°_{298} = 15.14$ eV (32)

$CH_3Br \rightarrow Br^- + CH_2^+ + H$ $\quad \Delta_r H°_{298} = 14.77$ eV (33)

This onset for F^- from CH_3F at 18.5 eV suggests that the equivalent reaction is probably also operative,

$CH_3F \rightarrow F^- + CH_2^+ + H$ $\quad \Delta_r H°_{298} = 16.47$ eV (34)

However, it is energetically possible that the highest-energy band, marked F3, in the three spectra of Figure 19 may correspond to dissociation to $Y^- + CH^+ + 2H$.

In addition to formation of Y^- with CH_3^+, cleavage of the C–Y bond following VUV excitation can also result in the formation of the ion pair $CH_3^- + Y^+$. Yet CH_3^- is not observed from any of the three molecules. Whatever the dynamics of ion-pair formation, these channels are forbidden by energetics, except possibly for the highest-energy bands from CH_3Cl and CH_3Br,

i.e. $CH_3F \rightarrow CH_3^- + F^+$ $\Delta_r H°_{298} = 22.15$ eV (35)

$CH_3Cl \rightarrow CH_3^- + Cl^+$ $\Delta_r H°_{298} = 16.53$ eV (36)

$CH_3Br \rightarrow CH_3^- + Br^+$ $\Delta_r H°_{298} = 14.76$ eV (37)

Cleavage of the C–H bond can likewise result in two ion pairs, $H^- + CH_2Y^-$ and $CH_2Y^- + H^+$. CH_2Y^- *is* observed from all three molecules, and absolute cross sections and quantum yields are shown in Figures 15–17 and in Table 8. Comparison to the yields of H^- is not possible due to the difficulties associated with quantifying the H^- signals due to the zero-blast effect.

6.4 Conclusions from ion-pair formation in non-symmetric molecules

The main conclusion from the work on non-symmetric molecules described in Sections 6.1–6.3 is that halogen atoms preferentially form their atomic anion following VUV excitation into Rydberg states of halogen-containing polyatomic molecules, and this dominates production of H^- or polyatomic fragment anions. Where two halogen anion channels are possible it appears that one anion is nearly always dominant. So, for example, F^-, and not Cl^-, preferentially forms from SF_5Cl and CF_3Cl. It is not clear whether this is due to the smaller mass, the smaller size, or the greater electronegativity of one anion *vs*. another. It does appear, however, that the dynamics of the crossing of the Rydberg state with the ion-pair continuum appears to be the dominant process that determines which anion is formed preferentially. Unfortunately, calculations of potential energy curves in this region of photon excitation, 10–20 eV, are very scarce even for molecules of high symmetry such as SF_6, CF_4 and CH_4. All other factors, such as the thermochemistry of the different

exit channels and the microscopic properties of the different anions (such as size, electron affinity, electronegativity or polarisability of the neutral atom), seem to be second-order effects.

7. Bond dissociation energies from ion-pair induced photochemistry

Using the inequality of eq. (II), the experimental *AE* values for anion formation at 298 K determined in this work on CF_3X and CH_3Y can be used to calculate an upper limit to the bond dissociation energy, D^o_{298}, when the *AE* value correlates to *single*-bond breaking ion-pair formation. When the unimolecular dissociation involves multiple bond-breaking or the formation of a new bond, calculations performed in this way become over-complicated and too many assumptions are made.

We consider the CH_3Y data first, and we remind the reader that we are using the sign convention for an electron affinity as given in Section 1. The *AE* values of Y^- from CH_3Y (Table 8) are used with the *IE* of the CH_3 radical (9.84 ± 0.01 eV [89]) and the *EA* of the respective halogen atom (F (3.40 eV); Cl (3.61 eV); Br (3.36 eV) [90]) for the C–Y bond dissociation energy. For the C–H energy, we use the *IE* of the H atom (13.61 eV [36]) and the *EA* of the respective counter radical (CH_2F (0.25 ± 0.18 eV), CH_2Cl (0.74 ± 0.16 eV) and CH_2Br (0.79 ± 0.14 eV) [91-93]). The resulting upper limits to bond dissociation energies are shown in Table 9, and compared with literature values [64]. Note that an alternative way to present the data for the H–CH_2X bonds is to use literature values for the bond dissociation energies, and calculate a lower limit to the electron affinity of the CH_2X radical. We then obtain $EA(CH_2F) \geq -0.2_0 \pm 0.2$ eV, $EA(CH_2Cl) \geq 0.7_5 \pm 0.2$ eV, and $EA(CH_2Br) \geq 0.9_3 \pm 0.2$ eV, all consistent within error limits of the literature values [91-93]. With the possible exception of the Br–CH_3 data where the values for D^o_{298} are slightly outside error limits, there is excellent consistency between the upper-limit values for $D^o_{298}(Y–CH_3)$ and $D^o_{298}(H–CH_2Y)$ obtained indirectly from this ion-pair work and the accepted literature values. Furthermore, the significant difference between the upper limit for $D^o_{298}(F–CH_3)$ from this work, 5.84 ± 0.02 eV, and the literature value, 4.77 ± 0.09 eV, is in excellent agreement with the large kinetic energy of over 1 eV measured in the CH_3^+ cation by Locht *et al.* for reaction (30) by ion kinetic energy analysis in photoionisation mass spectrometry

[96]. It is also interesting to note that the upper-limit value for both $D^{o}_{298}(Y–CH_3)$ and $D^{o}_{298}(H–CH_2Y)$ tends towards the literature value as the size of Y increases from F to Br. This trend is also observed in the data for the CF_3X series, see below. As the size of Y or X increases, the density of Rydberg states increases, increasing the likelyhood of a Rydberg state crossing with an ion-pair state at as low an energy as thermochemically possible, thereby reducing the inequality presented in equ. (II) ultimately to an equality.

We next consider the CF_3X (X = Cl, Br, I) data. The atomic anion thresholds were not measured with the high resolution which was performed with the CH_3Y series, so the errors in the upper limits to the bond energies, ± 0.2 eV, are correspondingly higher. The *AE* of F^- and Cl^- from CF_3Cl, F^- and Br^- from CF_3Br, and F^- and I^- from CF_3I (Table 6) can be used to determine upper limits to the bond energies at 298 K of $F–CF_2Cl$, $Cl–CF_3$, $F–CF_2Br$, $Br–CF_3$, $F–CF_2I$ and $I–CF_3$, respectively. Note that the Br^- data from CF_3Br may not strictly be valid, since formation of this anion is probably dominated by the dissociative electron attachment mechanism. The calculations of these values follow the same procedure as explained in the previous paragraph for the CH_3Y series. Thus to calculate $D^{o}_{298}(X–CF_3)$, we use the *EA* value of the CF_3 radical, 1.82 ± 0.05 eV [97], and *IE* values for Cl (12.97 eV), Br (11.82 eV) and I (10.45 eV) [36]. In addition $D^{o}_{298}(F–CF_3)$ is calculated from the $AE(F^-/CF_4)$, Section 5, and is also included in Table 9. Now the calculation is slightly different because CF_3^- was not observed from CF_4, but the $AE(F^-/CF_4)$ can be used to yield the same information if $EA(F)$ = 3.40 eV and $IE(CF_3)$ = 9.04 ± 0.04 eV are used instead [98]. Again, the consistency is noted between upper-limit values for $D^{o}_{298}(X–CF_3)$ obtained indirectly from this ion-pair work and the accepted literature values. Furthermore, as described in the preceding paragraph, the upper-limit value for D^{o}_{298} tends towards the accurate value as the size of X increases from F through to I. The data for the bond energy of $F–CF_2X$ is incomplete because the *IE* of the CF_2Br and CF_2I radicals are unknown.

The formation of F^- from CF_3I at onset arises from the dissociation reaction $CF_3I \rightarrow F^- + CF_2I^+$. Although an upper limit to $D^{o}_{298}(F–CF_2I)$ cannot be calculated, as described above, the information is available to calculate an upper limit to $D^{o}_{298}(F–CF_2I^+)$ if equation (XIV) is used,

$$AE_{298}(F^-) \geq IE(CF_3I) + D^o_{298}(F{-}CF_2I^+) - EA(F) \qquad \text{(XIV)}$$

The $AE_{298}(F^-)$ is 9.7 ± 0.2 eV (Table 6) and the $IE(CF_3I)$ is 10.37 eV [78], giving $D^o_{298}(F{-}CF_2I^+) \leq 2.7 \pm 0.2$ eV or 263 ± 19 kJ mol^{-1}. Since $D^o_{298}(F{-}CF_2I^+)$ is simply the enthalpy change for reaction (38),

$$CF_3I^+ \rightarrow CF_2I^+ + F \qquad \Delta_r H°_{298} \leq 263 \pm 19 \text{ kJ mol}^{-1} \qquad \text{(38)}$$

an upper limit to $\Delta_f H°_{298}(CF_2I^+)$ can be determined. Thus using standard values for CF_3I^+ and F, $\Delta_f H°_{298}(CF_2I^+)$ is calculated to be ≤ 598 ± 20 kJ mol^{-1}. A similar calculation for F^- from CF_3Br yields $D^o_{298}(F{-}CF_2Br^+) \leq 6.47 \pm 0.21$ eV and $\Delta_f H°_{298}(CF_2Br^+) \leq 1017 \pm 25$ kJ mol^{-1}. This latter value is consistent with a more accurate way of determining the enthalpy of formation of CF_2Br^+ from cleavage of the weakest bond in CF_2Br_2. Thus using threshold photoelectron photoion coincidence spectroscopy at the relatively modest resolution of *ca.* 0.03 eV, a more accurate upper limit value of 570 ± 9 kJ mol^{-1} at 298 K was obtained [99].

Finally, we note that the top half of Table 9 includes datum for the H–CH_3 bond energy from the $AE_{298}(H^-)$ from CH_4 [19]. The signal at threshold, 13.3 ± 0.1 eV, corresponds to *direct* ion-pair formation. This onset lies well above the first adiabatic *IE* of methane, 12.61 eV [100], but well below the second adiabatic *IE*, 22.39 eV [101]. The H^- peak at 15 eV, with onset at 13.3 eV, cannot therefore coincide with a Rydberg state of CH_4, and its broad shape and slow onset indicate direct ion-pair formation. Under these circumstances, given sufficient sensitivity in the experiment, the H^- signal from CH_4 should turn on at the thermochemical onset. The H–CH_3 bond energy determined from the H^- onset, 4.21 ± 0.11 eV, is, however, slightly less than the well-established literature value of 4.553 ± 0.004 eV [64]. This scientific impossibility could be accounted for by uncertainties in the thermochemistry, but more likely by contributions to the H^- signal from hotbands of CH_4 and/or by the presence of vibrationally-excited molecules possibly caused by electron excitation by photoelectrons. The bottom half of Table 9 completes the data for the other molecules studied in detail by ion-pair spectroscopy: SF_6, CF_4, SF_5CF_3 and SF_5Cl. Whilst there are no real surprises in the data, and one would not use this as the method of choice to determine the bond dissociation energy of a

neutral molecule, it is satisfying that all the data for the experimentally-determined and literature values of D^o_{298}(A–BC) are consistent. It is more likely that this method could be used to determine a lower limit for the *EA* of the radical A, assuming that both the values of D^o_{298}(A–BC) and *IE*(BC) are known.

8. General comments on Ion-pair formation in polyatomic molecules

The systems already described plus CH_2X_2, CF_2Y_2, CCl_2Z_2; CHX_3, CFY_3, $CClZ_3$; C_xH_y and C_mF_n

The results presented in Section 6 represent a minority of the polyatomic molecules in the gas phase that have been studied by VUV anion spectroscopy since 2005 at the Daresbury synchrotron source. In total, 24 molecules have been studied. Data for the 11 molecules reported so far in this Review plus the remaining 13 molecules (C_2H_4, C_2H_6, C_3H_8, C_2F_4, C_2F_6, C_3F_8, CH_2F_2, CHF_3, CH_2Cl_2, $CHCl_3$, CCl_4, CF_2Cl_2, $CFCl_3$) are collected in Table 10, and the spectra of these 13 molecules are shown in Figures 20-32. Full details can be found in the PhD thesis of one of the authors [22]. This forms the most comprehensive collection of information about anion formation, of which ion-pair formation is a particular example, from polyatomic molecules since the Berkowitz review [1]. Some of these molecules (CF_4, SF_6, CH_4, CH_3Y, CF_xCl_y, C_2H_4, C_2H_6 and C_3H_8) have previously been studied by the groups of Mitsuke and Baumgärtel [6-10,74,79]. All our work is in excellent agreement with these studies, but in most cases the enhanced signal-to-noise ratio of the spectra, the larger number of anions observed, and the addition of absolute cross sections and quantum yields represent a significant improvement. These data have not yet all been analysed in full, but certain trends are emerging which are described in this Section.

8.1 Appearance energies of anions and thermochemical thresholds

First, we compare the experimental appearance energy (AE_{298}) for anion formation, usually by ion-pair formation, with the thermochemically-determined threshold ($\Delta_r H^o_{298}$ for the relevant anion-forming dissociation reaction). We remind the reader that for the generic polyatomic molecule ABC,

$$AE_{298}(A^-) \geq D^o_{298}(A–BC) + IE(BC) - EA(A)$$

$$or\ IE(ABC) + D^o_{298}(A–BC^+) - EA(A)$$

$$or\ \Delta_r H^o_{298}(ABC \rightarrow A^- + BC^+) \qquad (XV)$$

The equality of these equations only holds true in the absence of a kinetic shift and/or a barrier in the exit channel. These data are shown in columns 4 and 6 of Table 10, and we reiterate that at our experimental resolution we are working within the approximation that *energy* and *enthalpy* changes are one and the same (Section 3). Thus $AE_{298}(A^-)$ must be greater than or equal to $\Delta_r H^o_{298}$, and this is indeed true for the majority of the results shown in Table 10. For the few instances where this inequality is not obeyed (*e.g.* H^- from CH_4), thermal effects, the presence of vibrationally-excited molecules, and/or uncertainty in the calculated $\Delta_r H°_{298}$ values are expected to be responsible. In most cases, when only one dissociation process is thermodynamically accessible, the reaction occurring at the AE_{298} value can unambiguously be identified to *single* bond-breaking ion-pair dissociation. *Multiple*-bond-breaking ion-pair reactions are assigned more tentatively, assuming the process yielding the least amount of excess energy prevails (*e.g.* $CF_3Cl \rightarrow Cl^- + CF_2^+ + F$ rather than $CF_3Cl \rightarrow Cl^- + CF_3^+$). This assumption is justified by experimental observations: it is common for the appearance of a feature in an ion-pair spectrum to correlate with a possible dissociation threshold.

The difference between AE_{298} and $\Delta_r H°_{298}$ is plotted in Figure 33a for all anions listed in Table 10 that result from *single* bond-breaking ion-pair dissociation. Quite arbitrarily, this energy difference is plotted as a function of the mass of the parent molecule. The random distribution of points in this graph is probably to be expected. However, if the points for H^- and F^- ions are plotted separately (Figures 33b and 33c, respectively), the distributions show an interesting trend; the points for H^- ions are clustered around $(AE_{298} - \Delta_r H°_{298}) = 0$, whilst those for F^- take larger values. This indicates that the dynamics for H^- ion-pair formation tend to allow for this anion to 'turn on' at the thermochemical threshold, favouring dissociation with low excess energy release. It is also interesting that the anion is H^- for four out of the five instances in Figure 33a where $(AE_{298} - \Delta_r H°_{298}) < 0$, the other being for Br^- from CH_3Br with a value of –0.04 eV. By

contrast, F^- ion pairs are formed with larger excess energies in the range 0.7–2.5 eV. These trends become even clearer when the dataset is limited to methane and the halo-substituted methanes (Figures 33d–33g), where the data for Cl^- and CY_3^- (*i.e.* CF_3^-, CH_2F^-, CH_2Cl^- and CH_2Br^-) anions are also isolated and plotted. Low excess energies are always observed for CY_3^- anion formation; all points in Figure 33g have values for ($AE_{298} - \Delta_r H°_{298}$) between 0 and 0.6 eV. In Figures 33e and 33f, for F^- and Cl^- ions from halo-substituted methanes, an apparent positive correlation between ($AE_{298} - \Delta_r H°_{298}$) and the mass of the parent molecule is observed. This is surprising given that the data were plotted against mass for no particular reason, other than to observe the scattering of ($AE_{298} - \Delta_r H°_{298}$) about the *y* axis. Indeed, the same correlation is observed if the *x* axis represents the total number of electrons in the molecule, or the molecular polarisability. There is no obvious explanation for this observation and ideally more data points are required if this trend is to be confirmed.

8.2 Ion-Pair formation below the ionisation energy

From an experimental point of view it is advantageous to detect ion pairs below the ionisation energy of the parent molecule; signal will then be observed against a zero background, and anions or cations can be detected with the confidence that they must originate from ion-pair formation. Energetically, it is possible for ion-pair formation to occur below the *IE*(ABC) if, for the generic reaction $ABC \rightarrow A^- + BC^+$, the electron affinity of A exceeds the bond dissociation energy of $A–BC^+$ (as discussed in Section 1). This condition is most likely satisfied when A is a halogen atom with a corresponding large value for its *EA*. Indeed, *theoretically*, this is true for every halogen-containing molecule in Table 10, with one exception: F^- from C_2F_4. Since the *EA*(F) is 3.40 eV, the *IE*(C_2F_4) is 10.12 eV and the *AE*(F^-) is 13.17 eV (Table 10), we deduce that $3.40 < D^o_{298}(F–C_2F_3^+) < 6.45$ eV. This is consistent with the value of 5.7 ± 0.2 eV from thermochemistry (Table 11, Column 2). The unsaturated, perfluorinated molecule C_2F_4 is a classic example of the 'perfluoro effect' [23]; the C–F bonds in C_2F_4 are strengthened by the combined inductive effect of four fluorine atoms at the expense of a significantly weakened C=C bond. Thus the $F–C_2F_3$ bond

dissociation energy, 5.66 ± 0.13 eV is greater than the H–C_2H_3 energy, 4.81 ± 0.03 eV [64]. Bond dissociation energies for ionised and neutral molecules described in this Review are shown in Table 11. However, the observation of ion-pair formation below the *IE* is not always restricted to instances where A is a halogen atom. Despite the small *EA* of the hydrogen atom, 0.754 eV [90], H^- ions may be observed below the *IE* for three out of the eleven hydrogen-containing molecules listed in Table 10: CH_2F_2, CHF_3 and $CHCl_3$. For these three molecules, $D^o(H–CHF_2^+$ *or* $H–CX_3^+) < 0.754$ eV (see Table 11).

From the data in Table 10, there are only four instances where the maximum value of the cross section, σ_{max}, was observed below the *IE* of the parent molecule: F^- from CF_4, Cl^- from CH_2Cl_2, Br^- from CH_3Br, and F^- from SF_6. In all other cases, σ_{max} was observed at a photon energy above the *IE*. It is also worth noting that, for the majority of the twenty four molecules studied, σ_{max} for producing *atomic* anions occurs between 16 and 22 eV, which is enough energy to access multiple-bond-breaking ion-pair dissociation channels. Exceptions to this are for CF_4, C_2F_6, SF_6, SF_5Cl, CH_3F, CH_3Cl, CH_2Cl_2 and CH_3Br, where the lowest-energy ion-pair dissociation reaction occurs at the cross-section maximum.

8.3 Quantum yields for anion formation

The quantum yield values, Φ, in Column 9 of Table 10 represent the probability for the formation of a given anion *via* an ion-pair reaction following the absorption of a photon by the parent molecule. Its value is calculated by dividing the anion cross section by the total photoabsorption cross section. A quantum yield value is always quoted at a given energy. Each quantum yield listed in the Table represents the maximum value calculated within the energy range studied. The largest value is 2.3×10^{-3} or 0.23 % (for both F^- from CH_3F and Cl^- from CH_3Cl), the smallest is 5.6×10^{-7} or 0.000056 % (for F_2^- from CF_4). The majority of the quantum yields lie between 5×10^{-4} and 1×10^{-6} (*i.e.* 0.05-0.0001 %).

By comparing these data for the twenty four molecules studied, some general statements can be made:

(a) Quantum yields for the production of an *atomic* anion are most often much greater than quantum yields for the production of a *molecular* anion. There are only a very few exceptions to this statement (*e.g.* CF_3^- *vs.* F^- formation from CHF_3).

(b) In molecules containing both hydrogen and halogen atoms, quantum yields for the production of the atomic halogen anion are greater than for production of H^- anions. Note, however, that when the H^- signal was similar to or weaker than that of the halogen anion, it was not possible to determine absolute cross sections and quantum yields for H^- formation due to the zero-blast effect (footnotes *p* and *q* in Table 10).

(c) For the fluoromethane series of molecules, the quantum yield at *E* (σ_{max}) for F^- formation decreases as the number of fluorine atoms increases: Φ (F^- from CH_3F) > Φ (F^- from CH_2F_2) > Φ (F^- from CHF_3) > Φ (F^- from CF_4). The opposite trend is observed for F^- anions produced from the chlorofluoromethanes: Φ (F^- from $CFCl_3$) < Φ (F^- from CF_2Cl_2) < Φ (F^- from CF_3Cl).

(d) For the chloromethane series of molecules, the quantum yield at *E* (σ_{max}) for Cl^- formation also decreases as the number of chlorine atoms increases: Φ (Cl^- from CH_3Cl) > Φ (Cl^- from CH_2Cl_2) > Φ (Cl^- from $CHCl_3$). Again, the opposite trend is observed for Cl^- anions produced from the chlorofluoromethanes: Φ (Cl^- from CF_3Cl) < Φ (Cl^- from CF_2Cl_2). Note that the Cl^- signal observed from $CFCl_3$ and CCl_4 is dominated by dissociative electron attachment, and the contribution to its signal from ion-pair formation is not known.

(e) For the hydrocarbon series of molecules, the quantum yield at *E* (σ_{max}) for H^- formation increases as the number of hydrogen atoms increases: Φ (H^- from CH_4) < Φ (H^- from C_2H_4) < Φ (H^- from C_2H_6) < Φ (H^- from C_3H_8). It is noted that the value for H^- from CH_4, 4.4×10^{-6}, is based on our value of 1.4×10^{-22} cm^2 for the cross section for H^- formation at 20.6 eV [19]. This is a factor of *ca.* 70 smaller than the value of the cross section quoted by Mitsuke *et al.* [7]. It is not clear what normalisation and correction factors have been applied to the signals by Mitsuke *et al.,* and in particular whether any mass discrimination correction for detection of *m/z* 1 anions in their quadrupole spectrometer has been made. Since our values for H^- from C_2H_6 and C_3H_8 are in much

closer agreement, it does not appear that the detection of *m/z* 1 anions is the reason, *per se*, for the anomalously high value of Mitsuke *et al.* for the cross section for H^- production from CH_4.

(f) In comparing fully hydrogenated and full fluorinated molecules (*e.g.* CH_4 *vs.* CF_4, C_3H_8 *vs.* C_3F_8), the maximum cross section for F^- production always exceeds that for H^- production. Thus for the molecules $CH(F)_4$, $C_2H(F)_4$, $C_2H(F)_6$ and $C_3H(F)_8$, in each case, in the range 10–25 eV the maximum value of $\sigma(F^-)$ is a factor of 2–18 times greater than the corresponding value for H^- formation.

These statements may be understood better if one considers the electronegativity of the individual atoms, and therefore the overall polarisation of the electron density across the molecule. Pauling electronegativities for the relevant atoms are: F (3.98), Cl (3.16), Br (2.96), I (2.66), S (2.58), C (2.55) and H (2.20) [116]. For example, the bond polarisation in CH_4 can be represented by $C^{\delta-}$–$H^{\delta+}$, but in CF_4 by $C^{\delta+}$–$F^{\delta-}$. The effects of fluorine substitution on the four hydrogen atoms in methane have been studied by Brundle *et al.* [107], where they calculate that in moving from CH_4 through the three hydrofluoromethanes to CF_4, the carbon atom surrenders over 1.6 electrons to the fluorines, mostly through polarisation of the C–X bonds. Qualitatively, therefore, one can explain point (f) above and appreciate that F^- formation from CF_4 might be more probable than H^- from CH_4. We can also consider the experimental data in point (c) for the fluoromethanes. Although the carbon atom gives up more charge as H atoms are substituted for F atoms in CF_4, the electron density on any *one* given F atom will be reduced when the total number of F atoms within the molecule increases. The same argument can be followed to explain the experimental data in (d) for the chloromethanes. For any chlorofluoromethane, however, the central carbon is always bonded to four highly electronegative species – the difference between electronegativities for F and Cl is relatively small. Now perhaps a statistical factor plays a part, whereby the number of F or Cl atoms determines which anion is formed in preference to the other; indeed the quantum yields at E (σ_{max}) for F^- and Cl^- from CF_2Cl_2 are almost identical (Table 10).

It is incorrect, however, to attempt to understand any of the above statements by considering absolute energetic quantities such as electron affinites or bond dissociation energies; these values simply determine

the asymptotic dissociation energy for the ion-pair state. It is also incorrect to assume that the polarity of the breaking bond is the *sole* factor to determine the relative quantum yields of atomic anions. This effect may contribute slightly but is probably not the dominant factor. All the evidence for the molecules studied in detail (Section 6) is that, assuming indirect formation of ion pairs *via* an excited neutral state, it is the dynamics of the crossing between the Rydberg and ion-pair states which is the most important factor, and indeed the probability for the excited state to decay by a different process. Therefore, the position of the ion-pair state along the reaction coordinate (*i.e.* the value for its equilibrium bond separation, r_e) and its shape are significant.

8.4 Competing ion-pair reactions

It is observed from many of these ion-pair studies that different anions from the same molecule display peaks in their ion yields at the same energy. These peaks most likely identify the same excited intermediate state, and this is further evidence that ion pairs are commonly formed by an indirect mechanism. Specific examples for CH_2F_2 and CF_3Cl are discussed below.

The spectra for anions produced from CH_2F_2 are shown in Figure 26. The first band in the H^- spectrum shows vibrational structure consistent with that observed by photoelectron spectroscopy for the ground state of $CH_2F_2^+$, $^2B_2$ [63,99]. The peaks in this band are assigned using the Rydberg formula to overlapping members of the *5p* and *6p* $^1B_2$ Rydberg series. The band at 12.56 eV most likely corresponds to the maximum of the vibrational distribution of the *5p* Rydberg series. The bands at 12.69, 12.82, 12.94, 13.07 and 13.20 eV correspond to vibrationally-resolved components of the *6p* Rydberg series with a quantum defect of *ca.* 0.55–0.65 [117]. It is clear that two different ion-pair dissociation channels are competing following excitation to the 5*p* Rydberg state, $CH_2F_2^* \rightarrow F^- + CH_2F^+$ and $CH_2F_2^* \rightarrow H^- + CHF_2^+$. However, the F^- channel no longer competes following excitation to higher vibrational members of the *6p* Rydberg state; the first peak in the F^- spectrum spans 11.8 to 13.1 eV only. The *6p* Rydberg state overlaps with the ground state of $CH_2F_2^+$, $^2B_2$; the adiabatic *IE* is 12.726 eV and the vertical *IE* is 13.141 eV [63].

Furthermore at 13.06 eV, $CH_2F_2^+$ becomes unstable with respect to H + CHF_2^+ [63]. This dissociation is therefore complementary to the $CH_2F_2^* \rightarrow H^- + CHF_2^+$ ion-pair dissociation, but *not* to $CH_2F_2^* \rightarrow F^- + CH_2F^+$. This may explain why the F^- dissociation channel diminishes at 13.1 eV, while that for H^- continues. Although an absolute cross section for H^- formation was not determined due to the zero-blast effect, its signal strength at *ca.* 12.6 eV is slightly weaker than but comparable to that of the F^- signal. The F^- cross section at this energy is *ca.* 5×10^{-21} cm^2.

Ion-pair formation from CF_3Cl was discussed in detail in Section 6.2. The F^- and Cl^- spectra (Figures 13 and 14) share some common features, and the two spectra are compared directly in Figure 34. F^- and Cl^- anions were both detected at 17.6 eV, but only the Cl^- ion yield displays a resolved peak at this energy. The range from 16–18 eV is the only region across the two spectra where the Cl^- cross section exceeds that for F^-. The two spectra cross at 18.4 eV and 28.2 eV, and between these energies the F^- cross section is significantly larger than that for Cl^-. The fact that features are observed in both spectra at similar energies suggests these do indeed represent competing decay channels from the same Rydberg states. Vertical ionisation energies for CF_3Cl^+ ^2E, $^2A_1$, ^2E and $^2A_1$ are 17.71, 20.20, 21.20 and 23.80 eV, respectively [77,118]. The features in the Cl^- spectrum at 17.6, 19.7 and 20.9 eV are assigned to high-lying Rydberg states ($n > 5$) converging on the , and ionisation limits, respectively. The shoulder at 22.5 eV is assigned as either the $3p\ ^1A_1$ or $4s\ ^1A_1$ Rydberg state converging on the ionisation limit.

Section 8.3 addressed *general* trends in quantum yield and cross section values, only comparing those in Table 10 quoted at E_{max}. The data for F^- and Cl^- from CF_3Cl, however, is one example showing that cross section and quantum yield values should be compared at the *same* energy; in this particular case, the values for F^- are a factor of *ca.* 6 greater than for Cl^- production at an energy of 21.0 eV. This point is perhaps obvious, but it serves to highlight the challenges in understanding why one particular anion has a higher probability for formation than another.

8.5 Anions formed by dissociative electron attachment

For a molecule under study by negative photoion spectroscopy, below the *IE* any anion produced can only result from an ion-pair reaction. Above the *IE*, however, photoelectrons are simultaneously produced, and negative ions can also result from an electron attachment process. Examples where this has been observed include: SF_5^- and SF_6^- from SF_6, SF_5^- from SF_5CF_3 (Sections 5.1 and 5.3); Br^- from CF_3Br and I^- from CF_3I (Section 6.2); SF_5^- from SF_5Cl (Section 6.1); Cl^- from $CFCl_3$ and Cl^- from CCl_4 (Table 10, Figures 30 and 32). The electron attachment process for the generic polyatomic molecule ABC can be described by:

$$ABC + h\nu \rightarrow ABC^+ + e^- \qquad (39)$$

$$ABC + e^- \rightarrow ABC^- \ \textit{or}\ A^- + BC \ \textit{or}\ A^- + B + C \qquad (40)$$

Four points are made when identifying such electron attachment processes:

(1) A plot of the anion signal as a function of gas pressure will be linear for ion-pair formation, but non-linear (with the rate of change in signal increasing with increasing pressure) if electron attachment is dominant. Figure 5 shows examples for F^- and SF_5^- from SF_6. Following reactions (39) and (40), a quadratic dependence of the signal of A^- with pressure of ABC is to be expected.

(2) ABC must have an electron attachment rate coefficient, k_a, of sufficient magnitude for this process to be observed at a rate comparable with ion-pair formation. Not surprisingly, the molecules listed above all have have very fast thermal k_a values, lying between 1×10^{-8} and 4×10^{-7} cm^3 molecule^{-1} s^{-1} (footnote *u* in Table 10). Molecules with slightly lower k_a values were also studied (*e.g.* $CHCl_3$ and CF_2Cl_2 ($k_a = 4.7 \times 10^{-9}$ and 1.9×10^{-9} cm^3 molecule^{-1} s^{-1}, respectively) [119]), but the anion signals were all attributed to ion-pair formation since they showed a linear dependence with pressure. It appears that there is a threshold rate coefficient of *ca.* 5×10^{-9} cm^3 molecule^{-1} s^{-1}, below which the value is too slow for anions to form effectively by dissociative electron attachment.

(3) There is usually only one anion produced by electron attachment from any given molecule which is detected by negative photoion spectroscopy (the exception being SF_6^- *and* SF_5^- being formed from SF_6). This anion always matches the dominant species identified from independent thermal electron attachment experiments in which the mass of the product anion is detected.

(4) The spectrum of an anion produced by electron attachment matches, to varying extent depending on the molecule and signal strength, the threshold photoelectron spectrum (TPES) for that molecule. In most cases peak positions are the same, but relative intensities of peaks can vary significantly.

The most interesting point is probably the final one. The similarities/differences between an anion spectrum produced predominantly by electron attachment and the molecular threshold photoelectron spectrum have already been mentioned for the molecules SF_6, SF_5CF_3, CF_3Br, CF_3I and SF_5Cl in Sections 5 and 6, and in detail in the original papers [17,18,21]. Taking SF_6 as the example where there is the closest similarity between the SF_6^- yield and the TPES of SF_6 (Figure 4), the only significant difference between the two spectra is the peak at 19.9 eV which appears *ca.* two times more intense in the SF_6^- spectrum. The same point about the intensity of this peak has been discussed by Yencha *et al* [40]. who compared their TPES of SF_6 with the ion yield of SF_6^- from SF_6 reported by Mitsuke *et al* [9]. The k_a value for this molecule is high, 2.4×10^{-7} cm^3 molecule^{-1} s^{-1}. The angular momentum of the attaching electron is composed of linear combinations of components with quantum numbers l=0 (*s* wave), l=1 (*p* wave), l=2 (*d* wave) *etc.* The cross section for non-dissociative electron attachment to SF_6 peaks at very low energy which is a characteristic of *s*-wave capture [47], but SF_6^- anions observed from reaction (8) will arise from *all* electrons integrated under the cross section *vs.* electron energy distribution. By contrast, the TPES arises only from low-energy electrons detected within the bandpass of the threshold analyser, *ca.* 4 meV in the experiment of Yencha *et al* [40]. In practice, the experimentally-observed resolution will depend upon a convolution of the electron energy distribution and the resolution of the photon source. In both experiments the monochromator resolution, *ca.* 0.4 nm or 130 meV at 19.9 eV, will probably dominate. Notwithstanding this point, there is no reason why the intensities of the TPES and SF_6^- spectra in Figure 4 should be *exactly* the same, and this may explain the small differences that have been observed both by us and by Yencha *et al.* We also note

that this difference is not be a particular property of SF_6, because a greater inconsistency in intensities in the threshold photoelectron and parent anion yields has been observed with another polyatomic molecule which attaches electron very rapidly, *cyclic*-C_5F_8 [120], with a k_a value, 3.6×10^{-7} cm^3 molecule^{-1} s^{-1}, similar to that of SF_6 [121]. We should note also that the yield of SF_5^- also show many similarities to the TPES of SF_6. The enthalpy change for the reaction $SF_6 + h\nu \rightarrow SF_5^- + F^+$ is 17.6 eV. Below this energy, therefore, SF_5^- can only form by dissociative electron attachment. Above this energy, there exists the possibility that a small amount of SF_5^- is produced *via* this ion-pair reaction.

Comparing all the molecules in which an anion is produced predominantly by electron attachment, there is unfortunately no general trend whether the 'agreement', however that is quantified, between the two spectra correlates with any physical property, such as the k_a value. As highlighted above for SF_6 and *c*-C_5F_8, the reasons for any differences cannot easily be explained. New data for Cl^- from $CFCl_3$ and CCl_4 are shown in Figures 32 and 30, respectively, and Table 10. Both spectra show a remarkable tendancy for the relative anion signal to increase with increasing photon energy, especially above *ca.* 22 eV; this is seen most clearly in comparing the Cl^- ion yield from CCl_4 with the TPES of this molecule (Figure 30). It is even possible that some of the features observed above 22 eV identify inner-valence-shell ionisation energies which are very weak or absent in the TPES. Furthermore, Cl^- signal *vs.* pressure plots recorded at these peak energies continue to maintain a non-linear dependence with pressure, as discussed in point (1) above. For the Cl^- from CCl_4 example, a close examination of the TPES does indeed reveal weak and partially resolved features between 24 and 30 eV.

9. Conclusions

The formation of ion pairs from polyatomic molecules is a weak process; quantum yields are typically less than *ca.* 10^{-3} or 0.1 %. The detection of ion-pair formation therefore requires a sensitive experimental apparatus, and most spectra could only be recorded at a relatively modest resolution of *ca.* 0.1–0.6 nm. Ion-pair formation is most commonly formed by an indirect mechanism *via* an initially excited Rydberg state of

the parent molecule. Many peaks in ion-pair spectra occur between adiabatic and vertical ionisation energy values of either the ground or an excited electronic state of the parent cation. Indeed, many of the strongest anion signals result following predissociation of high-lying Rydberg states ($n > 5$). It can be difficult to resolve these overlapping excited states, let alone assign them, especially when the resolution of the experiment is limited.

One of the most interesting questions raised is: why is one anion produced preferentially to another? This question can be asked when comparing the same anion from different molecules (*e.g.* Cl^- from CF_3Cl and CF_2Cl_2), different anions from different molecules (*e.g.* H^- from CH_4 and F^- from CF_4), and different anions from the same molecule (*e.g.* F^- and Cl^- from CF_3Cl). Some trends are apparent when comparing a series of similar molecules (*e.g.* the methyl halides, the fluoromethanes or the chloromethanes (Section 8.3)), but there is no common explaination. Another unanswered question is: why are some anions not observed at all? Examples include the absence of Cl^- anions from CF_3Cl below 16 eV *via* the reaction $CF_3Cl \rightarrow Cl^- + CF_3^+$ (Section 6.2), and the complete absence of Cl^- anions from SF_5Cl above 12 eV (Section 6.1).

Thermochemistry is a useful tool to identify the cation and neutral dissociation fragments accompanying the detected anion. However, conclusive assignments can only realistically be made at the onset for ion-pair formation when one unique dissociation reaction is energetically allowed. The ideal experiment would detect anion and cation fragments above the ionisation energy in coincidence, and perhaps this is where the future of ion-pair spectroscopy lies. Such coincidence experiments would identify both the anion *and* cation fragments [122], allowing for a more detailed analysis of ion-pair dissociation dynamics. Finally, it is noted that there is very little information known about ion-pair potential energy surfaces in polyatomic molecules, and the dynamics of dissociation from these surfaces. For example, one might be able to use equation (IV) to model the potential energy function of an ion-pair state if constants A and α can be derived from experimental results. It is to be hoped that the vast amount of experimental data presented in this Review will stimulate interest in theoreticians to tackle such problems.

Acknowledgements : We thank Professor Colin Latimer and Dr Ken Dunn (Queens University Belfast) for the use of their apparatus to record all the spectra reported in this Review, and for an incredibly enjoyable collaboration over the last five years. Without them, this work would never have happened. We also thank the Staff at the Daresbury Laboratory, especially Dr David Shaw, for help and guidance with the experiments, Ms Nicola Rogers for help with the analysis of the CH_3Y (Y = H,F,Cl,Br) spectra, Mr Andrew Rodgers for help with analysis of the CH_2F_2 and CH_2Cl_2 spectra, and Dr Michael Parkes (University College London) for many useful discussions. Finally, we thank the referee for helpful and constructive comments which we hope have improved the presentation and understanding of this Review. Beamtime from the CCLRC / STFC Research Council is acknowledged, and the initial collaboration between the Birmingham and Belfast groups came about, in part, through an EPSRC Network Grant on VUV Photophysics and Photochemistry, GR/N26234/01.

Note added in proof : The yield of Cl^- from $CHCl_3$ between 10 and 20 eV has very recently been published on the web (Chen *et al.,* J. Phys. Chem. A., DOI: 10.1021/jp2000927). No other anions are reported. The Cl^- spectrum shows its maximum signal at ca. 12 eV. The spectrum appears to show little relation to that observed by us (Fig. 29 of this review).

References

[1] J. Berkowitz, in *VUV and Soft X-ray Photoionisation*, edited by U. Becker and D.A. Shirley (Plenum, New York, 1996) p.263. ISBN: 0306450380.

[2] A. Terenin and B. Popov, Phys. Z. Sowjetunion, **2**, 299 (1932).

[3] K. P. Lawley and R. J. Donovan, J. Chem. Soc. Farad. Trans., **89**, 1885 (1993).

[4] V. H. Dibeler and J. A. Walker, J. Chem. Phys., **43**, 1842 (1965).

[5] M. Krauss, J. A. Walker and V. H. Dibeler, J. Res. Nat. Bur. Stand., **72A**, 281 (1968).

[6] K. Mitsuke, S. Suzuki, T. Imamura and I. Koyano, J. Chem. Phys., **94**, 6003 (1991).

[7] K. Mitsuke, H. Hattori and H. Yoshida, J. Chem. Phys., **99**, 6642 (1993).

[8] K. Mitsuke, S. Suzuki, T. Imamura and I. Koyano, J. Chem. Phys., **95**, 2398 (1991).

[9] K. Mitsuke, S. Suzuki, T. Imamura and I. Koyano, J. Chem. Phys., **93**, 8717 (1990).

[10] S. Suzuki, K. Mitsuke, T. Imamura and I. Koyano, J. Chem. Phys., **96**, 7500 (1992).

[11] S. X. Tian, Y. F. Lu, Y. F. Wang, Q. Feng, L. L. Chen, J. D. Sun, F. Y. Liu, X. B. Shan and L. S. Sheng, Chem. Phys. Letts., **496**, 254 (2010).

[12] K. Suto, Y. Sato, C. L. Reed, V. Skorokhodov, Y. Matsumi and M. Kawasaki, J. Phys. Chem. A., **101**, 1222 (1997).

[13] D. D. Xu, J. Huang, R. J. Price and W. M. Jackson, J. Phys. Chem. A., **108**, 9916 (2004).

[14] J. D. D. Martin and J. W. Hepburn, Phys. Rev. Letts., **79**, 3154 (1997).

[15] R. C. Shiell, X. K. Hu, Q. J. Hu and J. W. Hepburn, J. Phys. Chem. A., **104**, 4339 (2000).

[16] A. G. Suits and J. W. Hepburn, Ann. Rev. Phys. Chem., **57**, 431 (2006).

[17] M. J. Simpson, R. P. Tuckett, K. F. Dunn, C. A. Hunniford, C. J. Latimer and S. W. J. Scully, J. Chem. Phys., **128**, 124315 (2008).

[18] M. J. Simpson, R. P. Tuckett, K. F. Dunn, C. A. Hunniford and C. J. Latimer, J. Chem. Phys., **130**, 194302 (2009).

[19] N. J. Rogers, M. J. Simpson, R. P. Tuckett, K. F. Dunn and C. J. Latimer, Mol. Phys., **108**, 895 (2010).

[20] N. J. Rogers, M. J. Simpson, R. P. Tuckett, K. F. Dunn and C. J. Latimer, Phys. Chem. Chem. Phys., **12**, 10971 (2010).

[21] M. J. Simpson and R. P. Tuckett, J. Phys. Chem. A., **114**, 8043 (2010).

[22] M. J. Simpson, *Ph.D. Thesis, University of Birmingham* (2010) http://etheses.bham.ac.uk/1056/

[23] C. R. Brundle, H. Basch, M. B. Robin and N. A. Keubler, J. Amer. Chem. Soc., **94**, 1451 (1972).

[24] J. Berkowitz, *Photoabsorption, Photoionisation and Photoelectron Spectroscopy* (Academic Press London, 1979). ISBN: 0120916509

[25] C. Sandorfy, *The Role of Rydberg States in Spectroscopy and Photochemistry*, edited by C. Sandorfy (Kluwer Academic Publishers, London, 1999) p.1. ISBN: 0792355334

[26] C. E. Theodosiou, M. Inokuti and S. Manson, Atomic Data and Nuclear Data Tables, **35**, 473 (1986).

[27] M. W. Chase, J. Phys. Chem. Ref. Data Monograph, **17**, 1 (1998). ISBN: 1563968312.

[28] S. G. Lias, J. E. Bartmess, J. F. Liebman, J. L. Holmes, R. D. Levin and W. G. Mallard, J. Phys. Chem. Ref. Data, **17**, 1 (1988). ISBN: 0883185628.

[29] D. A. Shaw, D. M. P. Holland and I. C. Walker, J. Phys. B: At. Mol. Opt. Phys., **39**, 3549 (2006).

[30] J. C. Traeger and R. G. McLoughlin, J. Amer. Chem. Soc., **103**, 3647 (1981).

[31] C. R. Howle, S. Ali, R. P. Tuckett, D. A. Shaw and J. B. West, Nucl. Inst. Methods Phys. Res. Sect. B, **237**, 656 (2005)

[32] C. A. Hunniford, S. W. J. Scully, K. F. Dunn and C. J. Latimer, J. Phys. B.; At. Mol. Opt. Phys., **40**, 1225 (2007).

[33] K. F. Dunn, *private communication* (2010).

[34] S. W. J. Scully, *Ph.D. Thesis, Queens University Belfast* (2004).

[35] P. H. Dawson, *Quadrupole Mass Spectrometry and its Applications*, American Vacuum Society Classics, American Institute of Physics, New York (1995). ISBN: 1563964554.

[36] NIST Chemistry webbook, http://webbook.nist.gov/chemistry/

[37] P. M. Dehmer and W. A. Chupka, J. Chem. Phys., **62**, 4525 (1975).

[38] N. J. Mason, A. Dawes, R. Mukerji, E. A. Drage, E. Vasekova, S. M. Webb and P. Limao-Vieira, J. Phys. B.: At. Mol. Opt. Phys., **38**, 5893 (2005).

[39] D. M. P. Holland, D. A. Shaw, I. C. Walker, I. J. McEwen, E. Apra and M. F. Guest, J. Phys. B.: At. Mol. Opt. Phys., **38**, 2047 (2005).

[40] A. J. Yencha, D. B. Thompson, A. J. Cormack, D. R. Cooper, M. Zubek, P. Bolognesi and G. C. King, Chem. Phys., **216**, 227 (1997).

[41] J. C. Creasey, H. M. Jones, D. M. Smith, R. P. Tuckett, P. A. Hatherly, K. Codling and I. Powis, Chem. Phys., **174**, 441 (1993).

[42] R. Y. L. Chim, R. A. Kennedy, R. P. Tuckett, W. Zhou, G. K. Jarvis, D. J. Collins and P. A. Hatherly, J. Phys. Chem. A., **105**, 8403 (2001).

[43] D. M. P. Holland, D. A. Shaw, A. Hopkirk, M. A. MacDonald and S. M. McSweeney, J. Phys. B.: At. Mol. Opt. Phys., **25**, 4823 (1992).

[44] R. Y. L. Chim, R. A. Kennedy and R. P. Tuckett, Chem. Phys. Lett., **367**, 697 (2003).

[45] S. W. J. Scully, R. A. Mackie, R. Browning, K. F. Dunn and C. J. Latimer, J. Phys. B.: At. Mol. Opt. Phys., **35**, 2703 (2002).

[46] C. A. Mayhew, A. D. J. Critchley, D. C. Howse, V. Mikhailov and M. A. Parkes, Eur. Phys. J. D., **35**, 307 (2005).

[47] L. G. Christophorou and J. K. Olthoff, J. Phys. Chem. Ref. Data, **29**, 267 (2000).

[48] A. J. Yencha, A. Hopkirk, A. Hiraya, G. Dujardin, A. Kvaran, L. Hellner, M. J. Besnard-Ramage, R. J. Donovan, J. G. Goode, R. R. J. Maier, G. C. King and S. Spyrou, J. Elec. Spec. Rel. Phen., **70**, 29 (1994).

[49] G. A. Garcia, H. Soldi-Lose and L. Nahon, Rev. Sci. Instr., **80**, 023102 (2009).

[50] L. C. Lee, E. Phillips and D. L. Judge, J. Chem. Phys., **67**, 1237 (1977).

[51] J. F. M. Aarts, S. M. Mason and R. P. Tuckett, Mol. Phys., **60**, 761 (1987).

[52] D. M. P. Holland, A. W. Potts, A. B. Trofimov, J. Breidbach, J. Schirmer, R. Feifel, T. Richter, K. Godehusen, M. Martins, A. Tutay, M. Yalcinkaya, M. Al-Hada, S. Eriksson and L. Karlsson, Chem. Phys., **308**, 43 (2005).

[53] W. T. Sturges, T. J. Wallington, M. D. Hurley, K. P. Shine, K. Sihra, A. Engel, D. E. Oram, S. A. Penkett, R. Mulvaney and C. A. M. Brenninkmeijer, Science, **289**, 611 (2000).

[54] P. A. Kendall, N. J. Mason, G. A. Buchanan, G. Marston, P. Tegeder, A. Dawes, S. Eden, P. Limao-Viera and D. A. Newnham, Chem. Phys., **287**, 137 (2003).

[55] P. A. Kendall and N. J. Mason, J. Elec. Spec. Rel. Phen., **120**, 27 (2001).

[56] R. P. Tuckett, Adv. Fluorine Sci., (Elsevier) **1**, 89 (2006). ISBN: 9780444528117.

[57] W. Xu, C. Xiao, Q. Li, Y. Xie and H. F. Schaefer, Mol. Phys., **102**, 1415 (2004).

[58] C. Atterbury, A. D. J. Critchley, R. A. Kennedy, C. A. Mayhew and R. P. Tuckett, Phys. Chem. Chem. Phys., **4**, 2206 (2002).

[59] S. T. Arnold, T. M. Miller, A. A. Viggiano and C. A. Mayhew, Int. J. Mass Spectrom., **223**, 403 (2003).

[60] R. A. Kennedy and C. A. Mayhew, Int. J. Mass Spectrom., **206**, AR1 (2001).

[61] J. A. Ruiz, A. Kivimaki, M. Stankiewicz, E. M. Garcia, M. Coreno, S. Ali, J. Koperski, E. Rachlew, G. Serrano, V. Feyer and R. P. Tuckett, Phys. Chem. Chem. Phys., **8**, 5199 (2006).

[62] P. Limao-Viera, S. Eden, P. A. Kendall, N. J. Mason, A. Giuliani, J. Heinesch, M. J. Hubin-Franskin, J. Delwiche and S. V. Hoffmann, Int. J. Mass Spectrom., **233**, 335 (2004).

[63] J. N. Harvey, N. J. Rogers, R. P. Tuckett, A. Bodi and T. Gerber, *unpublished data from Swiss Light Source.*

[64] D. R. Lide, *Handbook of Chemistry and Physics*, 88th edition (CRC Press, Boca Raton, 2008) Section 9, 61. ISBN: 9780849304880.

[65] J. Bellet, R. Jurek and J. Chanussot, J. Mol. Spectrosc., **78**, 16 (1979).

[66] C. J. Marsden and L. S. Bartell, Inorg. Chem., **15**, 3004 (1976).

[67] A. P. Klyagina, A. A. Levin and G. L. Gutzev, Chem. Phys. Lett., **77**, 365 (1981).

[68] R. L. DeKock, B. R. Higginson and D. R. Lloyd, J. Chem. Soc. Farad. Disc., **54**, 84 (1972).

[69] R. Y. L. Chim, P. Cicman, T. D. Mark, C. A. Mayhew, P. Scheier and R. P. Tuckett, Int. J. Mass Spectrom., **261**, 208 (2007).

[70] M. A. Parkes, *private communication* (2007).

[71] J. M. van Doren, T. M. Miller, A. A. Viggiano, P. Spanel, D. Smith, J. C. Bopp and J. Troe, J. Chem. Phys., **128**, 094309 (2008).

[72] M. Braun, M. W. Ruf, H. Hotop, P. Cicman, P. Scheier, T. D. Mark, E. Illenberger, R. P. Tuckett and C. A. Mayhew, Int. J. Mass Spectrom., **252**, 234 (2006).

[73] M. Fenzlaff, R. Gerhard and E. Illenberger, J. Chem. Phys., **88**, 149 (1988).

[74] H. W. Jochims, W. Lohr and H. Baumgartel, Ber. Buns. Phys. Chem., **80**, 130 (1976).

[75] S. Ali, *Ph.D. Thesis, University of Birmingham* (2007) http://etheses.bham.ac.uk/897/

[76] S. Eden, P. Limao-Vieira, S. V. Hoffmann and N. J. Mason, Chem. Phys., **323**, 313 (2006).

[77] J. C. Creasey, D. M. Smith, R. P. Tuckett, K. R. Yoxall, K. Codling and P. A. Hatherly, J. Phys. Chem., **100**, 4350 (1996).

[78] N. A. Macleod, S. Wang, J. Hennessy, T. Ridley, K. P. Lawley and R. J. Donovan, J. Chem. Soc. Farad. Trans., **94**, 2689 (1998).

[79] H. Schenk, H. Oertel and H. Baumgartel, Ber. Buns. Phys. Chem., **83**, 683 (1979).

[80] I. Powis, O. Dutuit, M. Richard-Viard and P. M. Guyon, J. Chem. Phys., **92**, 1643 (1990).

[81] R. Locht, B. Leyh, A. Hoxha, D. Dehareng, H. W. Jochims and H. Baumgartel, Chem. Phys., **257**, 283 (2000).

[82] R. Locht, B. Leyh, A. Hoxha, D. Dehareng, K. Hottmann, H. W. Jochims and H. Baumgartel, Chem. Phys., **272**, 259 (2001).

[83] R. Locht, B. Leyh, H. W. Jochims and H. Baumgartel, Chem. Phys., **317**, 73 (2005).

[84] J. W. Au, G. Cooper, G. R. Burton, T. N. Olney and C. E. Brion, Chem. Phys., **173**, 209 (1993).

[85] L. Karlsson, R. Jadrny, L. Mattsson, F. T. Chau and K. Siegbahn, Phys. Scripta, **16**, 225 (1977).

[86] R. Locht, B. Leyh, D. Dehareng, K. Hottmann, H. W. Jochims and H. Baumgartel, Chem. Phys., **323**, 458 (2006).

[87] R. Locht, B. Leyh, A. Hoxha, D. Dehareng, K. Hottmann, H. W. Jochims and H. Baumgartel, Chem. Phys., **272**, 293 (2001).

[88] C. Y. R. Wu, L. C. Lee and D. L. Judge, J. Chem. Phys., **71**, 5221 (1979).

[89] A. M. Schulenburg, C. Alcaraz, G. Grassi and F. Merkt, J. Chem. Phys., **125**, 104310 (2006).

[90] J. C. Rienstra-Kiracofe, G. S. Tschumper, H. F. Schaeffer, S. Nandi and G. B. Ellison, Chem. Rev., **102**, 231 (2002).

[91] S. T. Graul and R. R. Squires, J. Amer. Chem. Soc., **112**, 2517 (1990).

[92] S. Ingemann and N. M. M. Nibbering, J. Chem. Soc. Perkin Trans. 2, 837 (1985).

[93] P. M. Hierl, M. J. Henchman and J. F. Paulson, Int. J. Mass Spectrom. Ion Proc., **117**, 475 (1992).

[94] M. Bilde, J. Sehested, T. E. Mogelberg, T. J. Wallington and O. J. Nielsen, J. Phys. Chem., **100**, 7050 (1996).

[95] M. K. Gilles, A. A. Turnipseed, R. K. Talukdar, Y. Rudich, P. W. Villalta, L. G. Huey, J. B. Burkholder and A. R. Ravishankara, J. Phys. Chem., **100**, 14005 (1996).

[96] R. Locht, J. Momigny, E. Ruhl and H. Baumgartel, Chem. Phys., **117**, 305 (1987).

[97] H. J. Deyerl, L. S. Alconcel and R. E. Continetti, J. Phys. Chem. A., **105**, 552 (2001).

[98] G. A. Garcia, P. M. Guyon and I. Powis, J. Phys. Chem. A., **105**, 8296 (2001).

[99] D. P. Seccombe, R. P. Tuckett and B. O. Fisher, J. Chem. Phys., **114**, 4074 (2001).

[100] J. W. Rabalais, T. Bergman, L. O. Werme, L. Karlsson and K. Siegbahn, Phys. Scripta, **3**, 13 (1971).

[101] M Carlsson Gothe, B. Wannberg, L. Karlsson, S. Svensson, P. Baltzer, F. T. Chau and M. Y. Adam, J. Chem. Phys., **94**, 2536 (1991).

[102] B. A. Williams and T. A. Cool, J. Chem. Phys., **94**, 6358 (1991).

[103] A. J. C. Nicholson, J. Chem. Phys., **43**, 1171 (1965).

[104] G. Bieri and L. Asbrink, J. Elec. Spec. Rel. Phen., **20**, 149 (1980).

[105] S. Eden, P. Limao-Vieira, P. A. Kendall, N. J. Mason, J. Deleiche, M. J. Hubin-Franskin, T. Tanaka, M. Kitajima, H. Tanaka, H. Cho and S. V. Hoffmann, Chem. Phys., **297**, 257 (2004).

[106] G. K. Jarvis, K. J. Boyle, C. A. Mayhew and R. P. Tuckett, J. Phys. Chem. A., **102**, 3219 (1998).

[107] C. R. Brundle, M. B. Robin and H. Basch, J. Chem. Phys., **53**, 2196 (1970).

[108] A. F. Lago, J. P. Kercher, A. Bodi, B. Sztaray, B. Miller, D. Wurzelmann and T. Baer, J. Phys. Chem. A., **109**, 1802 (2005).

[109] D. P. Seccombe, R. Y. L. Chim, G. K. Jarvis and R. P. Tuckett, Phys. Chem. Chem. Phys., **2**, 769 (2000).

[110] T. Pradeep and D. A. Shirley, J. Elec. Spec. Rel. Phen., **66**, 125 (1993).

[111] J. Berkowitz, *Atomic and Molecular Photoabsorption: Absolute Total Cross Sections* (Academic Press, London, 2002). ISBN: 9780120918416

[112] K. Kameta, S. Machida, M. Kitajima, M. Ukai, N. Kouchi, Y. Hatano and K. Ito, J. Elec. Spec. Rel. Phen., **79**, 391 (1996).

[113] D. P. Seccombe, R. Y. L. Chim, R. P. Tuckett, H. W. Jochims and H. Baumgartel, J. Chem. Phys., **114**, 4058 (2001).

[114] R. Y. L. Chim, *Ph.D. Thesis, University of Birmingham* (2003) http://etheses.bham.ac.uk/1526/

[115] D. P. Seccombe, *unpublished data.*

[116] D. F. Shriver and P. W. Atkins, *Inorganic Chemistry, 4th ed.*, (Oxford University Press, 2006). ISBN: 9780199264636.

[117] A. N. Rodgers, M. J. Simpson and R. P. Tuckett, *unpublished data*.

[118] T. Cvitas, H. Gusten and L. Klasinc, J. Chem. Phys., **67**, 2687 (1977).

[119] S. J. Burns, J. M. Matthews and D. L. McFadden, J. Phys. Chem., **100**, 19436 (1996).

[120] M. A. Parkes, *Ph.D. Thesis, University of Birmingham* (2008) http://etheses.bham.ac.uk/74/

[121] R. Y. Pai, L. G. Christophorou and A. A. Christodoulides, J. Chem. Phys., **70**, 1169 (1979).

[122] H. Yoshida and K. Mitsuke, J. Elec. Spec. Rel. Phen., **79**, 487 (1996).

Table 1 : Sensitivity factors, *S*, for detection of the sample gases by the ion gauge detector used in the experiments relative to N_2 gas ($S = 1$). The true gas pressure is given by the (Ion Gauge Reading) / *S*.

N_2	1.0	O_2	0.9_5						
CF_4	1.7	SF_6	2.7	SF_5CF_3	3.2	CH_4	1.5	CCl_4	5.4
CF_4	1.7	CF_3Cl	2.6	CF_2Cl_2	3.5	$CFCl_3$	4.1	CCl_4	5.4
CH_4	1.5	CH_3F	*1.55* #	CH_2F_2	*1.6* #	CHF_3	*1.65* #	CF_4	1.7
CH_4	1.5	CH_3Cl	3.0	CH_2Cl_2	3.7	$CHCl_3$	4.8	CCl_4	5.4
CH_4	1.5	CH_3F	*1.6* #	CH_3Cl	3.0	CH_3Br	3.7	CH_3I	4.2
CF_4	1.7	CF_3H	*1.65* #	CF_3Cl	2.6	CF_3Br	*3.9* #	CF_3I	*4.4* #
CH_4	1.5	C_2H_4	2.3	C_2H_6	2.6	C_3H_8	3.7		
CF_4	1.7	C_2F_4	*2.5* #	C_2F_6	*2.9* #	C_3F_8	*4.1* #		
SF_6	2.7	SF_5Cl	*3.6* #	SF_5CF_3	3.2				

Group additivity effects [33,34] are used to estimate these values, given in italics, where the data have not been measured.

Table 2 : Appearance energies, cross sections, and quantum yields for anions observed from photoexcitation of SF_6, CF_4, and SF_5CF_3.

Molecule [*AIE* [a] / eV]	Anion	*AE* [b] / eV	Cross section [c] / cm^2	Energy [d] / eV	Quantum Yield [e]
SF_6 [15.1]	F^-	12.7	7.1×10^{-21}	14.2	2.4×10^{-4}
	F_2^-	16.3	1.4×10^{-22}	18.3	1.9×10^{-6}
	SF_5^-	15.1	– [f]	17.5	– [g]
	SF_6^-	15.1	– [f]	17.1	– [g]
CF_4 [15.4]	F^-	13.0	1.4×10^{-21}	14.0	2.8×10^{-5}
	F_2^-	20.1	4.0×10^{-23}	21.6	5.6×10^{-7}
SF_5CF_3 [12.9]	F^-	11.05	3.4×10^{-20}	16.9	3.4×10^{-4}
	F_2^-	16.1	1.2×10^{-21}	17.9	1.1×10^{-5}
	SF^-	24.0	2.8×10^{-22}	28.8	2.4×10^{-6}
	SF_2^-	20.2	3.9×10^{-22}	24.2	2.5×10^{-6}
	SF_3^-	15.4	1.0×10^{-20}	17.6	1.0×10^{-4}
	SF_4^-	13.0	1.3×10^{-20}	14.1	1.7×10^{-4}
	SF_5^-	12.9	– [f]	17.0	– [g]

[a] Adiabatic ionisation energy. Values are taken from the observed onset of ionisation for SF_6 [40], CF_4 [41], and SF_5CF_3 [42].

[b] Appearance energy (*AE*) from this work. The error is estimated to be ± 0.2 eV (except for F^- from SF_5CF_3 for which the error is ± 0.05 eV), based on the resolution and step size used to record ion yields.

[c] Cross section for anion production following photoexcitation of the parent molecule.

[d] Energy of strongest peak. It is at this energy, where appropriate, where cross section and quantum yield measurements are taken.

[e] Quantum yields for anion production, obtained by dividing the anion cross section (column 4) by the total photoabsorption cross section. The latter values are given for SF_6, CF_4 and SF_5CF_3 in refs [43,44,39].

[f] Normalisation of the signal strength to determine an absolute cross section is not possible because of the non-linear dependence of signal with pressure.

[g] Quantum yield cannot be determined because the cross section is not defined.

Table 3 : Peak positions and energy spacings, in eV, for the vibrational states observed in the F^- ion yield from CF_4 in the photon energy range 20.9 to 22.1 eV. Spectrum recorded with a stepsize of 0.01 eV and a resolution of *ca.* 0.1 eV.

$3t_2 \rightarrow 4p\ ^1T_2$					$3t_2 \rightarrow 5p\ ^1T_2$				$3t_2 \rightarrow 6p\ ^1T_2$				
ΔE^a	E^b		E^c	ΔE^d	ΔE^a	E^b		E^c	ΔE^d	ΔE^a	E^b		E^c	ΔE^d
	(υ_1, 0, 0, 0) [e]													
	υ_1 =													
	20.90	4	20.87											
0.09				0.09										
	20.99	5	20.96											
0.09				0.11										
	21.08	6	21.07			(υ_1, 0, 0, 0) [e]								
0.10				0.09		υ_1 =								
	21.18	7	21.16			21.18	2	21.16						
					0.09				0.07					
						21.27	3	21.23						
					0.09				0.11					
						21.36	4	21.34			(υ_1, 0, 0, 0) [e]			
					0.09	*21.38*			0.11		υ_1 =			
						21.45	5	21.45			21.45	2	21.45	
					0.10	*21.48* *21.53*			0.09	0.10	*21.48* *21.53*			0.09
						21.55	6	21.54			21.55	3	21.54	
					0.09				0.10	0.09				0.10
						21.64	7	21.64			21.64	4	21.64	
					0.09				0.07	0.09				0.07
						21.73	8	21.71			21.73	5	21.71	
					0.08	*21.75*			0.11	0.08	*21.75*			0.11
						21.81	9	21.82			21.81	6	21.82	
						21.85				0.10	*21.85*			0.09
											21.91	7	21.91	
														0.09
												8	22.00	
														0.08
												9	22.08	

[a] Energy spacing between vibrational states, in eV (this work).

[b] Energy of peak maximum, in eV (this work). Values in italics show the energies of weak shoulders.

[c] Energy of peak maximum, in eV, taken from Mitsuke *et al* [8].

[d] Energy spacing between vibrational states, in eV, taken from Mitsuke *et al* [8].

[e] Assignments for the vibrational quantum number in the ν_1 mode of CF_4*. These assignments are taken from the ion-pair study of Mitsuke *et al* [8]. and the photoabsorption study of Lee *et al* [50].

Table 4 : F^- quantum yields (Φ_F-) measured at energies both below and above the onsets of ionisation for SF_6, CF_4 and SF_5CF_3. Total photoabsorption cross sections for SF_6, CF_4 and SF_5CF_3 are taken from refs [43,44,39].

Molecule	**Φ_F- below onset of ionisation**	**Φ_F- above onset of ionisation**
SF_6	2.4×10^{-4} at 14.2 eV	1.5×10^{-5} at 24.6 eV
CF_4	2.8×10^{-5} at 14.0 eV	9.3×10^{-6} at 21.8 eV
SF_5CF_3	1.5×10^{-4} at 11.7 eV	3.4×10^{-4} at 16.9 eV

Table 5 : Rydberg assignments to features observed in the F^- ion yield recorded following the photoexcitation of SF_5Cl, recorded with a stepsize of 0.05 eV and a wavelength resolution of 0.6 nm.

Feature [a]	E / eV [b]	IE [c]	δ [d]	assignment [e]
2	14.06	14.79 ($A\ ^2A_1$)	1.68	$(15a_1)^{-1}\ 6p$
3	16.8_0	18.07 ($\widetilde{F}\ ^2A_1$)	1.73	$(14a_1)^{-1}\ 5p$
4	20.6_5	21.0 ($J\ ^2A_1$) 21.9 ($K\ ^2E$)	1.80 1.70	$(13a_1)^{-1}\ 8p$ $(5e)^{-1}\ 5p$
5	21.6_5	21.9 ($K\ ^2E$)	1.62	$(5e)^{-1}\ 9p$
6	23.2_0	25.1 ($L\ ^2A_1$)	1.33	$(12a_1)^{-1}\ 4p$
7	23.9_5	25.1 ($L\ ^2A_1$)	1.56	$(12a_1)^{-1}\ 5p$
8	24.6_0	25.1 ($L\ ^2A_1$)	1.78	$(12a_1)^{-1}\ 7p$

[a] Feature in the F^- ion yield as labelled in Figure 11.

[b] Photon energy of the feature (Figure 11). The uncertainty in these values is estimated to be ± 0.01 eV for feature 2, ± 0.1 eV for features 3–8.

[c] The electronic state of SF_5Cl^+ to which the assigned Rydberg state converges. Values of the vertical ionisation energy are taken from DeKock *et al.* [68].

[d] Value of the quantum defect calculated from the Rydberg formula, eq. (V).

[e] Rydberg orbital assignment. The numbering scheme for the MOs of SF_5Cl (Figure 10) is that used by Klyagina *et al*. and Parkes [67,70], where both core and valence orbitals are counted.

Table 6 : Appearance energies, cross sections and quantum yields for anions observed from photoexcitation of CF_3Cl, CF_3Br and CF_3I.

Molecule [AIE [a] / eV]	Anion	AE [b] (eV)	Cross section maximum [c] / cm^2	Energy [d] / eV	Quantum yield [e]
CF_3Cl [12.4]	F^-	16.0	1.5×10^{-20}	21.0	1.8×10^{-4}
	Cl^-	16.1	2.3×10^{-21}	20.9	2.9×10^{-5}
	F_2^-	*ca.* 21 [f]	6.8×10^{-23}	22.7	8.5×10^{-7}
	FCl^-	*ca.* 18 [f]	6.5×10^{-23}	20.8	8.0×10^{-7}
	CF^-	25.5 [g]	1.6×10^{-22}	27.3	– [h]
	CF_2^-	20.2	1.5×10^{-22}	21.3	1.8×10^{-6}
	CF_3^-	15.5	2.8×10^{-22}	18.1	3.5×10^{-6}
CF_3Br [11.5]	F^-	14.7	9.7×10^{-21}	19.6	1.2×10^{-4}
	Br^-	15.1	– [j]	–	– [j]
	F_2^-	*ca.* 19 [f]	2.8×10^{-22}	20.4	3.4×10^{-6}
	FBr^-	*ca.* 18 [f]	5.5×10^{-22}	20.4	6.6×10^{-6}
	CF^-	23.6	3.4×10^{-22}	25.6	5.2×10^{-6}
	CF_2^-	18.2	4.9×10^{-22}	19.5	5.8×10^{-6}
	CF_3^-	13.6	2.5×10^{-22}	14.8	4.0×10^{-6}
CF_3I [10.4]	F^-	9.7	1.1×10^{-20}	20.4	– [k]
	I^-	8.8	– [j]	–	– [j]
	F_2^-	*ca.* 17 [f]	8.5×10^{-23}	20.1	– [k]
	CF^-	21.6	1.1×10^{-22}	23.6	– [k]
	CF_2^-	16.0	4.6×10^{-22}	16.8	– [k]
	CF_3^-	11.0	5.7×10^{-22}	12.7	– [k]

[a] Adiabatic ionisation energy for CF_3Cl [77], CF_3Br [77] and CF_3I [78].

[b] Appearance energy (AE) from this work. The error is estimated to be ± 0.2 eV, based on the resolution and step size used to record the ion yields.

[c] Cross section for anion production following photoexcitation of the parent molecule.

[d] Energy of peak maximum at which cross section and quantum yield measurements are taken.

[e] Quantum yields for anion production, obtained by dividing cross sections for anions (column 4) by total photoabsorption cross sections. The latter values are given for CF_3Cl and CF_3Br [74,75].

[f] Cannot state AE with any confidence due to poor signal/noise.

[g] There is some ambiguity surrounding the mass of anions detected contributing to the CF^- ion yield from CF_3Cl. The signal observed in the range 16–25 eV is thought to arise from Cl^- ions, and the value of 25.5 eV represents our interpretation of the true onset of CF^- anions.

[h] Quantum yield is not calculated because photoabsorption cross section for CF_3Cl is not available at this energy.

[j] The Br^- and I^- ion yields are significantly influenced by anions arising from dissociative electron attachment. Cross sections, and hence quantum yields, cannot therefore be defined. The one exception is I^- at 9.0 for which we estimate a cross section of 3.8×10^{-21} cm^2 and a quantum yield of 8×10^{-5} (see Section 6.2 of text).

[k] Quantum yields cannot be calculated, because photoabsorption data for CF_3I are limited to photon energies < 12 eV.

Table 7 : Comparison of data obtained for ion-pair formation of F^- from SF_6, SF_5Cl and SF_5CF_3. A separate comparison for CF_4 and CF_3Cl is also included.

Molecule	*AIE* [a] / eV	*AE*(F^-) [b] / eV	Reaction at *AE* [c]	E(σ_{max}) [d] / eV	Reaction at σ_{max} [c]
SF_6	15.1	12.7 ± 0.2	$SF_6 \rightarrow F^- + SF_5^+$	14.2	$SF_6 \rightarrow F^- + SF_5^+$
SF_5Cl	12.3	12.7 ± 0.2	not known	14.06	$SF_5Cl \rightarrow F^- + SF_4^+ + Cl$
SF_5CF_3	12.9	11.05 ± 0.05	$SF_5CF_3 \rightarrow F^- + CF_3^+ + SF_4$	16.9	not known
CF_4	15.4	13.0 ± 0.2	$CF_4 \rightarrow F^- + CF_3^+$	14.0	$CF_4 \rightarrow F^- + CF_3^+$
CF_3Cl	12.4	16.0 ± 0.2	$CF_3Cl \rightarrow F^- + CF_2^+ + Cl$	21.0	not known

[a] Adiabatic ionisation energy for SF_6 [40], SF_5Cl [68,69], SF_5CF_3 [42], CF_3Cl [77] and CF_4 [48].

[b] Appearance energy of F^- anions, this work.

[c] The ion-pair reactions are assigned by comparing calculated enthalpies of reaction with onsets to features observed in the anion ion yield spectra.

[d] The energy for maximum cross section for production of F^-.

Table 8 : Appearance energies, cross sections and quantum yields for anions observed from photoexcitation of CH_3F, CH_3Cl, CH_3Br and CH_4.

Molecule	Anion	AE_{298} / eV	Cross section / cm^2	Energy of cross section maximum / eV	Quantum Yield [g]
CH_3F	F^-	12.28 ± 0.02 [a]	1.2×10^{-19}	13.4	2.3×10^{-3}
CH_3F	CF^-	24.4 ± 0.2 [b,c]	4.2×10^{-23}	27.2	1.5×10^{-6}
CH_3F	CHF^-	21.5 ± 0.2 [b]	8.8×10^{-23}	22.4	2.2×10^{-6}
CH_3F	CH_2F^-	18.2 ± 0.2 [b]	4.1×10^{-23}	19.7	8.9×10^{-7}
CH_3Cl	Cl^-	10.04 ± 0.02 [a]	1.2×10^{-19}	11.3	2.3×10^{-3}
CH_3Cl	CH_2Cl^-	17.2 ± 0.2 [b]	7.6×10^{-21}	18.2	1.0×10^{-4}
CH_3Br	H^-	12.1 ± 0.2 [d]	– [f]	14.0	–
CH_3Br	Br^-	9.46 ± 0.02 [a]	2.5×10^{-20}	10.0	4.1×10^{-4}
CH_3Br	$CHBr^-$	*ca.* 20 [e]	1.3×10^{-22}	22.4	3.3×10^{-6}
CH_3Br	CH_2Br^-	17.1 ± 0.2 [b]	5.6×10^{-22}	17.8	8.1×10^{-6}
CH_4	H^-	13.30 ± 0.10	1.4×10^{-22} [h]	20.6	4.4×10^{-6}
CH_4	CH^-	22.5 ± 0.2	5.9×10^{-23}	29.3	4.6×10^{-6}
CH_4	CH_2^-	22.2 ± 0.2	2.8×10^{-23}	24.9	1.3×10^{-6}

[a] Appearance energy (*AE*) from this work (Figure 18).

[b] Appearance energy (*AE*) from this work (Figures 15–17).

[c] *AE*(CF^-) given here assumes that the peak at 22.5 eV in Figure 15b is overlap of CHF^- signal.

[d] *AE* is difficult to determine as scan starts as 12 eV, and a subtraction method has been implemented to allow for the zero-blast effect.

[e] Cannot determine *AE* with confidence due to poor signal-to-noise ratio. The signal may have contributions from CH_2Br^-.

[f] Cross section cannot be determined due to the zero-blast effect, discussed in text (Section 6.3).

[g] Quantum yields for anion production are obtained by dividing the anion cross section by the total absorption cross section. The latter values for CH_3F, CH_3Cl, CH_3Br and CH_4 are taken from references [81-84].

[h] The H^- anion is dominant, so an absolute cross section can be determined.

Table 9 : Upper limits to experimentally-determined bond dissociation energies and comparison with literature values.

Bond	D^{o}_{298} / eV	
	This work	**Literature value** [a]
$H - CH_3$	4.21 ± 0.11	4.553 ± 0.004
$F - CH_3$	$\leq 5.84 \pm 0.02$ [b]	4.77 ± 0.09
$Cl - CH_3$	$\leq 3.81 \pm 0.02$ [b]	3.63 ± 0.02
$Br - CH_3$	$\leq 2.98 \pm 0.02$ [b]	3.05 ± 0.02
$H - CH_2F$	$\leq 4.8_4 \pm 0.2_7$ [c]	4.39 ± 0.04
$H - CH_2Cl$	$\leq 4.3_3 \pm 0.2_6$ [c]	4.34 ± 0.02
$H - CH_2Br$	$\leq 4.2_8 \pm 0.2_4$ [c]	4.43 ± 0.02
$F - CF_3$	$\leq 7.4 \pm 0.2$ [d]	5.67 ± 0.02
$Cl - CF_3$	$\leq 4.4 \pm 0.2$ [e]	3.79 ± 0.04
$Br - CF_3$	$\leq 3.6 \pm 0.2$ [e]	3.07 ± 0.01
$I - CF_3$	$\leq 2.4 \pm 0.2$ [e]	2.35 ± 0.01
$F - CF_2Cl$	$\leq 11.1 \pm 0.2$	5.30 [f]
$F - CF_2Br$	$\leq 18.1 - IE(CF_2Br)$	5.09 [j]
$F - CF_2I$	$\leq 13.1 - IE(CF_2I)$	5.40 [j]
$F - SF_5$	$\leq 6.3 \pm 0.3$	4.06 [f]
$F - CF_3$	$\leq 7.4 \pm 0.2$	5.67 ± 0.02
$F_5S - CF_3$	– [g]	3.86 ± 0.45 [k]
$F - SF_4CF_3$	$\leq 14.5 - IE(SF_4CF_3)$	n/a
$F - SF_4Cl$	$\leq 4.8 \pm 0.3$ [h]	3.70 [m]
$Cl - SF_5$	$\leq 4.4 \pm 0.3$	2.54 [m]

[a] Reference [64].

[b] Calculated from the *AE* of Y^- formation from CH_3Y. The compound errors have contributions from the errors in *AE*(Y^-), typically 0.02 eV, and the error in *IE*(CH_3), 0.01 eV.

[c] Calculated from the *AE* of CH_2Y^- formation from CH_3Y, in Figures 15–17. The errors are dominated by errors in *AE* (CH_2Y^-), typically 0.2 eV.

[d] Calculated from the *AE*(F^-) from CF_4 [17].

[e] Calculated from the *AE* of X^- formation from CF_3X.

[f] Error not quoted.

[g] CF_3^- and SF_5^- are either not observed, or are not formed by ion-pair formation.

[h] Uses an enthalpy of formation of SF_4Cl^+ of +327 kJ mol^{-1} [69].

[j] Calculated assuming the enthalpies of formation at 298 K of the CF_2Br and CF_2I radicals are –238 and –144 kJ mol^{-1}, respectively [94,95]

[k] Value at 0 K [56].

[m] Calculated assuming the enthalpies of formation of SF_4Cl and SF_5 are –761 and –915 kJ mol^{-1}, respectively [69]. Errors are often not quoted and difficult to estimate, but probably an error in the bond energy of ± 0.20 eV is realistic.

Table 10 : Summary of data collected for anion production following VUV photoexcitation of twenty four gas-phase polyatomic molecules. Data recorded at the Daresbury Synchrotron Radiation Source between 2005 and 2008.

Molecule	*AIE* [a] / eV	Anion	AE_{298} [b] / eV	Reaction at AE_{298} [c]	$\Delta_r H°_{298}$ [d] / eV	σ_{max} [e] / cm^2	$E(\sigma_{max})$ [f] / eV	$\Phi(\sigma_{max})$ [g]
1	2	3	4	5	6	7	8	9
CH_4	12.61	H^-	13.30 ± 0.10	$CH_4 \rightarrow H^- + CH_3^+$	13.7	1.4×10^{-22}	20.6	4.4×10^{-6}
C_2H_4 [h]	10.51	H^-	13.06 ± 0.10	$C_2H_4 \rightarrow H^- + C_2H_3^+$	12.5	8.3×10^{-22}	18.0	1.4×10^{-5}
C_2H_6 [h]	11.52	H^-	12.00 ± 0.10	$C_2H_6 \rightarrow H^- + C_2H_5^+$	11.9	1.7×10^{-21}	19.3	2.7×10^{-5}
C_3H_8 [h]	10.9	H^-	13.2 ± 0.2	$C_3H_8 \rightarrow H^- + C_3H_7^+$	11.7	3.3×10^{-21}	18.6	3.3×10^{-5}
CF_4 [j]	15.4	F^-	13.0 ± 0.2	$CF_4 \rightarrow F^- + CF_3^+$	11.3	1.4×10^{-21}	14.0	2.8×10^{-5}
		F_2^-	20.1 ± 0.2	$CF_4 \rightarrow F_2^- + CF^+ + F$	19.3	4.0×10^{-23}	21.6	5.6×10^{-7}
C_2F_4 [h]	10.12	F^-	13.17 ± 0.05	$C_2F_4 \rightarrow F^- + C_2F_3^+$	12.4	1.7×10^{-20}	16.5	– [m]
		CF^-	22.4 ± 0.5	$C_2F_4 \rightarrow CF^- + CF^+ + 2F$	19.7	2.4×10^{-22}	27.5	– [m]
C_2F_6 [h]	13.4	F^-	13.62 ± 0.10	$C_2F_6 \rightarrow F^- + C_2F_5^+$	11.5	7.4×10^{-21}	14.7	– [n]
C_3F_8 [h]	13.0	F^-	13.1 ± 0.2	$C_3F_8 \rightarrow F^- + C_3F_7^+$	12.2	4.7×10^{-21}	23.4	– [m]
		CF_2^-	20.4 ± 0.2	– [k]	–	4.9×10^{-22}	21.8	– [m]
CH_3F [w]	12.53	H^- [p]	–	–	–	–	–	–
		F^-	12.28 ± 0.02	$CH_3F \rightarrow F^- + CH_3^+$	11.2	1.2×10^{-19}	13.4	2.3×10^{-3}
		CF^-	24.4 ± 0.2	$CH_3F \rightarrow CF^- + H^+ + 2H$	22.1	4.2×10^{-23}	27.2	1.5×10^{-6}
		CHF^-	21.5 ± 0.2	$CH_3F \rightarrow CHF^- + H^+ + H$	21.7	8.8×10^{-23}	22.4	2.2×10^{-6}
		CH_2F^-	18.2 ± 0.2	$CH_3F \rightarrow CH_2F^- + H^+$	17.7	4.1×10^{-23}	19.7	8.9×10^{-7}
CH_2F_2 [h]	12.729	H^- [q]	12.08 ± 0.05 [r]	$CH_2F_2 \rightarrow H^- + CHF_2^+$	12.5 [r]	–	–	–
		F^-	11.86 ± 0.05	$CH_2F_2 \rightarrow F^- + CH_2F^+$	10.7	6.6×10^{-21}	18.8	1.4×10^{-4}
		F_2^-	17.20 ± 0.05	$CH_2F_2 \rightarrow F_2^- + CH_2^+$	15.9	3.3×10^{-22}	18.5	6.9×10^{-6}
CHF_3 [h]	13.8	H^- [q]	12.82 ± 0.05 [r]	$CHF_3 \rightarrow H^- + CF_3^+$	12.9 [r]	–	–	–
		F^-	≤ 12.4 [s]	$CHF_3 \rightarrow F^- + CHF_2^+$	11.0	4.5×10^{-21}	23.1	8.2×10^{-5}
		CF_3^-	16.6 ± 0.2	$CHF_3 \rightarrow CF_3^- + H^+$	16.5	2.7×10^{-20}	18.0	4.4×10^{-4}
CH_3Cl [w]	11.29	H^- [p]	–	–	–	–	–	–
		Cl^-	10.04 ± 0.02	$CH_3Cl \rightarrow Cl^- + CH_3^+$	9.9	1.2×10^{-19}	11.3	2.3×10^{-3}
		CH_2Cl^-	17.2 ± 0.2	$CH_3Cl \rightarrow CH_2Cl^- + H^+$	17.3	7.6×10^{-21}	18.2	1.0×10^{-4}
CH_2Cl_2 [h]	11.326	H^- [q]	11.5 ± 0.2 [r]	$CH_2Cl_2 \rightarrow H^- + CHCl_2^+$	11.7 [r]	–	–	–
		Cl^-	9.31 ± 0.05	$CH_2Cl_2 \rightarrow Cl^- + CH_2Cl^+$	8.6	6.6×10^{-20}	10.1	1.0×10^{-3}
		Cl_2^-	13.74 ± 0.10	$CH_2Cl_2 \rightarrow Cl_2^- + CH_2^+$	13.0	1.4×10^{-21}	16.0	1.5×10^{-5}
$CHCl_3$ [h]	11.30	H^- [q]	11.2 ± 0.2	$CHCl_3 \rightarrow H^- + CCl_3^+$	11.2	–	–	–
		Cl^-	9.26 ± 0.05	$CHCl_3 \rightarrow Cl^- + CHCl_2^+$	7.9	7.0×10^{-21}	20.3	5.4×10^{-5}
		CH^-	22.7 ± 0.2	$CHCl_3 \rightarrow CH^- + Cl^+ + 2Cl$	22.8	3.7×10^{-22}	24.8	5.7×10^{-6}
		CCl^-	19.3 ± 0.5	– [t]	–	5.7×10^{-22}	20.3	4.4×10^{-6}

CCl_4 [h]	11.30	Cl^- [u]	11.35 ± 0.05	$[CCl_4 + e^- \rightarrow CCl_3 + Cl^-]$	–	–	–	–
		CCl^-	21.2 ± 0.2	– [t]	–	1.6×10^{-21}	23.8	1.7×10^{-5}
CF_3Cl [x]	12.4	F^-	16.0 ± 0.2	$CF_3Cl \rightarrow F^- + CF_2^+ + Cl$	15.6	1.5×10^{-20}	21.0	1.8×10^{-4}
		Cl^-	16.1 ± 0.2	$CF_3Cl \rightarrow Cl^- + CF_2^+ + F$	15.4	2.3×10^{-21}	20.9	2.9×10^{-5}
		F_2^-	21 ± 2	$CF_3Cl \rightarrow F_2^- + Cl^+ + CF$	21.1	6.8×10^{-23}	22.7	8.5×10^{-7}
		FCl^-	18 ± 2	– [t]	–	6.5×10^{-23}	20.8	8.0×10^{-7}
		CF^-	25.5 ± 0.2	– [k]	–	1.6×10^{-22}	27.3	– [m]
		CF_2^-	20.2 ± 0.2	$CF_3Cl \rightarrow CF_2^- + Cl^+ + F$	20.3	1.5×10^{-22}	21.3	1.8×10^{-6}
		CF_3^-	15.5 ± 0.2	$CF_3Cl \rightarrow CF_3^- + Cl^+$	14.9	2.8×10^{-22}	18.1	3.5×10^{-6}
CF_2Cl_2 [h]	11.734	F^-	12.2 ± 0.1	$CF_2Cl_2 \rightarrow F^- + CFCl_2^+$	9.8	1.1×10^{-20}	19.1	1.0×10^{-4}
		Cl^-	10.35 ± 0.1	$CF_2Cl_2 \rightarrow Cl^- + CF_2Cl^+$	8.2	1.3×10^{-20}	20.0	1.2×10^{-4}
		CF^-	23.5 ± 0.5	– [k]	–	2.2×10^{-22}	25.6	– [m]
$CFCl_3$ [h]	11.53	F^-	14.4 ± 0.2	$CFCl_3 \rightarrow F^- + CCl_2^+ + Cl$	13.7	1.2×10^{-21}	18.3	1.0×10^{-5}
		Cl^- [u]	11.54 ± 0.10	$[CFCl_3 + e^- \rightarrow CFCl_2 + Cl^-]$	–	–	–	–
CH_3Br [w]	10.54	H^- [q]	12.1 ± 0.2	$CH_3Br \rightarrow H^- + CH_2Br^+$	11.6	–	–	–
		Br^-	9.46 ± 0.02	$CH_3Br \rightarrow Br^- + CH_3^+$	9.5	2.5×10^{-20}	10.0	4.1×10^{-4}
		$CHBr^-$	20 ± 2	$CH_3Br \rightarrow CHBr^- + H^+ + H$	20.9	1.3×10^{-22}	22.4	3.3×10^{-6}
		CH_2Br^-	17.1 ± 0.2	$CH_3Br \rightarrow CH_2Br^- + H^+$	17.3	5.6×10^{-22}	17.8	8.1×10^{-6}
CF_3Br [x]	11.5	F^-	14.7 ± 0.2	$CF_3Br \rightarrow F^- + CF_2^+ + Br$	14.9	9.7×10^{-21}	19.6	1.2×10^{-4}
		Br^- [u]	15.1 ± 0.2	$[CF_3Br + e^- \rightarrow CF_3 + Br^-]$	–	–	–	–
		F_2^-	19 ± 0.2	$CF_3Br \rightarrow F_2^- + Br^+ + CF$	19.2	2.8×10^{-22}	20.4	3.4×10^{-6}
		FBr^-	18 ± 2	– [t]	–	5.5×10^{-22}	20.4	6.6×10^{-6}
		CF^-	23.6 ± 0.2	– [k]	–	3.4×10^{-22}	25.6	5.2×10^{-6}
		CF_2^-	18.2 ± 0.2	$CF_3Br \rightarrow CF_2^- + Br^+ + F$	18.5	4.9×10^{-22}	19.5	5.8×10^{-6}
		CF_3^-	13.6 ± 0.2	$CF_3Br \rightarrow CF_3^- + Br^+$	13.1	2.5×10^{-22}	14.8	4.0×10^{-6}
CF_3I [x]	10.37	F^-	9.7 ± 0.2	$CF_3I \rightarrow F^- + CF_2I^+$	9.7	1.1×10^{-20}	20.4	– [m]
		I^- [z]	8.8 ± 0.2	$CF_3I \rightarrow I^- + CF_3^+$	8.3	–	–	–
		F_2^-	17 ± 2	$CF_3I \rightarrow F_2^- + I^+ + CF$	17.2	8.5×10^{-23}	20.1	– [m]
		CF^-	21.6 ± 0.2	- [k]	-	1.1×10^{-22}	23.6	– [m]
		CF_2^-	16.0 ± 0.2	$CF_3I \rightarrow CF_2^- + I^+ + F$	16.4	4.6×10^{-22}	16.8	– [m]
		CF_3^-	11.0 ± 0.2	$CF_3I \rightarrow CF_3^- + I^+$	11.0	5.7×10^{-22}	12.7	– [m]
SF_6 [j]	15.116	F^-	12.7 ± 0.2	$SF_6 \rightarrow F^- + SF_5^+$	10.4	7.1×10^{-21}	14.2	2.4×10^{-4}
		F_2^-	16.3 ± 0.2	$SF_6 \rightarrow F_2^- + SF_3^+ + F$	14.1	1.4×10^{-22}	18.3	1.9×10^{-6}
		SF_5^- [u]	15.1 ± 0.2	$[SF_6 + e^- \rightarrow F + SF_5^-]$	–	–	–	–
		SF_6^- [u]	15.1 ± 0.2	$[SF_6 + e^- \rightarrow SF_6^-]$	–	–	–	–
SF_5Cl [y]	12.3	F^-	12.7 ± 0.2	– [k]	–	6.1×10^{-20}	14.1	– [m]
		Cl^-	10.6 ± 0.2	$SF_5Cl \rightarrow Cl^- + SF_5^+$	8.7	–	10.9	–
		SF_5^-	–	$[SF_5Cl + e^- \rightarrow Cl + SF_5^-]$	–	–	–	–

		F^-	11.05 ± 0.05	$SF_5CF_3 \rightarrow F^- + CF_3^+ + SF_4$	11.5	3.4×10^{-20}	16.9	3.4×10^{-4}
		F_2^-	16.1 ± 0.2	$SF_5CF_3 \rightarrow F_2^- + CF_3^+ + SF_3$	14.3	1.2×10^{-21}	17.9	1.1×10^{-5}
		SF^-	24.0 ± 0.2	$SF_5CF_3 \rightarrow SF^- + CF_3^+ + 4F$	23.0	2.8×10^{-22}	28.8	2.4×10^{-6}
SF_5CF_3 [j]	12.9	SF_2^-	20.2 ± 0.2	$SF_5CF_3 \rightarrow SF_2^- + CF_3^+ + 3F$	20.0	3.9×10^{-22}	24.2	2.5×10^{-6}
		SF_3^-	15.4 ± 0.2	$SF_5CF_3 \rightarrow SF_3^- + CF_3^+ + 2F$	16.0	1.0×10^{-20}	17.6	1.0×10^{-4}
		SF_4^-	13.0 ± 0.2	$SF_5CF_3 \rightarrow SF_4^- + CF_3^+ + F$	13.4	1.3×10^{-20}	14.1	1.7×10^{-4}
		SF_5^- [u]	12.9 ± 0.2	$[SF_5CF_3 + e^- \rightarrow CF_3 + SF_5^-]$	–	–	–	–

[a] Adiabatic ionisation energy (*AIE*) values are taken from the following sources: CH_4 [100]; C_2H_4 [102]; C_2H_6 [103]; C_3H_8 [104]; CF_4 [48]; C_2F_4 [105]; C_2F_6 [106]; C_3F_8 [106]; CH_3F [85]; CH_2F_2 [63]; CHF_3 [107]; CH_3Cl [85]; CH_2Cl_2 [108]; $CHCl_3$ [109]; CCl_4 [63]; CF_3Cl [77]; CF_2Cl_2 [110]; $CFCl_3$ [109]; CH_3Br [86]; CF_3Br [77]; CF_3I [78]; SF_6 [40]; SF_5Cl [68]; SF_5CF_3 [42].

[b] Experimentally determined appearance energy at 298 K.

[c] Reaction occurring at onset.

[d] $\Delta_r H^o_{298}$ for the reaction in column 5, calculated from standard enthalpies of formation.

[e] Absolute value for the ion-pair cross section (σ) at its maximum.

[f] Energy (*E*) at which the ion-pair cross section reaches its maximum.

[g] Quantum yield (Φ) for ion-pair formation at *E* (σ_{max}). The ion-pair cross section is divided by the total photoabsorption cross section. Data for σ_{abs} from the following sources (for molecules not listed here see references in column 1): C_2H_4 [111]; C_2H_6 [112]; C_3H_8 [112]; CH_2F_2 [113]; CHF_3 [75]; CH_2Cl_2 [114]; $CHCl_3$ [115]; CCl_4 [75]; CF_2Cl_2 [113]; $CFCl_3$ [115].

[h] Data for this molecule are presented in Section 8 and Figures 20–32.

[j] Data in columns 3–9 for CF_4, SF_6 and SF_5CF_3 are taken from Section 5 and Table 2.

[k] The reaction occurring at the *AE* for this anion is not known due to the many different dissociation channels that are thermochemically open.

[m] Ion-pair quantum yield cannot be calculated because σ_{abs} is not known over the required energy range.

[n] Total photoabsorption cross section for C_2F_6 is reported from 16–62 eV and so $\Phi(\sigma_{max})$, at 14.7 eV, cannot be calculated. However, Φ for F^- formation at 17.7 eV is 4.8×10^{-5} [σ_{abs} (C_2F_6, 17.7 eV) = 7.3×10^{-17} cm^2] [50].

[p] H^- detected at *m/z* 1, but the signal was significantly weaker than the dominant anion. The H^- ion yield matches that of the dominant anion, presumably because of the *zero blast* effect in the quadrupole mass spectrometer [35], and cannot therefore be trusted.

[q] H^- detected at *m/z* 1, but the signal was of similar intensity to that of other anions. The H^- ion yield is unique, but it may contain contributions from other anions due to the *zero blast* effect [35]. Only limited information can

therefore be obtained. For example, absolute cross sections cannot be determined for H^- ion-pair formation unless it is the dominant anion [19,20].

[r] The fact that $\Delta_r H°_{298}$ exceeds AE_{298} may result from other anions being detected due to the *zero blast* effect (see notes *p* and *q*), giving an *AE* lower than it should be. Alternatively, thermal effects (*i.e.* hotbands) could cause the AE_{298} to precede $\Delta_r H°_{298}$.

[t] $\Delta_f H°_{298}$ is not known for CCl^-, FCl^- and FBr^-.

[u] Anion signal increases non-linearly with increasing parent gas pressure. Anion production is dominated by a two-step electron attachment process where photoionisation provides the source of electrons. All molecules have fast thermal electron attachment rate coefficients exceeding 10^{-8} cm^3 $molecule^{-1}$ s^{-1}.

[w] Data in columns 3–9 for CH_3Y molecules (Y = F, Cl, Br) are taken from Section 6.3 and Table 8.

[x] Data in columns 3–9 for CF_3X molecules (X = Cl,Br,I) are taken from Section 6.2 and Table 6.

[y] Data in columns 3–9 for SF_5Cl are taken from Section 6.1.

[z] The I^- yield at $E \geq 10.4$ eV is dominated by dissociative electron attachment to CF_3I (see note *u*). However, below 10.4 eV the observed I^- signal can only arise by ion-pair dissociation. Using absorption cross sections from Eden *et al.* [76], the cross section for I^- formation at 9.0 eV is 3.8×10^{-21} cm^2 with a corresponding quantum yield of 8×10^{-5}.

Table 11 : Bond dissociation energies of cations, D^{o+}, and neutral polyatomic molecules, D^o, at 298 K.

Cation	$D^{o+}_{therm.}$ [a] / eV	$D^{o+}_{expt.}$ [b] / eV	Neutral	$D^o_{lit.}$ [c] / eV
$H - C_2H_3^+$	2.7 ± 0.3	≤ (3.3 ± 0.2)	$H - C_2H_3$	4.81 ± 0.03
$H - C_2H_5^+$	1.1 ± 0.1	≤ (1.2 ± 0.2)	$H - C_2H_5$	4.36 ± 0.01
$H - C_3H_7^+$	1.6 ± 0.4	≤ (3.1 ± 0.3)	$H - C_3H_7$	4.38 ± 0.02
$H - CH_3^+$	1.8 ± 0.2	≤ (1.4 ± 0.1)	$H - CH_3$	4.553 ± 0.004
$H - CH_2F^+$	0.9 ± 0.4	– [d]	$H - CH_2F$	4.39 ± 0.04
$H - CH_2Cl^+$	1.8 ± 0.4	– [d]	$H - CH_2Cl$	4.34 ± 0.02
$H - CH_2Br^+$	1.8 ± 0.4	≤ (2.3 ± 0.2)	$H - CH_2Br$	4.43 ± 0.02
$H - CHF_2^+$	0.4 ± 0.3	≤ (0.1 ± 0.1)	$H - CHF_2$	4.48 ± 0.04
$H - CHCl_2^+$	1.1 ± 0.4	≤ (0.9 ± 0.2)	$H - CHCl_2$	4.15 ± 0.02
$H - CF_3^+$	–0.1 ± 0.4	≤ (–0.2 ± 0.2)	$H - CF_3$	4.61 ± 0.03
$H - CCl_3^+$	0.7 ± 0.3	≤ (0.7 ± 0.3)	$H - CCl_3$	4.07 ± 0.03
$F - CH_3^+$	2.1 ± 0.3	≤ (3.2 ± 0.1)	$F - CH_3$	4.77 ± 0.09
$F - CH_2F^+$	1.4 ± 0.2	≤ (2.5 ± 0.1)	$F - CH_2F$	5.14 ± 0.09
$F - CHF_2^+$	0.6 ± 0.3	≤ (2.0 ± 0.4)	$F - CHF_2$	5.53 ± 0.06
$F - CFCl_2^+$	1.5 ± 0.2	≤ (3.9 ± 0.1)	$F - CFCl_2$	5.00 ± 0.11
$F - CF_2Cl^+$	1.2 ± 0.3	– [e]	$F - CF_2Cl$	5.30
$F - CF_2Br^+$	2.0 ± 0.3	– [e]	$F - CF_2Br$	5.09 [h]
$F - CF_2I^+$	2.7 ± 0.2 [g]	≤ (2.7 ± 0.2)	$F - CF_2I$	5.40 [h]
$F - CF_3^+$	–0.7 ± 0.3	≤ (1.0 ± 0.3)	$F - CF_3$	5.67 ± 0.02
$F - CCl_3^+$	0.9 ± 0.2	– [e]	$F - CCl_3$	4.55 ± 0.04
$F - SF_5^+$	–1.4 ± 0.3	≤ (1.0 ± 0.2)	$F - SF_5$	4.06
$F - SF_4Cl^+$	2.7 ± 0.3	– [e]	$F - SF_4Cl$	3.70 [j]
$F - SF_4CF_3^+$	?	– [e]	$F - SF_4CF_3$	?
$F - C_2F_3^+$	5.7 ± 0.2	≤ (6.5 ± 0.1)	$F - C_2F_3$	5.66 ± 0.13
$F - C_2F_5^+$	1.5 ± 0.3	≤ (3.6 ± 0.2)	$F - C_2F_5$	5.52 ± 0.07
$F - C_3F_7^+$	2.6 ± 0.3	≤ (3.5 ± 0.3)	$F - C_3F_7$	6.15
$Cl - CH_3^+$	2.2 ± 0.2	≤ (2.4 ± 0.1)	$Cl - CH_3$	3.63 ± 0.02
$Cl - CH_2Cl^+$	0.9 ± 0.2	≤ (1.6 ± 0.1)	$Cl - CH_2Cl$	3.50 ± 0.03
$Cl - CHCl_2^+$	0.2 ± 0.2	≤ (1.6 ± 0.1)	$Cl - CHCl_2$	3.22 ± 0.02
$Cl - CFCl_2^+$	0.0 ± 0.2	– [f]	$Cl - CFCl_2$	3.33 ± 0.09
$Cl - CF_2Cl^+$	0.1 ± 0.2	≤ (2.2 ± 0.1)	$Cl - CF_2Cl$	3.46 ± 0.11
$Cl - CF_3^+$	0.4 ± 0.3	– [e]	$Cl - CF_3$	3.79 ± 0.04

$Cl - CCl_3^+$	-0.4 ± 0.2	– [f]	$Cl - CCl_3$	3.07
$Cl - SF_5^+$	0.0 ± 0.2	$\leq (1.9 \pm 0.3)$	$Cl - SF_5$	2.54
$Br - CH_3^+$	2.3 ± 0.1	$\leq (2.3 \pm 0.1)$	$Br - CH_3$	3.05 ± 0.02
$Br - CF_3^+$	0.6 ± 0.1	– [e]	$Br - CF_3$	3.07 ± 0.01
$I - CF_3^+$	1.0 ± 0.1	$\leq (1.5 \pm 0.2)$	$I - CF_3$	2.35 ± 0.01
$H_2FC - H^+$	5.4 ± 0.2	$\leq (5.9 \pm 0.3)$	$H_2FC - H$	4.39 ± 0.04
$H_2ClC - H^+$	6.7 ± 0.2	$\leq (6.6 \pm 0.3)$	$H_2ClC - H$	4.34 ± 0.02
$H_2BrC - H^+$	7.5 ± 0.2	$\leq (7.3 \pm 0.3)$	$H_2BrC - H$	4.43 ± 0.02
$F_3C - H^+$	4.5 ± 0.1	$\leq (4.6 \pm 0.3)$	$F_3C - H$	4.61 ± 0.03
$F_3C - Cl^+$	4.4 ± 0.1	$\leq (4.9 \pm 0.3)$	$F_3C - Cl$	3.79 ± 0.04
$F_3C - Br^+$	3.4 ± 0.1	$\leq (3.9 \pm 0.3)$	$F_3C - Br$	3.07 ± 0.01
$F_3C - I^+$	2.4 ± 0.1	$\leq (2.4 \pm 0.3)$	$F_3C - I$	2.35 ± 0.01
$F_5S - F^+$	6.3 ± 0.3	– [f]	$F_5S - F$	4.06
$F_5S - CF_3^+$	-0.4 ± 0.4	– [f]	$F_5S - CF_3$	3.86 ± 0.45 [k]
$F_5S - Cl^+$	3.0 ± 0.3	– [f]	$F_5S - Cl$	2.54 [j]

---

[a] Thermochemical ionic bond dissociation energy at 298 K (D^{o+}_{therm}) for the bond shown in the first column. This value is calculated from the equation $D^{o+}_{therm} = \Delta_r H°_{298} - IE(ABC) + EA(A)$, where $\Delta_r H°_{298}$ is the enthalpy change for the reaction $ABC \rightarrow A^- + BC^+$, *IE* is an ionisation energy and *EA* an electron affinity. $\Delta_r H°_{298}$ and *IE* values are included in Table 10. The *EA* values for H, F, Cl, Br and I are 0.754, 3.401, 3.613 eV, 3.364 and 3.059 eV, respectively [90].

[b] Experimental ionic bond dissociation energy at 298 K (D^{o+}_{expt}) for the bond shown in the first column. This value is calculated from $D^{o+}_{expt} \leq AE(A^-) - IE(ABC) + EA(A)$, where AE is the appearance energy of A^- detected from the reaction $ABC \rightarrow A^- + BC^+$, IE is an ionisation energy and EA an electron affinity. The AE and IE values are included in Table 10.

[c] Neutral bond dissociation energy at 298 K for the bond shown in the fourth column from reference [64].

[d] Experimental data not available because an accurate value for $AE(H^-)$ could not be obtained in either case due to the zero-blast effect [35].

[e] Experimental data not available because ion-pair formation involves production of a neutral species in addition to the anion-cation pair.

[f] Experimental data not available because production of the the anion is probably dominated by dissociative electron attachment, and not by ion-pair formation.

[g] Assumes F^- turns on at the thermochemical threshold for $CF_3I \rightarrow F^- + CF_2I^+$ (see Section 7).

[h] Not quoted in reference [64]. Calculated from $\Delta_r H^o_{298}$ for the neutral dissociation reaction $ABC \rightarrow A + BC$. Data for $\Delta_f H^o_{298}$ of CF_2Br and CF_2I radicals are indirect values taken from references [94,95].

[j] Not quoted in reference [64]. Calculated from $\Delta_r H^o_{298}$ for the neutral dissociation reaction $ABC \rightarrow A + BC$. Data for $\Delta_f H^o_{298}$ of SF_4Cl and SF_5 radicals are taken from reference [69].

[k] Value at 0 K [56].

Figure Captions

Figure 1 : (a) Potential energy (V) as a function of bond distance (r) showing *direct* ion-pair formation process for the generic reaction ABC + hν $\rightarrow$ A^- + BC^+. E_{ip} represents the asymptotic ion-pair dissociation energy. (b) Potential energy (V) as a function of bond distance (r) showing *indirect* ion-pair formation process *via* predissociation of a neutral excited state (ABC*), *i.e.* ABC + hν $\rightarrow$ (ABC*) $\rightarrow$ A^- + BC^+.

Figure 2 : The experimental endstation used at Daresbury for detecting negative photoions as a function of photon energy. QMS is a Hiden HAL IV quadrupole mass spectrometer, PMT a photomultiplier tube.

Figure 3 : Graph to determine the relative mass sensitivity, M, of the Hiden Analytical HAL IV quadrupole mass spectrometer as a function of m/z. Sample gases include CF_4, SF_6, SF_5CF_3, CH_3F, CH_3Cl, CH_3Br, CH_2Cl_2, CF_2Cl_2, $CFCl_3$, C_2H_4, C_2H_6, C_3H_8, C_2F_4, C_2F_6, C_3F_8, 2-C_4F_8, *c*-C_4F_8 and *c*-C_5F_8, allowing ions of mass ranging from 12–212 u to be observed (solid squares). The mass spectrum of each sample was measured with 70 eV electron impact ionisation, and compared with the NIST spectrum [36]. At each m/z value, the % yield from NIST is divided by the % yield from the QMS spectrum, and the data are normalised to unity arbitrarily at m/z 69 (*i.e.* CF_3^+). The solid line shows the best fit to a third-order polynomial.

Figure 4 : Cross sections for anion production following photoexcitation of SF_6. The SF_5^- and SF_6^- spectra are not on an absolute scale. Ion yields were recorded as a function of photon energy between 12 and 35 eV with a step size of 0.1 eV and a wavelength resolution of 0.6 nm. This resolution is equivalent to 0.07 eV at 12 eV, 0.6 eV at 35 eV. The ion yields are compared with the threshold photoelectron spectrum of SF_6 [41].

Figure 5 : Pressure dependence of F^- and SF_5^- anion signals from SF_6. A linear pressure dependence, shown by F^-, indicates the anion arises from a one-step, unimolecular ion-pair dissociation. A non-linear pressure dependence, shown by SF_5^-, suggests a more complicated, multi-step process is involved in formation of the anion.

Figure 6 : Cross sections for anion production following photoexcitation of CF_4. (a) and (b) F^- and F_2^- ion yields recorded as a function of photon energy between 12 and 35 eV with a step size of 0.1 eV and a wavelength resolution of 0.6 nm. The cross sections are on an absolute scale. (c) and (d) F^- and F_2^- ion yields from Scully [34] recorded over a narrower energy range at a higher resolution of 0.05 and 0.2 nm, respectively. The cross sections are now on a relative scale. (e) Threshold photoelectron spectrum of CF_4 for comparison [41].

Figure 7 : F^- signal from CF_4 in the photon energy range 20 to 23.5 eV with a step size of 0.01 eV and a wavelength resolution of 0.2 nm. This resolution is equivalent to 0.1 eV at 22 eV. Vibrational progressions of the ν_1 totally symmetric stretching mode in CF_4^* *np* Rydberg states converging on the CF_4^+ $\tilde{C}\,^2T_2$ state are shown by combs. The vertical ionisation energy for CF_4^+ $\tilde{C}\,^2T_2$ is 22.04 eV [41], shown by a red arrow. A previously-unobserved feature is observed at 22.82 eV, shown by the orange arrow. It is assigned to a Rydberg state converging to CF_4^+ $\tilde{D}\,^2A_1$.

Figure 8 : Cross sections for anion production following photoexcitation of SF_5CF_3. Ion yields were recorded as a function of photon energy between 10.5 and 35.0 eV with a step size of 0.1 eV and a wavelength resolution of 0.6 nm. Solid red arrows in spectra (a) – (f) show enthalpy values of the thermochemical thresholds calculated for reactions (12) – (17), respectively.

Figure 9 : Cross sections for anion production following photoexcitation of SF_5CF_3. The SF_5^- spectrum cannot be put onto an absolute scale. Ion yields were recorded as a function of photon energy between 10.5 and 35.0 eV with a step size of 0.1 eV and a wavelength resolution of 0.6 nm. The ion yields are compared with the threshold photoelectron spectrum (shown in red) of SF_5CF_3 [42].

Figure 10 : Valence molecular orbitals assigned to energy maxima of features (indicated by solid lines with numeric values, in eV) observed in experimental photoelectron spectra for SF_6 [40,41] and SF_5Cl [68,69], and the correlation between the orbitals. Orbitals in parenthesis are thought to lie close in energy but have not yet been resolved in experimental spectra.

Figure 11 : Cross section for F^- formation from SF_5Cl. (a) Spectrum from 12 to 30 eV recorded with a step size of 0.05 eV and a wavelength resolution of 0.6 nm. (b) Spectrum from 12.5 to 15.0 eV recorded with a step size of 0.005 eV and a wavelength resolution of 0.12 nm. (c) An expansion of (a) between 15 and 26 eV. All of the observable features in the F^- cross section are labelled 1-8 in spectra (b) and (c), see Section 6.1 of text.

Figure 12 : The observation of Cl^- anions following photoexcitation of SF_5Cl in the range 8 to 15 eV. The spectrum was recorded with a step size of 0.1 eV and a wavelength resolution of 0.6 nm. The spectrum could not be put onto an absolute scale, but the cross section is probably less than *ca.* 10^{-22} cm^2.

Figure 13 : Cross sections for F^- production following photoexcitation of (a) CF_3Cl, and (b) CF_3Br between 12 and 32 eV. The total photoabsorption spectra [75], threshold photoelectron spectra [77], and total fluorescence yields [75] for CF_3Cl and CF_3Br are included for comparative purposes. (c) Cross section for F^- production following photoexcitation of CF_3I between 8 and 32 eV. The threshold photoelectron spectrum [80] and total fluorescence yield [75] are included. All F^- ion yields were recorded with a step size of 0.1 eV and a wavelength resolution of 0.6 nm. This resolution is equivalent to *ca.* 0.2 eV at 20 eV.

Figure 14 : (a) Cross section for Cl^- production following photoexcitation of CF_3Cl in the energy range 12-34 eV. The total photoabsorption spectrum [75], threshold photoelectron spectrum [77], and total fluorescence yield [75] for CF_3Cl are included for comparative purposes. The Cl^- ion yield was recorded with a step size of 0.1 eV and a wavelength resolution of 0.6 nm. (b) Cross section for Br^- production following photoexcitation of CF_3Br between 12 and 28 eV, with the threshold photoelectron spectrum superimposed on top [77]. (c) I^- ion yield recorded following photoexcitation of CF_3I between 8 and 28 eV, with the 8–12 eV range expanded by a factor of 30. The threshold photoelectron spectrum [80] is superimposed on top of the I^- ion yield. The anion spectra cannot be put onto an absolute scale because the signals are shown to change non-linearly with pressure. The peak at 9.0 eV in the I^- spectrum, however, can only result from ion-pair formation and the cross section at this energy is 3.8×10^{-21} cm^2.

Figure 15 : Absolute cross sections for F^-, CF^-, CHF^- and CH_2F^- production following vacuum-UV photoexcitation of CH_3F. Ion yields were measured between 12 and 32 eV at a wavelength resolution of 0.6 nm. Solid arrows show the energies of the thermochemical thresholds calculated for all possible dissociation reactions. The relevant channels to the text are (1) corresponding to formation of $F^- + CH_3^+$, (7) to formation of $CHF^- + H^+ + H$, and (8) to formation of $CH_2F^- + H^+$.

Figure 16 : Absolute cross sections for Cl^- and CH_2Cl^- production following vacuum-UV photoexcitation of CH_3Cl. Ion yields were measured between 8 and 34 eV at a wavelength resolution of 0.6 nm. Solid arrows (9) and (12) show the energies of the thermochemical thresholds calculated for formation of $Cl^- + CH_3^+$ and $CH_2Cl^- + H^+$, respectively.

Figure 17 : Relative (H^-) and absolute (Br^-, $CHBr^-$, CH_2Br^-) cross sections for anion production following vacuum-UV photoexcitation of CH_3Br. Ion yields were measured at a wavelength resolution of 0.6 nm. Solid arrows (13), (16) and (21) show the energies of the thermochemical thresholds calculated for formation of $H^- + CH_2Br^+$, $Br^- + CH_3^+$ and $CH_2Br^- + H^+$, respectively.

Figure 18 : The threshold region for production of Y^- from CH_3Y recorded with a stepsize of 0.005 eV and a wavelength resolution of 0.2 nm, corresponding to *ca.* 0.02 eV at 12 eV. Absolute cross sections are not shown because the calibration signals of F^- from CF_4 and SF_6 were not measured at this resolution. (i) and (ii) show the energies of the adiabatic and vertical ionisation energy of the first photoelectron band of CH_3F [85]. (iii) shows the energy of the adiabatic ionisation energy of the first band of CH_3Cl, ionisation to CH_3Cl^+ $\tilde{X}$ ^2E where the spin-orbit splitting is very small, 0.027 eV [85]. (iv) and (v) show the energies of the adiabatic ionisation energy of the two spin-orbit components of CH_3Br^+ $\tilde{X}$ $^2E_{3/2}$ and $^2E_{1/2}$ where the spin-orbit splitting is much larger, 0.320 eV [86].

Figure 19 : Relative cross sections for production of Y^- from CH_3Y between 14 and 28 eV recorded at a resolution of 0.6 nm. The arrows show the vertical ionisation energies of the fourth photoelectron band, ionisation to $\tilde{C}$ $^2A_1$. A progression with

approximate spacing of 0.27 eV is observed in feature 3 of the Cl^- / CH_3Cl spectrum, probably corresponding to vibrational structure in the $(2a_1)^{-1}4s$ Rydberg state of CH_3Cl [88].

Figure 20： Cross section for formation of H^- from C_2H_4 in the range 12–35 eV. The spectrum was recorded with a wavelength resolution of 0.6 nm and a step size of 0.05 eV. The appearance energy, 13.06 eV, was determined from a higher-resolution scan, recording the onset region with a resolution of 0.2 nm and a step size of 0.02 eV.

Figure 21： Cross section for formation of H^- from C_2H_6. **(a)** in the range 12–30 eV with a step size of 0.05 eV and a resolution of 0.6 nm; **(b)** in the range 18–21 eV with a step size of 0.01 eV and a wavelength resolution of 0.12 nm. The appearance energy, 12.00 eV, was determined from a higher-resolution scan, recording the onset region with a wavelength resolution of 0.3 nm and a step size of 0.02 eV.

Figure 22： Cross section for formation of H^- from C_3H_8. **(a)** in the range 12–28 eV with a step size of 0.05 eV and a resolution of 0.6 nm; **(b)** two separate scans covering the range 12–24 eV at improved resolution, from 12.0–17.5 eV recorded with a step size of 0.02 eV and a wavelength resolution of 0.2nm, and from 16–24 eV recorded with a step size of 0.01 eV and a resolution of 0.12 nm. The appearance energy, 13.2 eV, is indicated.

Figure 23： Yields of anions from VUV photoexcitation of C_2F_4: (a) F^- absolute cross sections in the range 13–32 eV, the scan recorded with a step size of 0.05 eV and a wavelength resolution of 0.6 nm; (b) three higher-resolution F^- scans covering the range 12.7–20.4 eV, all with a step size of 0.01 eV and a resolution of 0.2 nm. The appearance energy of F^-, 13.17 eV, is indicated. (c) Yield of CF^- in the range 21–32 eV recorded with a step size of 0.1 eV and a resolution of 0.6 nm.

Figure 24： Cross section for formation of F^- from C_2F_6 in the range 13–32 eV with a step size of 0.02 eV and a wavelength resolution of 0.2 nm. The appearance energy, 13.62 eV, is indicated.

Figure 25： Yield of anions from photoexcitation of C_3F_8: (a) F^- absolute cross sections in the range 12–30 eV, the scan recorded with a step size of 0.05 eV and a wavelength resolution of 0.6 nm; (b) F^- spectrum covering the range 19.5–22.5 eV range with a step size of 0.01 eV and a resolution of 0.12 nm; (c) F^- spectrum covering the range 22.5–26.0 eV range with a step size of 0.01 eV and a resolution of 0.12 nm. The appearance energy of F^-, 13.1 eV, is indicated. (d) Yield of CF_2^- in the range 19–26 eV recorded with a step size of 0.1 eV and a resolution of 0.6 nm.

Figure 26： Ion yields for anions observed following photoexcitation of CH_2F_2. **(a)** H^- ion yield in the range 11.5–30.0 eV recorded with a step size of 0.02 eV and a wavelength resolution of 0.2 nm. Due to the zero blast effect in the quadrupole mass spectrometer, the signal detected at this *m/z* value of 1 may also contain contributions from other ions present (*i.e.* F^- and F_2^-). An

absolute cross section cannot therefore be determined, and it is possible that the observed features do not all result exclusively from H^- anions. **(b)** Higher-resolution scan of H^- covering the range 12.0–13.7 eV recorded with a step size of 0.005 eV and a resolution of 0.1 nm. A similar scan of the peak at 12.56 eV in the F^- spectrum was structureless and did *not* reproduce that in (b) for H^-. **(c)** Yield and cross section for F^- in the range 11.5–30.0 eV recorded with a step size of 0.02 eV and a resolution of 0.2 nm. **(d)** Yield and cross section for F_2^- in the range 16.5–25.5 eV recorded with a step size of 0.02 eV and a resolution of 0.2 nm. For all three anions, the appearance energies are indicated.

Figure 27 : Ion yields for anions observed following photoexcitation of CHF_3. The appearance energies of H^- and CF_3^- are indicated. **(a)** H^- ion yield in the photon energy range 12–25 eV recorded with a step size of 0.02 eV and a wavelength resolution of 0.3 nm. As in Figure 26, the signal at *m/z* 1 may also contain contributions from other ions present (*i.e.* F^- and CF_3^-), so the absolute cross section values cannot be determined. **(b)** Yield and cross section for F^- in the range 12–25 eV recorded in four separate scans: (i) dotted line, 12.0–15.3 eV, with a step size of 0.1 eV and a resolution of 0.6 nm; (ii) solid line, 15.3–18.1 eV, with a step size of 0.01 eV and a resolution of 0.2 nm; (iii) solid line, 18.4–22.3 eV, with a step size of 0.01 eV and a resolution of 0.16 nm; (iv) solid line, 22.8–24.4 eV with a step size of 0.005 eV and a resolution of 0.12 nm. The rise in signal of F^- for $h\nu <$ 12.4 eV arises from second order radiation, since a scan from 8–12 eV using a LiF window showed only background signal. **(c)** Yield and cross section for CF_3^- in the range 12–27 eV recorded with a step size of 0.1 eV and a resolution of 0.6 nm.

Figure 28 : Ion yields for anions observed following photoexcitation of CH_2Cl_2. **(a)** H^- ion yield in the range 11–30.0 eV recorded with a step size of 0.02 eV and a wavelength resolution of 0.2 nm. As in Figures 26 and 27, the H^- signal may also contain contributions from other ions present (*i.e.* Cl^- and Cl_2^-), so its absolute cross section cannot be determined. **(b)** Yield and cross section for Cl^- in the range 9–30 eV recorded with a step size of 0.02 eV and a resolution of 0.2 nm. **(c)** Higher-resolution Cl^- scan from 9.0–12.5 eV recorded with a step size of 0.01 eV and a resolution of 0.12 nm. **(d)** Yield and cross section for Cl_2^- in the range 12–18 eV recorded with a step size of 0.02 eV and a resolution of 0.2 nm. For all three anions, the appearance energies are indicated.

Figure 29 : Ion yields for anions observed following photoexcitation of $CHCl_3$. **(a)** Three separate scans are merged to generate the H^- ion yield: (i) from 8–15 eV with a step size of 0.05 eV and a wavelength resolution of 0.6 nm; (ii) from 15.0–19.5 eV with a step size of 0.02 eV and a resolution of 0.2 nm; (iii) from 19.5–32.0 eV with a step size of 0.05 eV and a resolution of 0.6 nm. The H^- signal may contain contributions from other ions present (*i.e.* CH^-, Cl^- and CCl^-). **(b)** Yield and cross section for Cl^- in the range 8–32 eV generated by merging three scans: (i) from 8.60–10.64 eV with a step size of 0.02 eV and a resolution of 0.4 nm; (ii) from 10.65–16.80 eV with a step size of 0.05 eV and a resolution of 0.6 nm; (iii) from 16.85–32.00 eV with a step size of 0.05 eV and a resolution of 0.6 nm. **(c)** Yield and cross section for CH^- in the range 20–32 eV recorded with a step size of 0.05 eV and a resolution of 0.6 nm. **(d)** Yield and cross section for CCl^- in the range 14–32 eV recorded with a step size of 0.1 eV and a resolution of 0.6 nm. For all four anions, the appearance energies are indicated.

Figure 30 : Ion yields for anions observed following photoexcitation of CCl_4. **(a)** Three scans have been merged to generate the Cl^- ion yield: (i) from 10.5–17.2 eV with a step size of 0.01 eV and a wavelength resolution of 0.2 nm; (ii) from 17.2–22.0 eV

with a step size of 0.02 eV and a resolution of 0.2 nm; (iii) from 22–32 eV with a step size of 0.02 eV and a resolution of 0.2 nm. The Cl^- signal at 16.45 *and* 24.9 eV increases non-linearly with gas pressure; absolute cross sections cannot be determined because the formation of Cl^- is dominated by the dissociative electron attachment. **(b)** Threshold photoelectron spectrum of CCl_4 [63], and the similarity of the peak positions with those in the Cl^- ion yield in (a) is noted. **(c)** Yield and cross section for CCl^- in the range 20–32 eV recorded with a step size of 0.05 eV and a resolution of 0.6 nm. For both anions, the appearance energies are indicated.

Figure 31 : Ion yields for anions observed following photoexcitation of CF_2Cl_2. **(a)** Two scans have been merged to generate the yield and cross section for F^-: (i) from 10.0–17.7 eV with a step size of 0.02 eV and a wavelength resolution of 0.2 nm; (ii) from 17.7–30.0 eV with a step size of 0.05 eV and a resolution of 0.6 nm. **(b)** Likewise, two scans have been merged to generate the yield and cross section for Cl^-: (i) from 10.0–12.5 eV with a step size of 0.01 eV and a resolution of 0.2 nm; (ii) from 13.9–32.0 eV with a step size of 0.05 eV and a resolution of 0.6 nm. **(c)** Yield and cross section for CF^- formation in the range 20–30 eV recorded with a step size of 0.1 eV and a resolution of 0.6 nm. For all three anions, the appearance energies are indicated.

Figure 32 : Ion yields for anions observed following photoexcitation of $CFCl_3$. **(a)** Two scans have been merged to generate the Cl^- yield: (i) from 11–16 eV recorded with a step size of 0.02 eV and a wavelength resolution of 0.3 nm, and (ii) from 16–32 eV recorded with a step size of 0.05 eV and a resolution of 0.6 nm. The Cl^- signal at 12.2, 18.2, 21.7 and 25.4 eV in all cases was shown to increase non-linearly with pressure of $CFCl_3$, so absolute cross sections cannot be determined because the formation of Cl^- is dominated by electron attachment attachment. **(b)** Yield and cross section for F^- (which *is* formed by ion-pair formation) from 14–32 eV recorded with a step size of 0.05 eV and a resolution of 0.6 nm.

Figure 33 : (a) The distribution of $(AE_{298} - \Delta_r H°_{298})$ for all anions produced from a single bond-breaking ion-pair dissociation reaction (see Table 10). (b) The sub-set from (a) showing H^-, (c) the sub-set from (a) showing F^- anions. (d) – (g). Data extracted from (a) for methane and the halo-substituted methanes only. CY_n^- in (g) includes data for CF_3^-, CH_2F^-, CH_2Cl^- and CH_2Br^-.

Figure 34 : The F^- and Cl^- cross sections recorded following the VUV photoexcitation of CF_3Cl, taken from Figures 13 and 14. The most intense peak at 21.0 eV with a cross section of $150 * 10^{-22}$ cm^2 corresponds to the F^- channel, the more structured but weaker spectrum to the Cl^- channel. Only the range 14–30 eV is shown. The complete spectra are presented and discussed in Section 6.2.

Figure 1

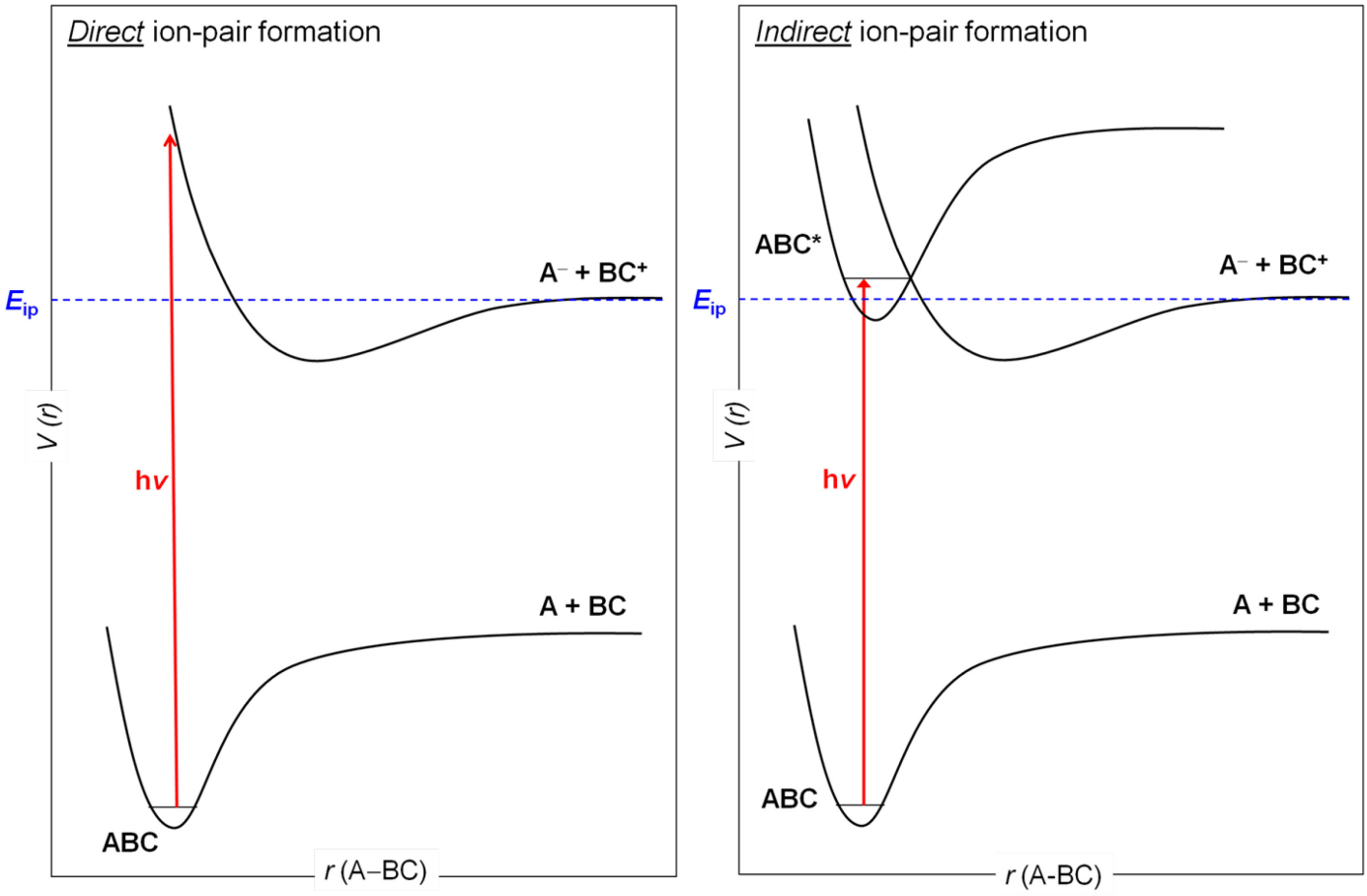
Direct ion-pair formation
A⁻ + BC⁺
E_ip
V (r)
hν
A + BC
ABC
r (A–BC)
Indirect ion-pair formation
ABC*
A⁻ + BC⁺
E_ip
V (r)
hν
A + BC
ABC
r (A-BC)

Figure 2

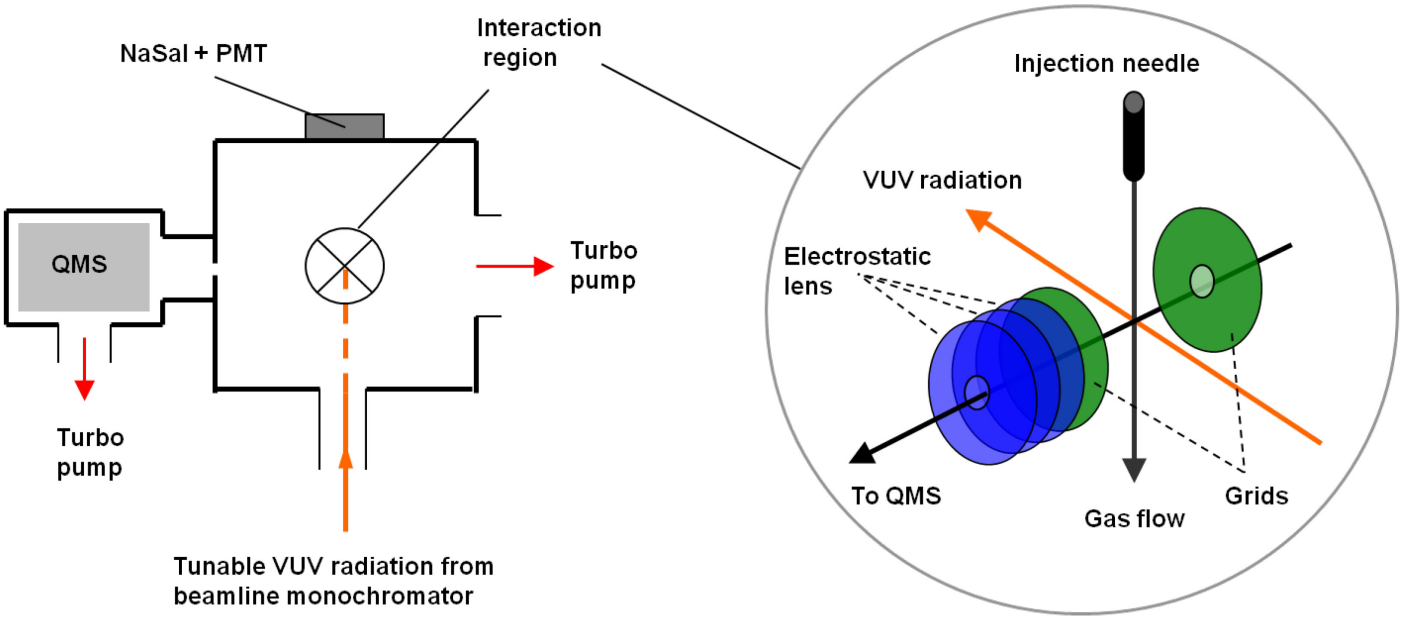
NaSal + PMT
Interaction region
Injection needle
VUV radiation
Electrostatic lens
QMS
Turbo pump
Turbo pump
To QMS
Gas flow
Grids
Tunable VUV radiation from beamline monochromator

Figure 3

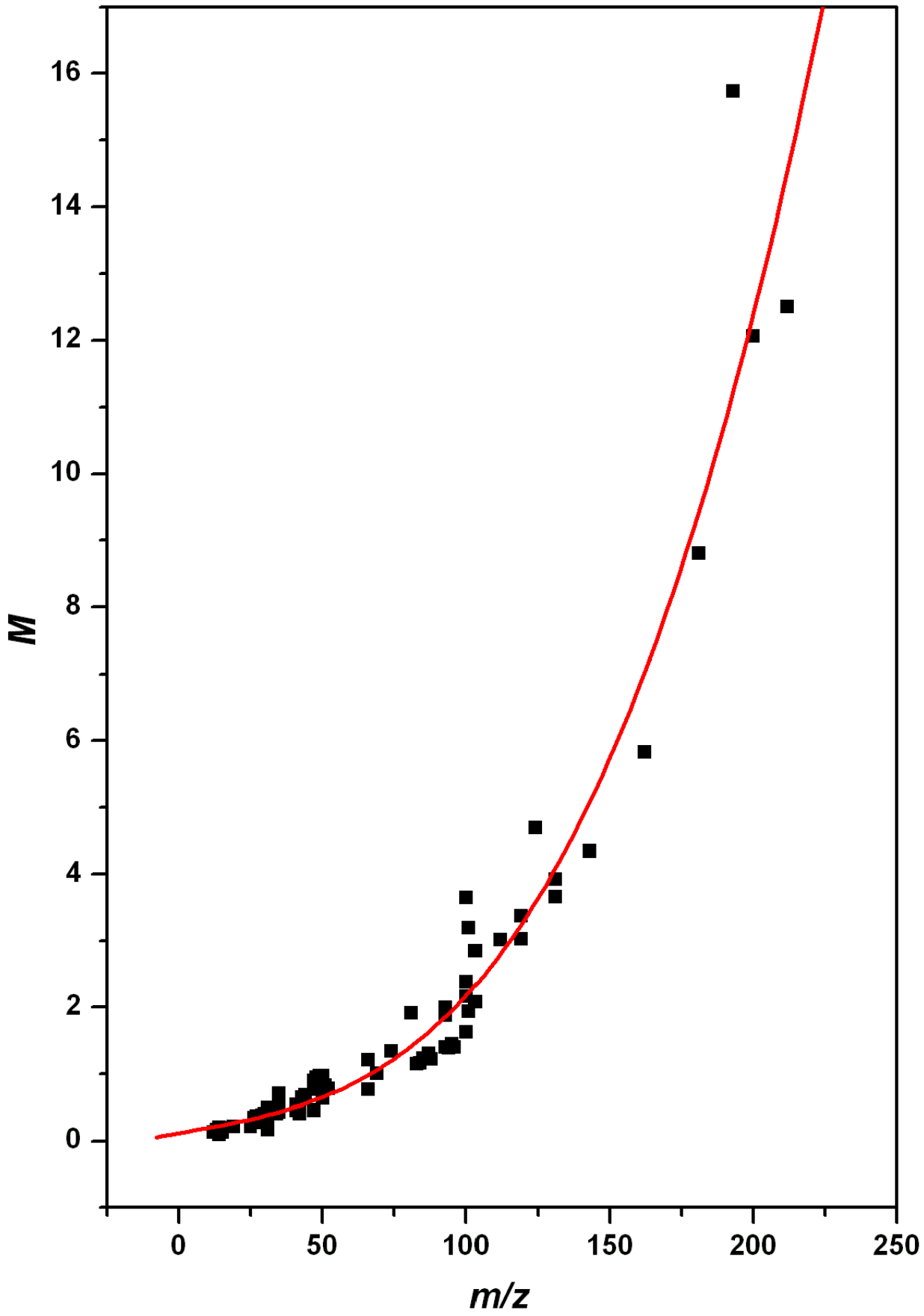

Figure 4

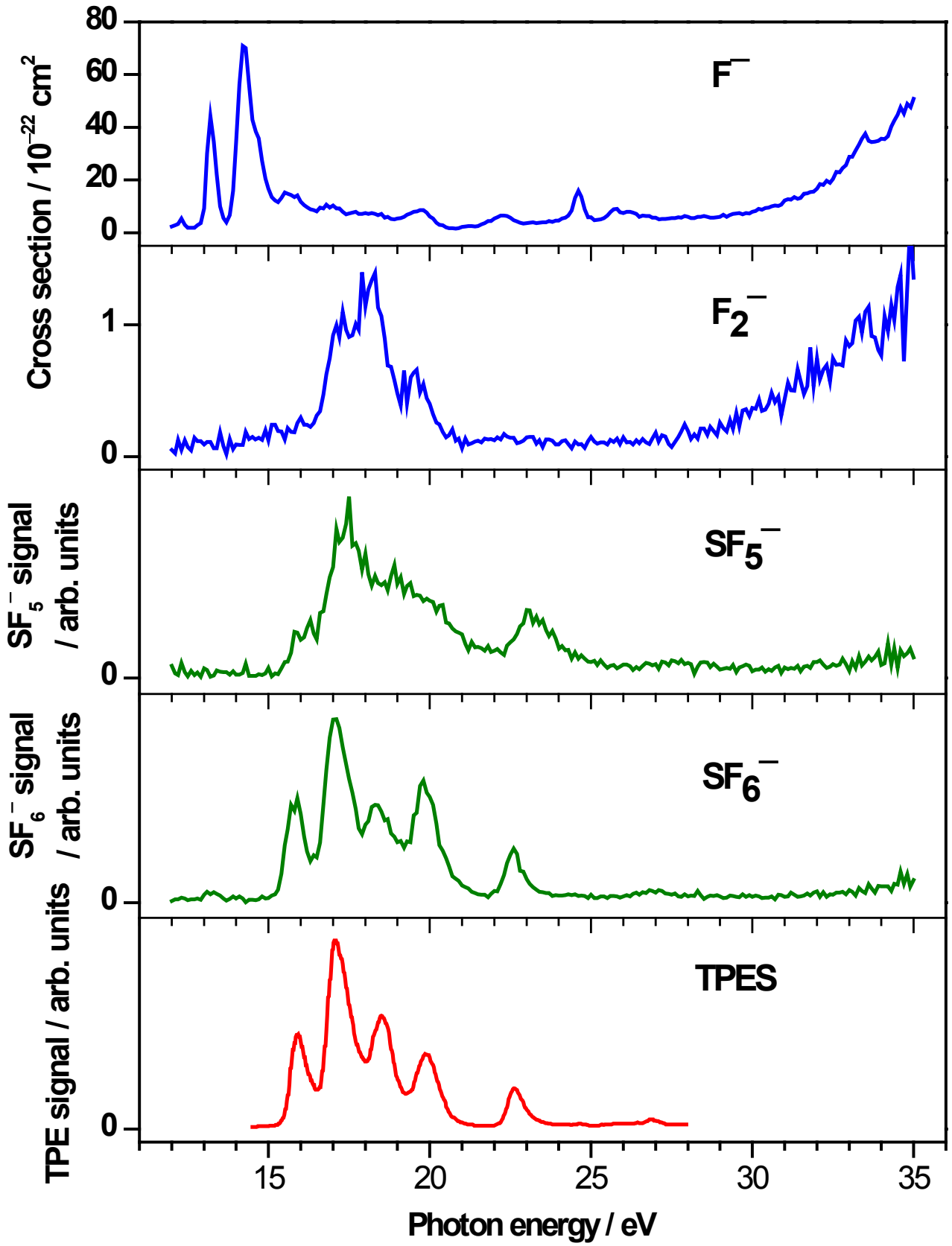
Cross section / 10^{-22} cm^2
80
60
40
20
0
F^-
1
0
F_2^-
SF_5^- signal / arb. units
0
SF_5^-
SF_6^- signal / arb. units
0
SF_6^-
TPE signal / arb. units
0
TPES
15
20
25
30
35
Photon energy / eV

Figure 5

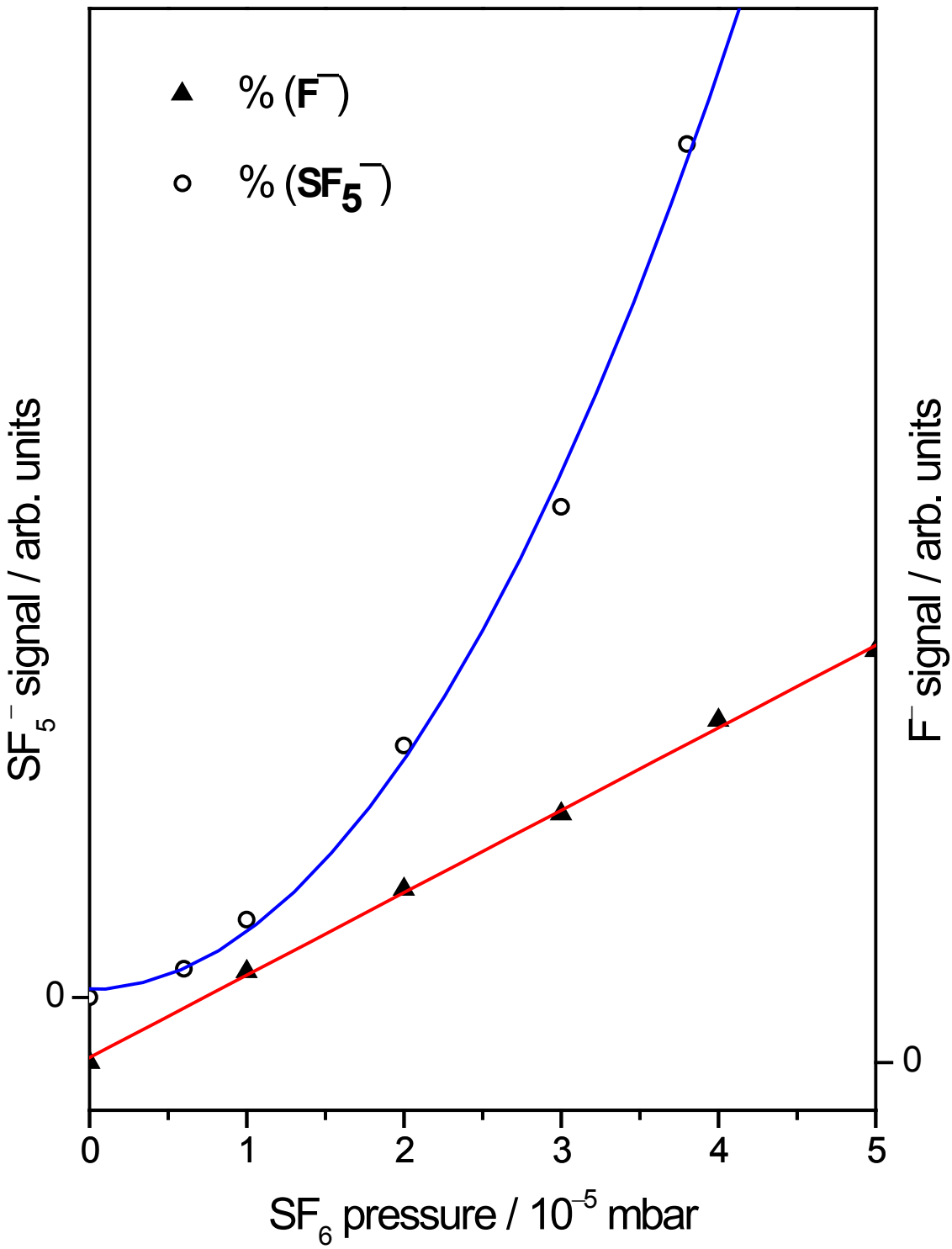
% (F⁻)
% (SF5⁻)
SF5⁻ signal / arb. units
F⁻ signal / arb. units
0
0
0
1
2
3
4
5
SF6 pressure / 10⁻⁵ mbar

Figure 6

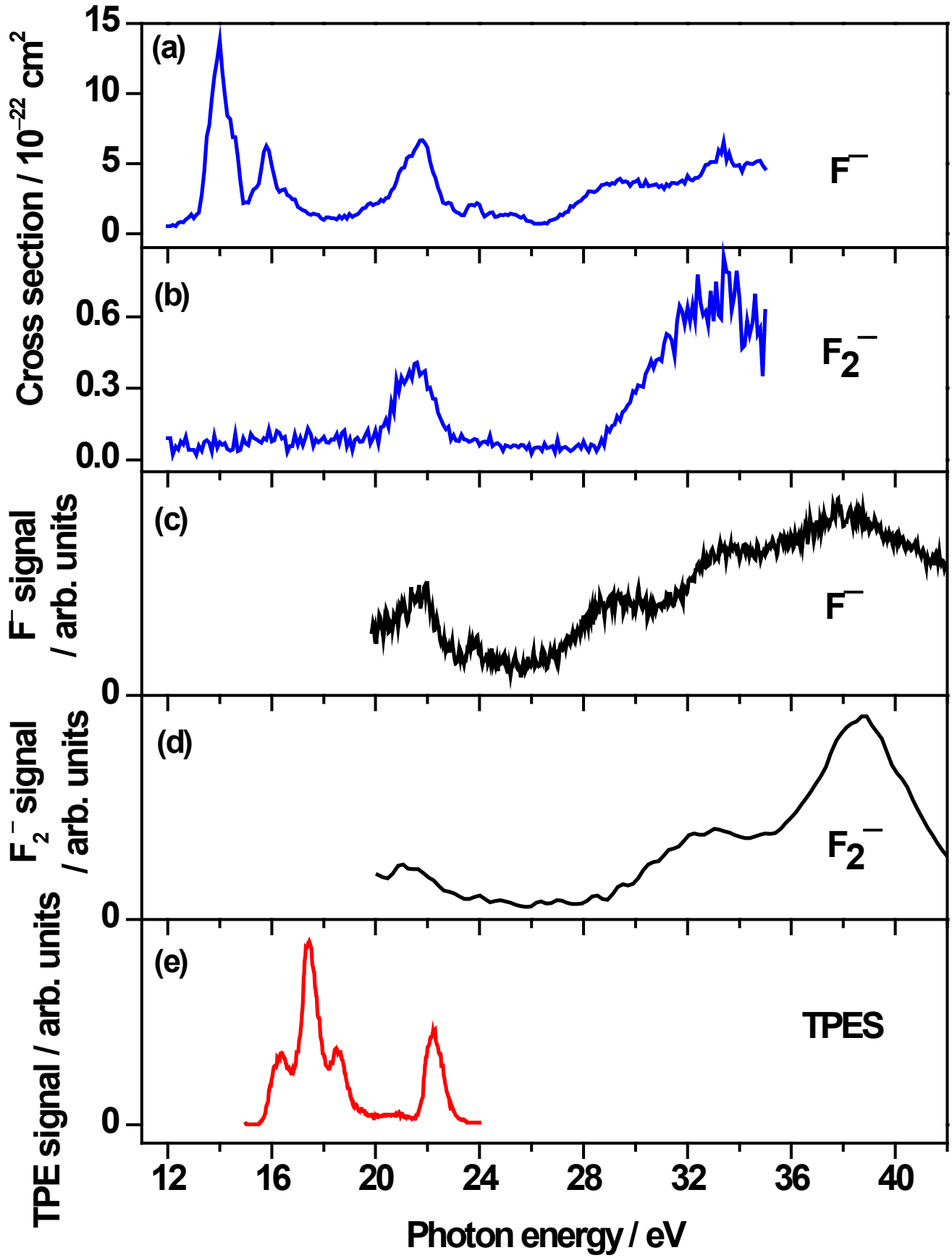
(a)
(b)
(c)
(d)
(e)
F⁻
F₂⁻
F⁻
F₂⁻
TPES
Cross section / 10⁻²² cm²
F⁻ signal / arb. units
F₂⁻ signal / arb. units
TPE signal / arb. units
Photon energy / eV
15
10
5
0
0.6
0.3
0.0
12
16
20
24
28
32
36
40

Figure 7

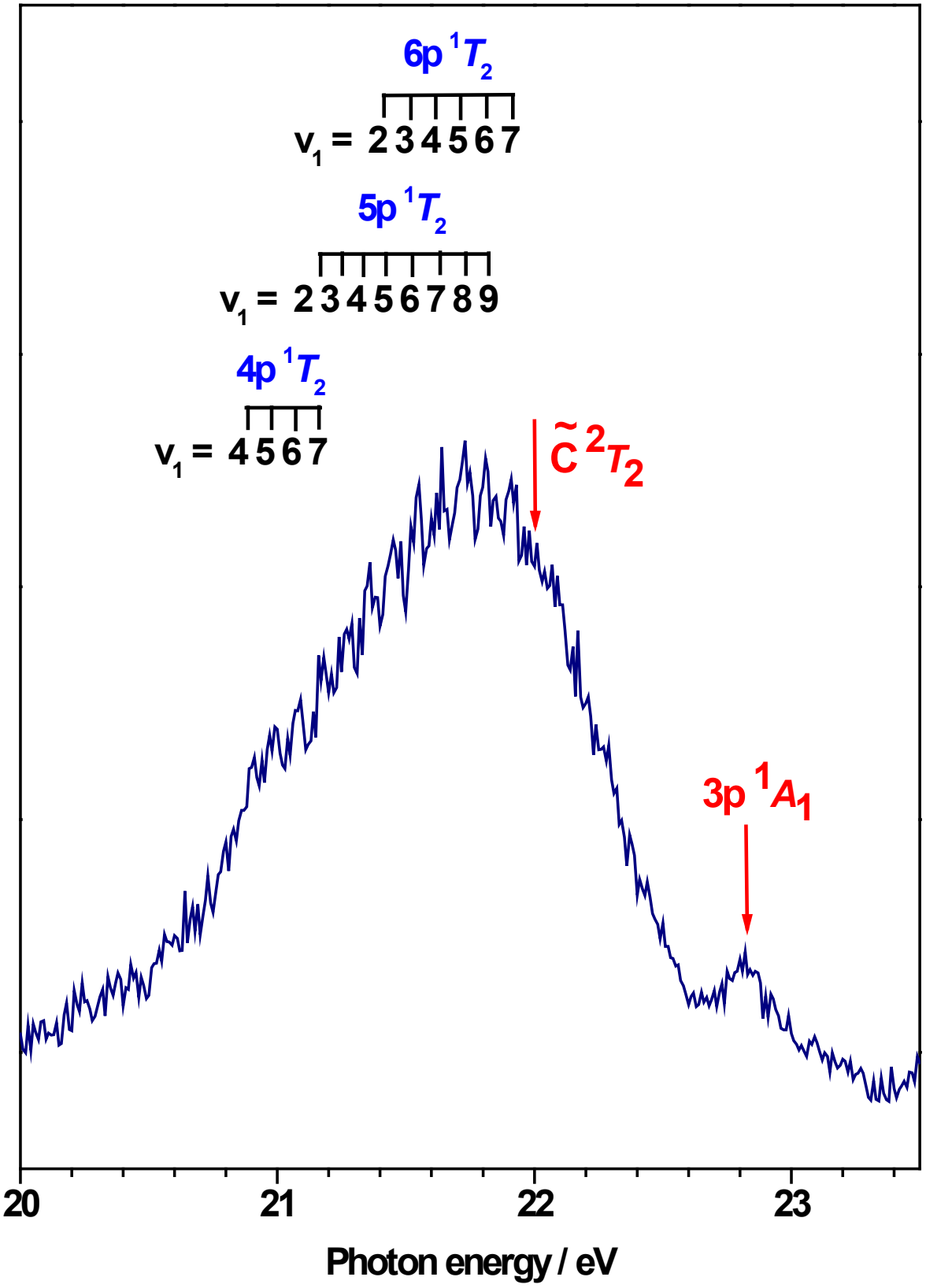
6p $^1T_2$
v_1 = 2 3 4 5 6 7
5p $^1T_2$
v_1 = 2 3 4 5 6 7 8 9
4p $^1T_2$
v_1 = 4 5 6 7
$\tilde{C}\,^2T_2$
3p $^1A_1$
20
21
22
23
Photon energy / eV

Figure 8

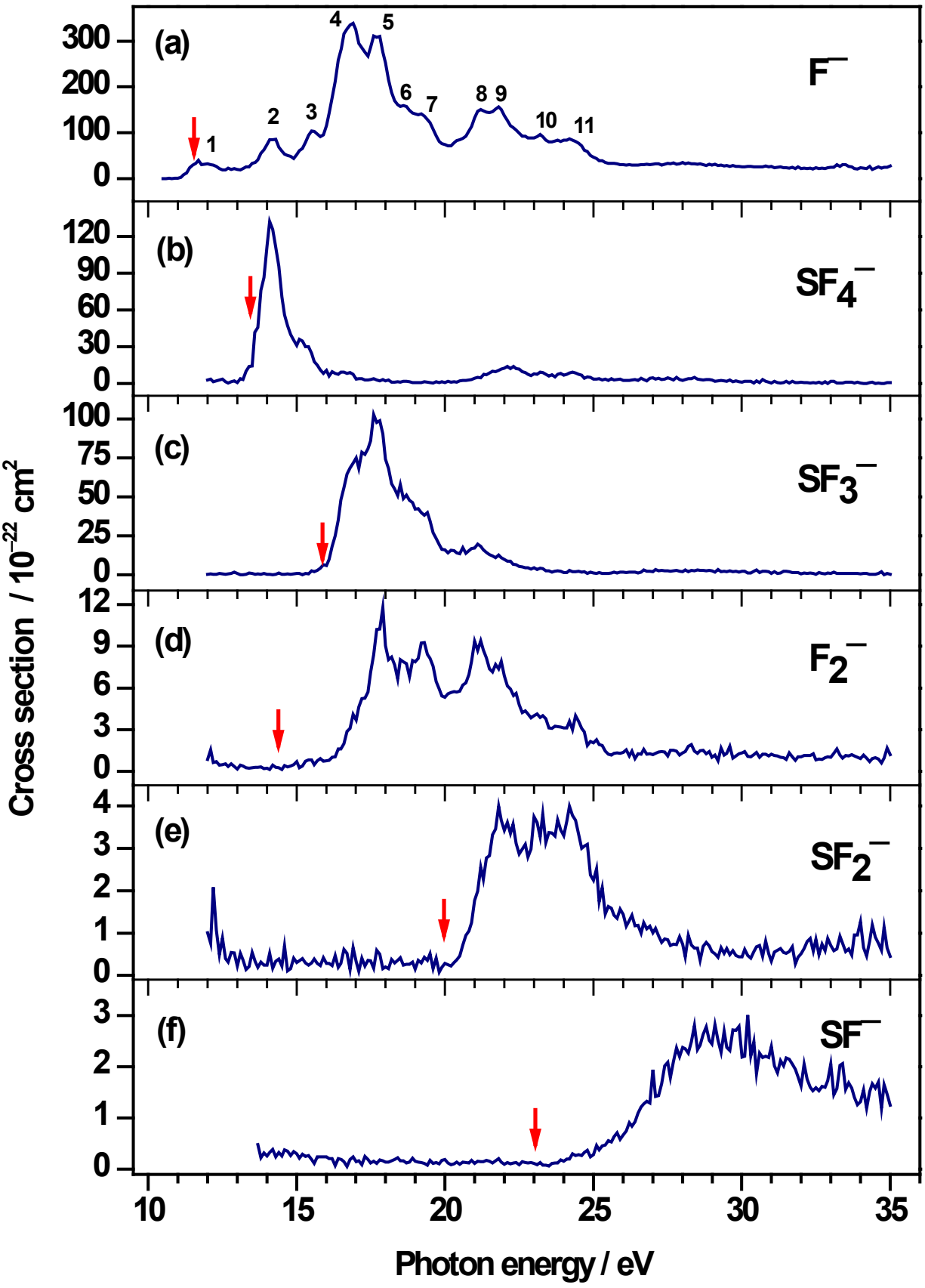
(a)
F⁻
(b)
SF4⁻
(c)
SF3⁻
(d)
F2⁻
(e)
SF2⁻
(f)
SF⁻
1
2
3
4
5
6
7
8
9
10
11
Cross section / 10⁻²² cm²
Photon energy / eV

Figure 9

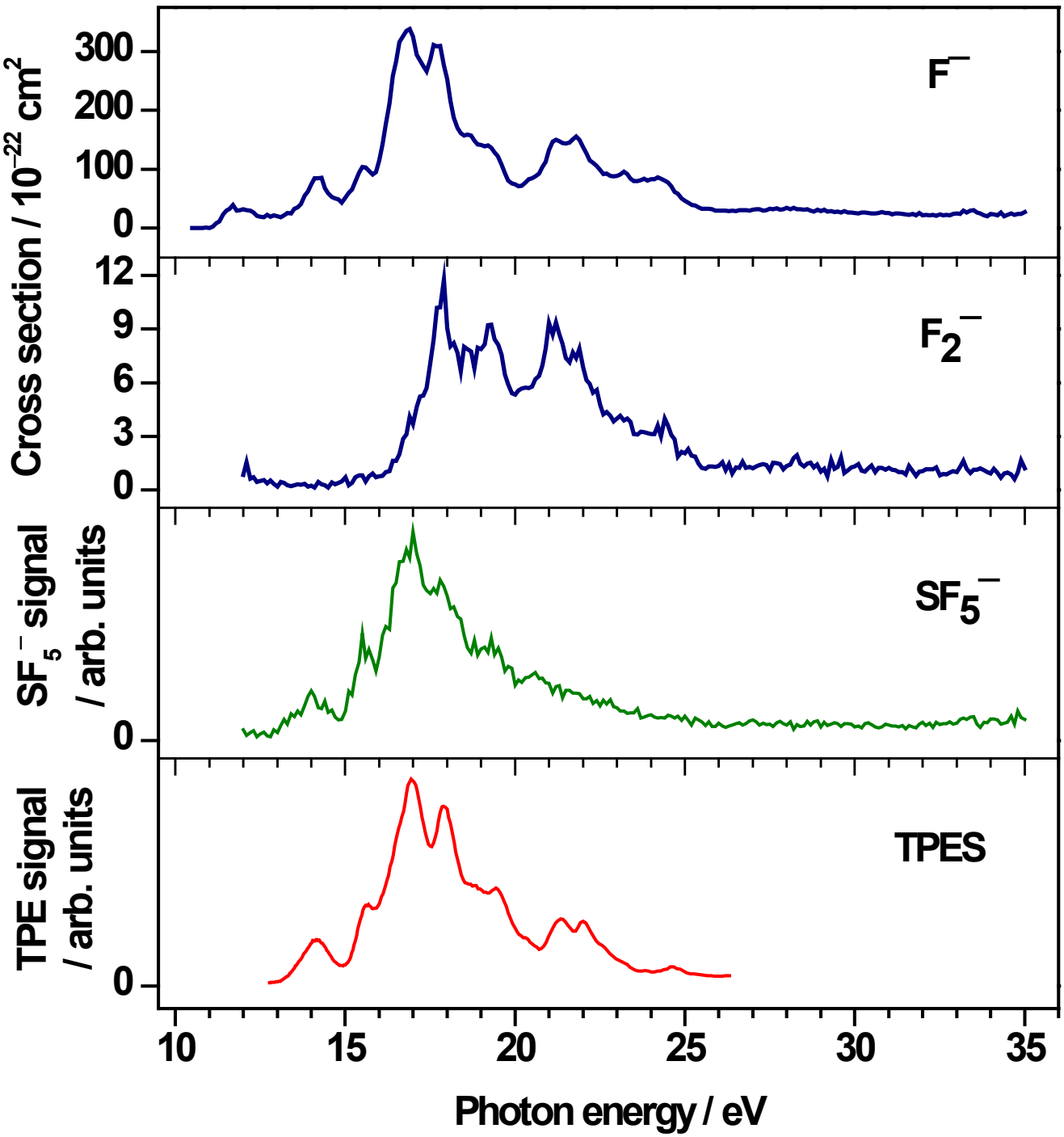
Cross section / 10^{-22} cm^2
300
200
100
0
F^-
12
9
6
3
0
F_2^-
SF_5^- signal / arb. units
0
SF_5^-
TPE signal / arb. units
0
TPES
10
15
20
25
30
35
Photon energy / eV

Figure 10

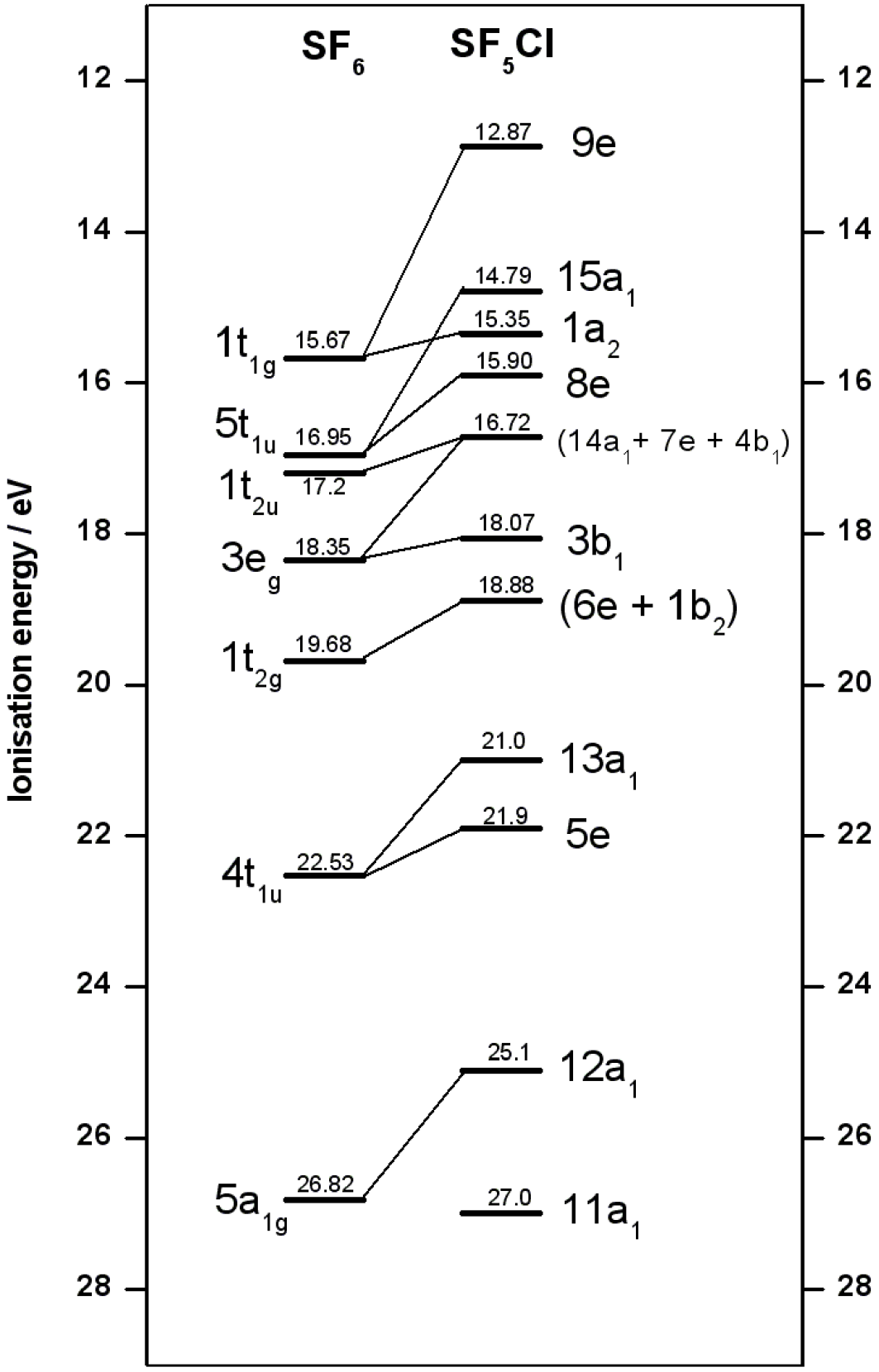
SF6
SF5Cl
Ionisation energy / eV
12
14
16
18
20
22
24
26
28
12.87
9e
14.79
15a1
15.35
1a2
15.67
1t1g
15.90
8e
5t1u
16.95
16.72
(14a1 + 7e + 4b1)
1t2u
17.2
18.07
3b1
3eg
18.35
18.88
(6e + 1b2)
1t2g
19.68
21.0
13a1
21.9
5e
4t1u
22.53
25.1
12a1
5a1g
26.82
27.0
11a1

Figure 11

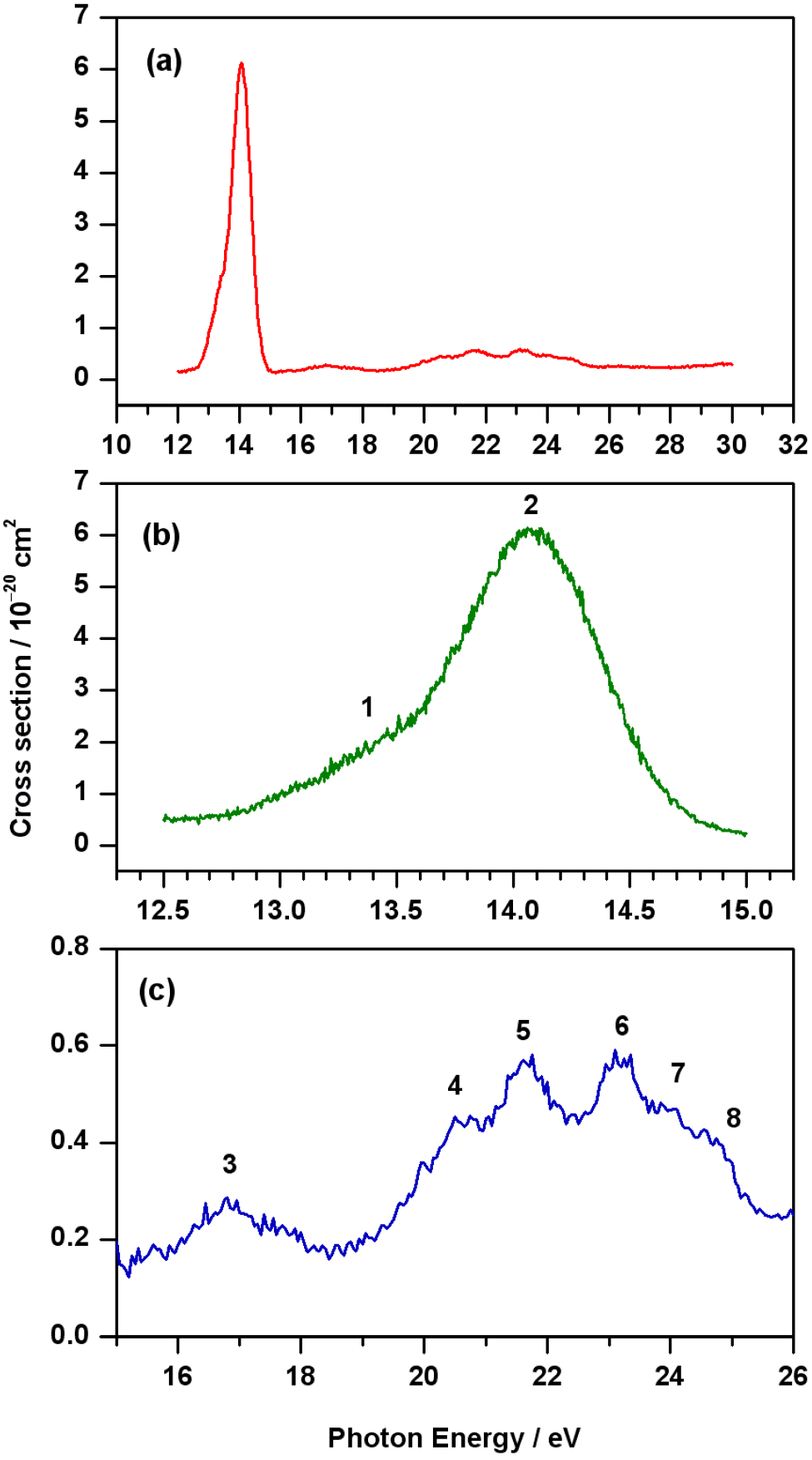

Figure 12

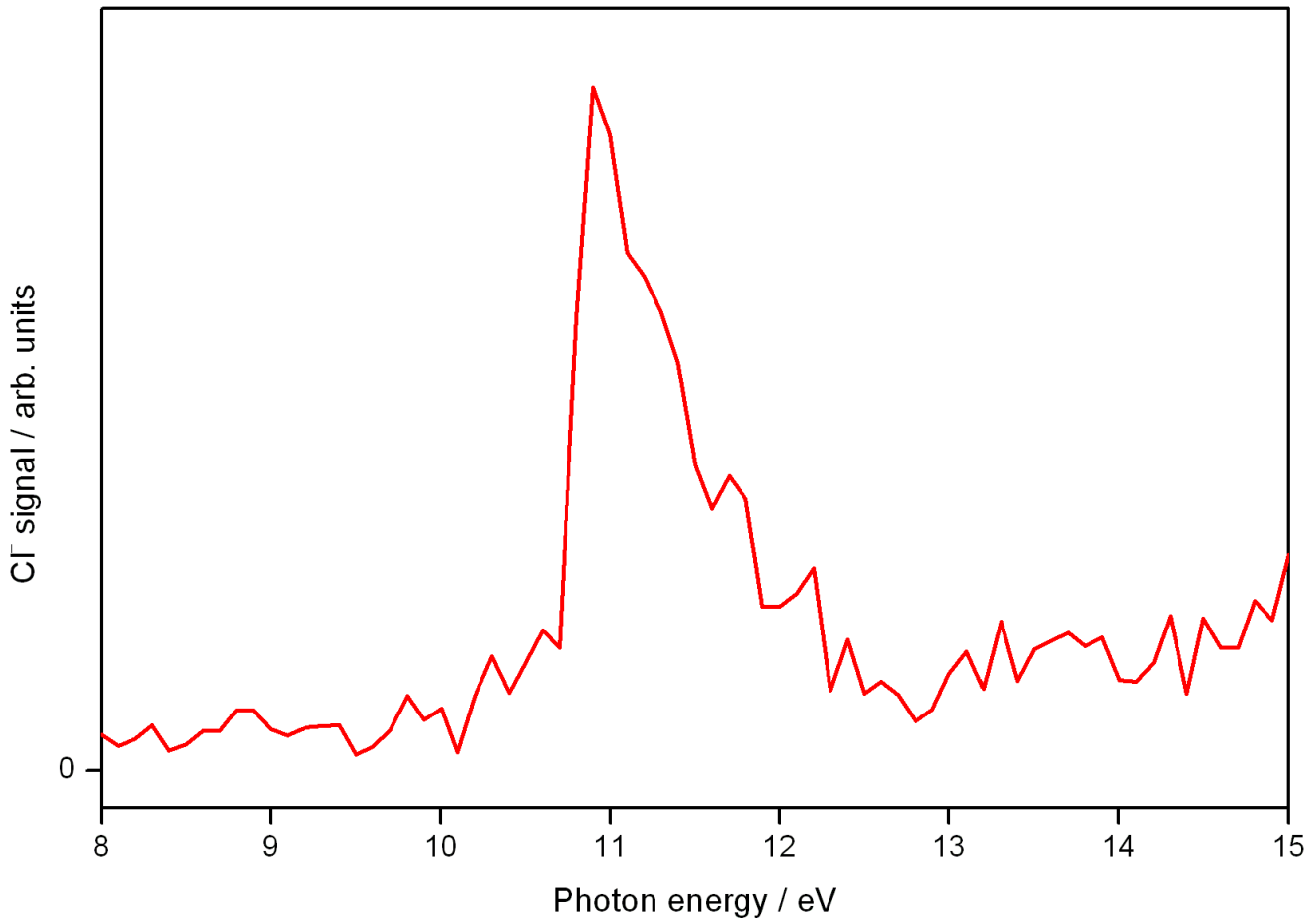

Figure 13

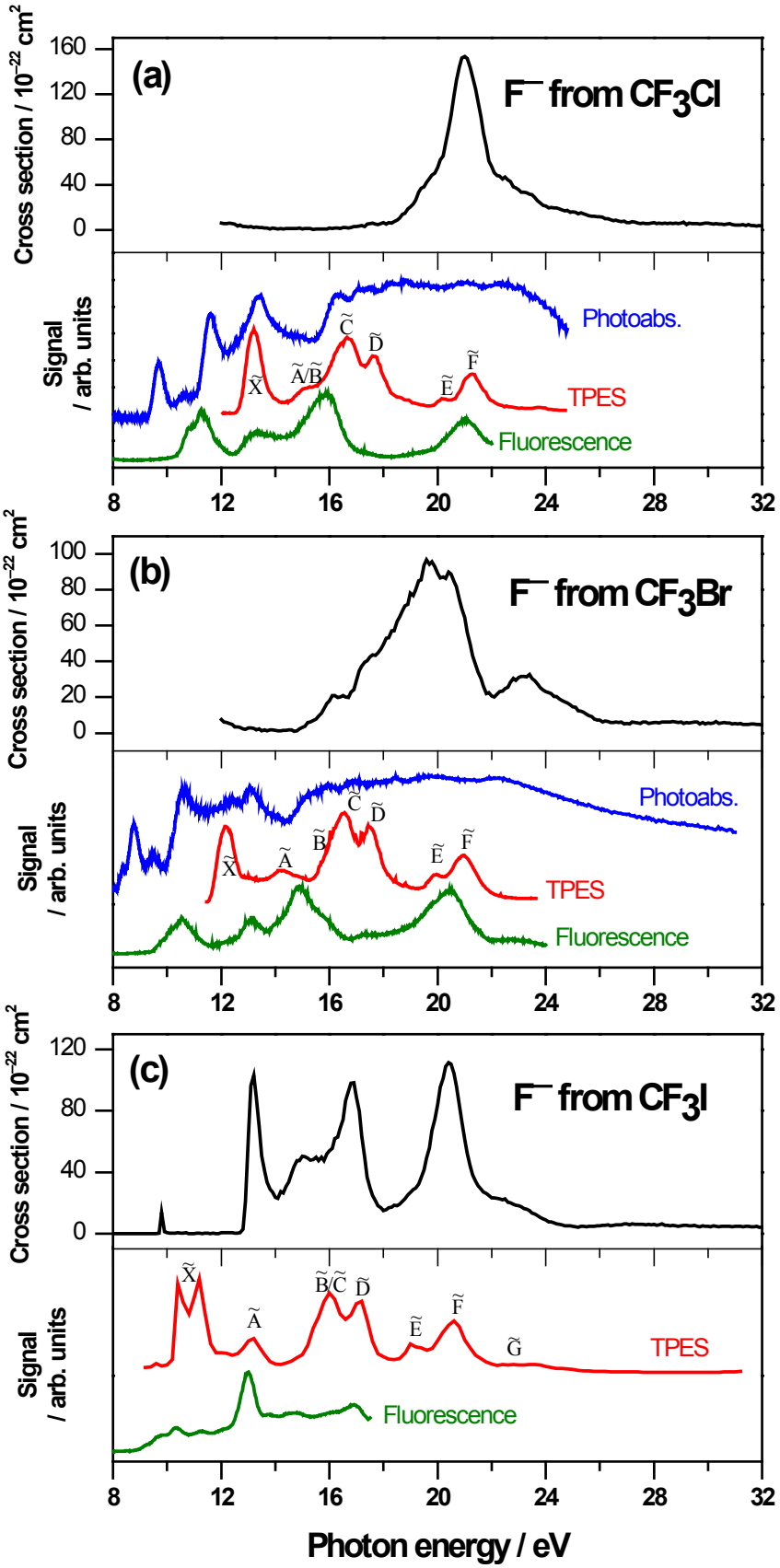
(a)
F⁻ from CF3Cl
Cross section / 10⁻²² cm²
Signal / arb. units
Photoabs.
TPES
Fluorescence
X̃
Ã/B̃
C̃
D̃
Ẽ
F̃
(b)
F⁻ from CF3Br
Ã
B̃
(c)
F⁻ from CF3I
G̃
Photon energy / eV

Figure 14

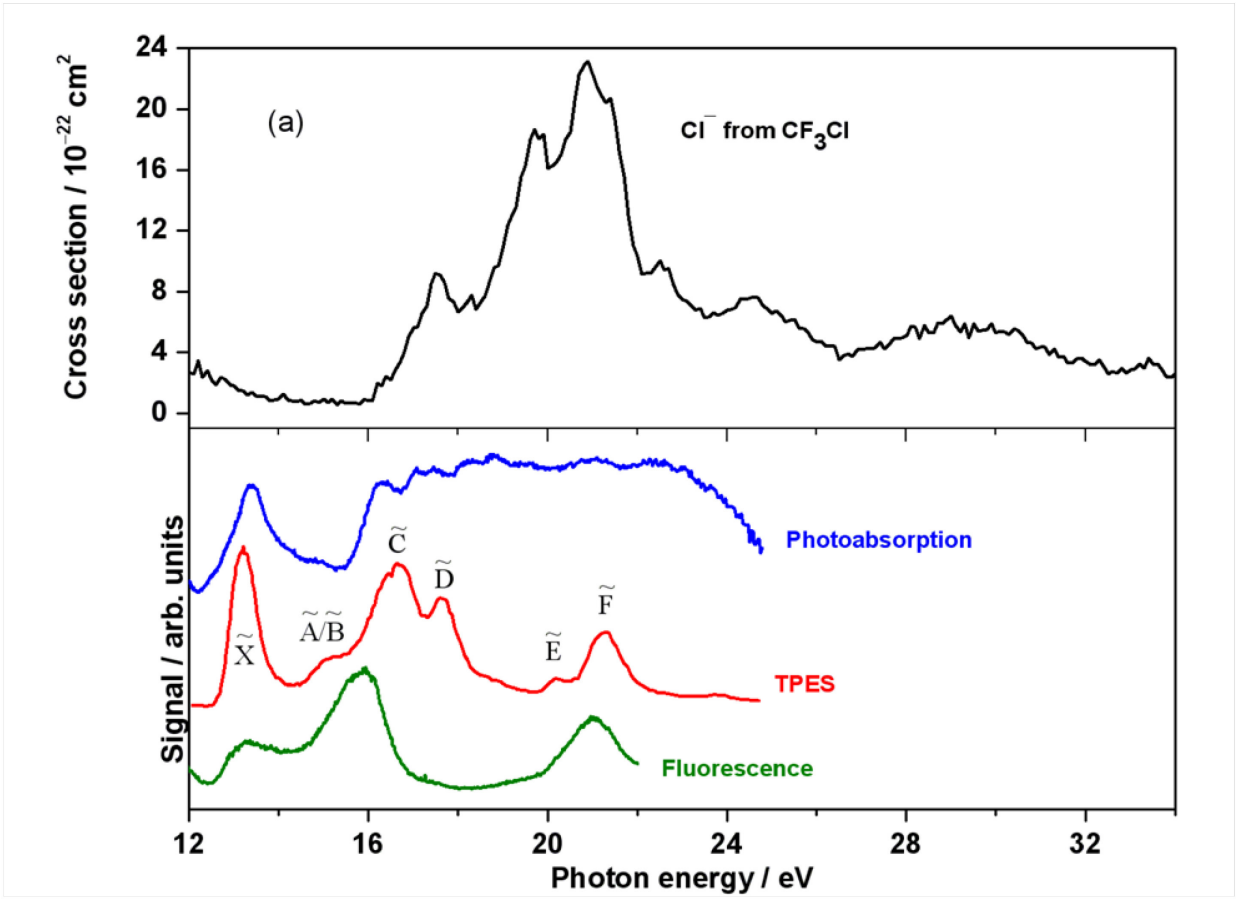
(a)
Cl⁻ from CF3Cl
Cross section / 10⁻²² cm²
Signal / arb. units
Photoabsorption
TPES
Fluorescence
X̃
Ã/B̃
C̃
D̃
Ẽ
F̃
Photon energy / eV

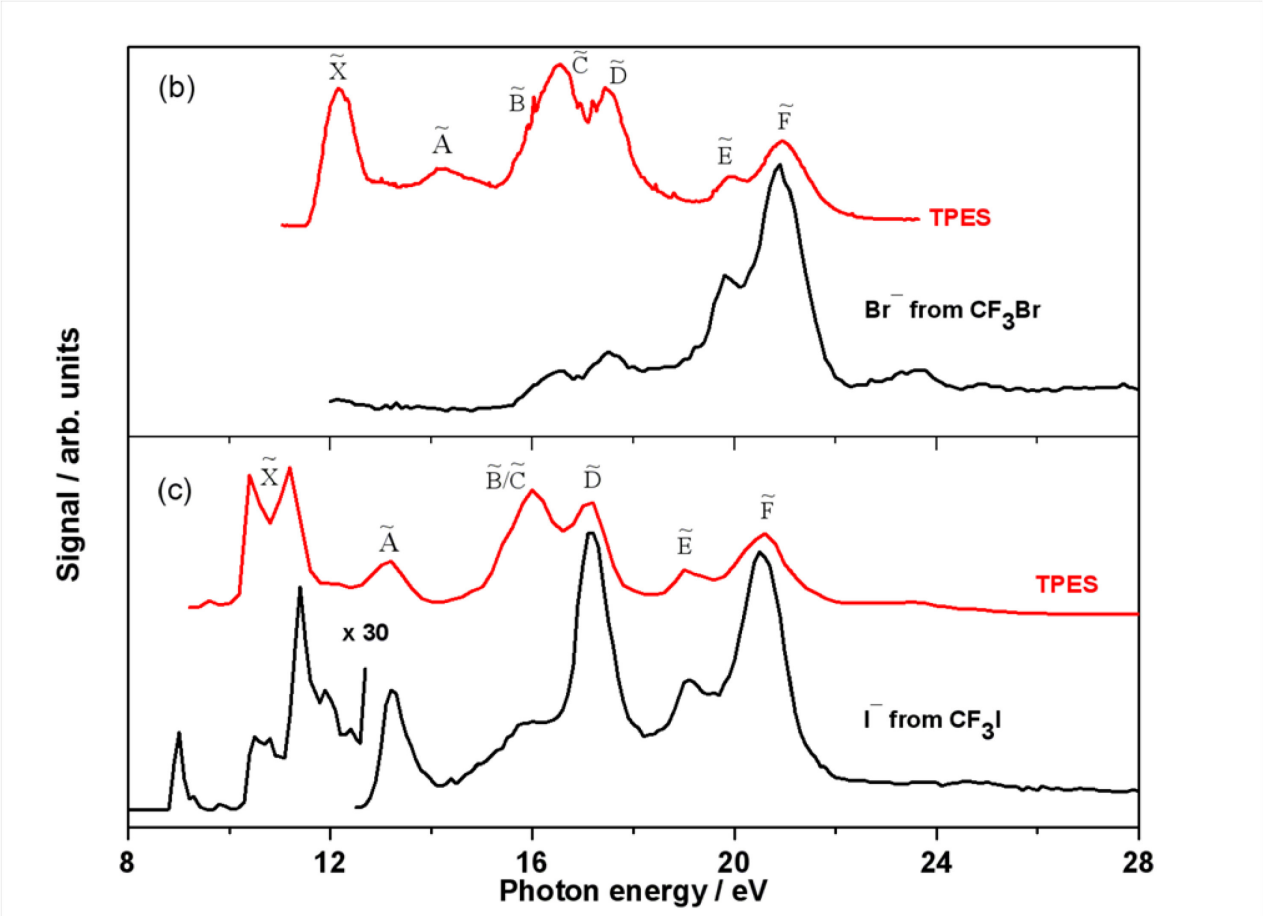
(b)
Br⁻ from CF3Br
TPES
(c)
I⁻ from CF3I
x 30
Signal / arb. units
Photon energy / eV

Figure 15

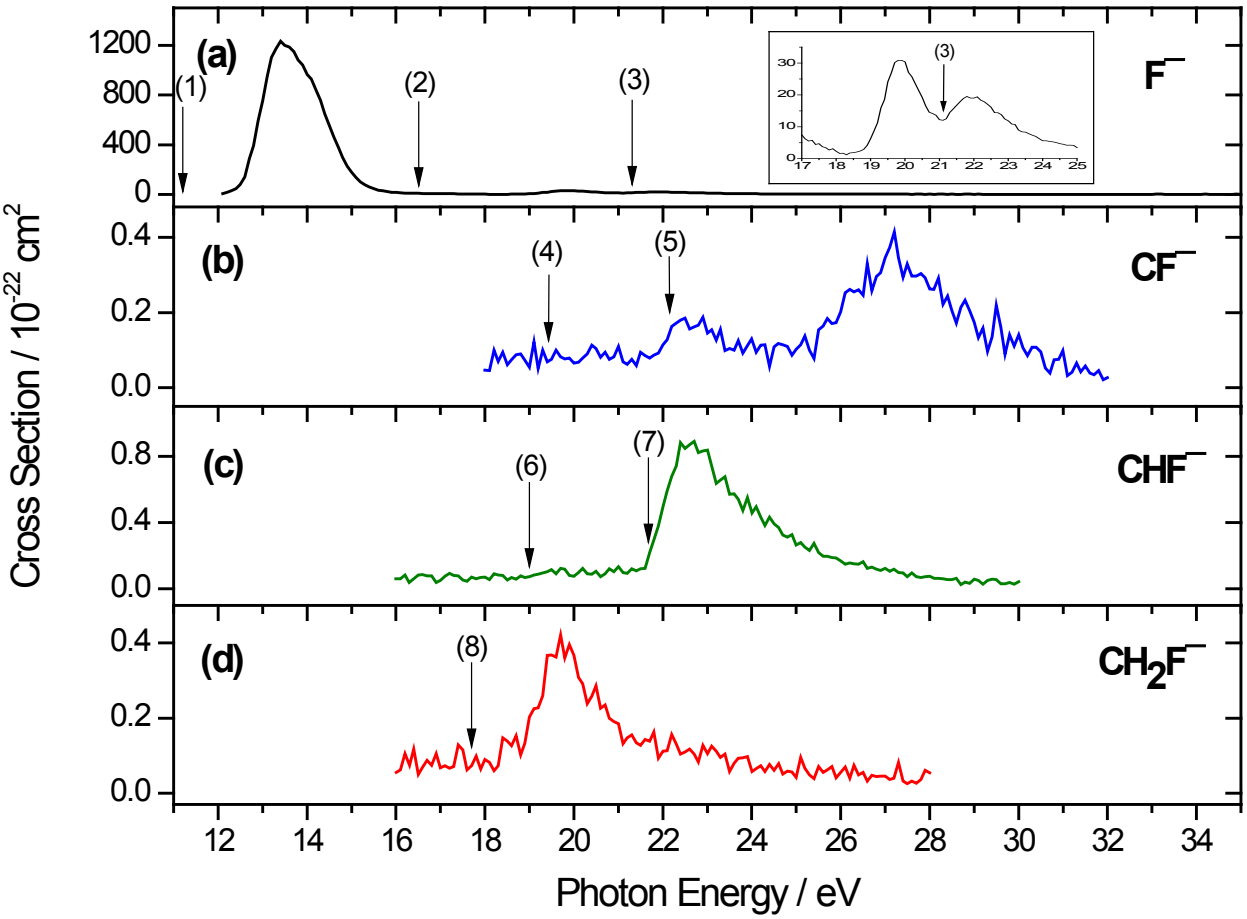
(a)
(b)
(c)
(d)
(1)
(2)
(3)
(4)
(5)
(6)
(7)
(8)
F⁻
CF⁻
CHF⁻
CH2F⁻
Cross Section / 10-22 cm2
Photon Energy / eV

Figure 16

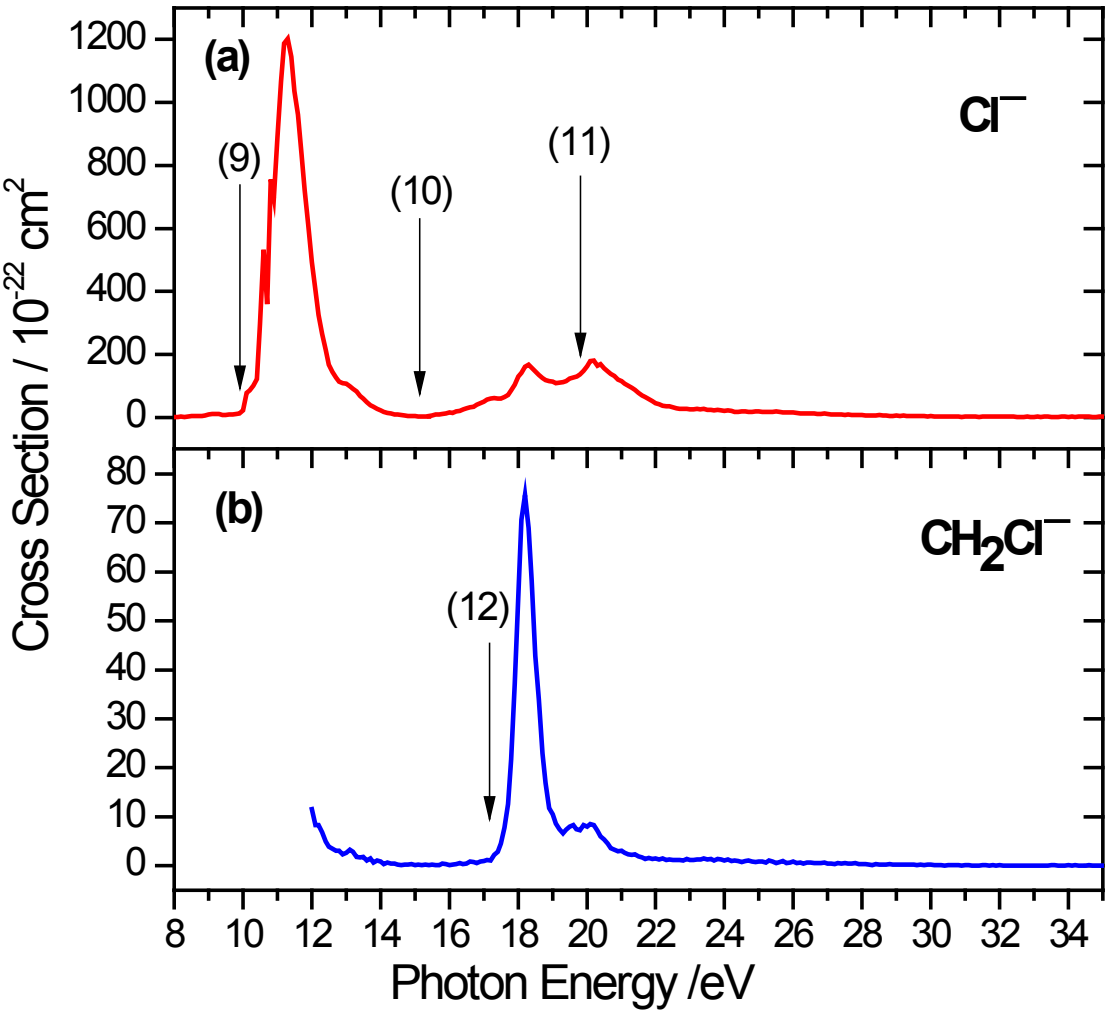

Figure 17

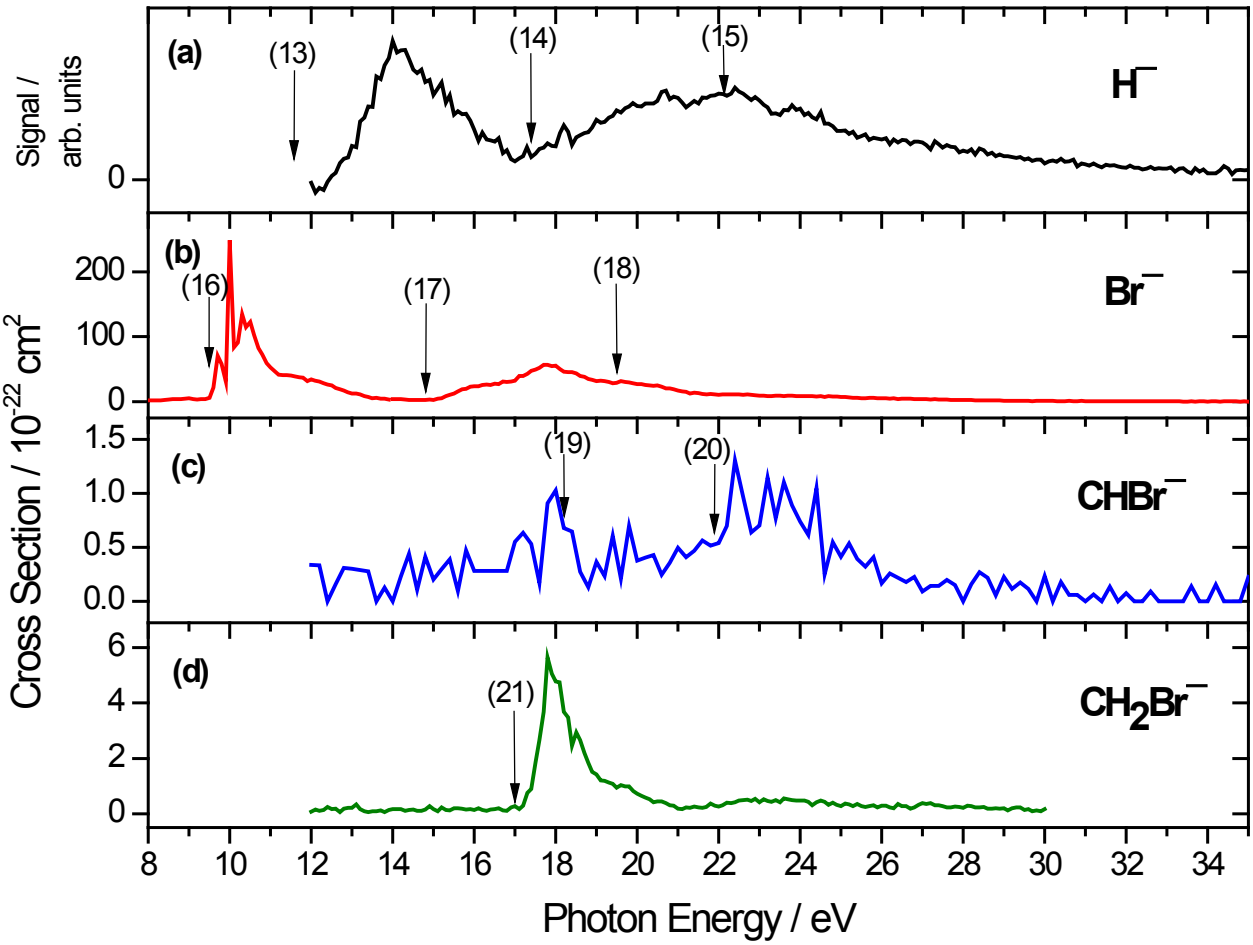
(a)
(13)
(14)
(15)
H⁻
Signal / arb. units
(b)
(16)
(17)
(18)
Br⁻
(c)
(19)
(20)
CHBr⁻
(d)
(21)
CH2Br⁻
Cross Section / 10-22 cm2
Photon Energy / eV

Figure 18

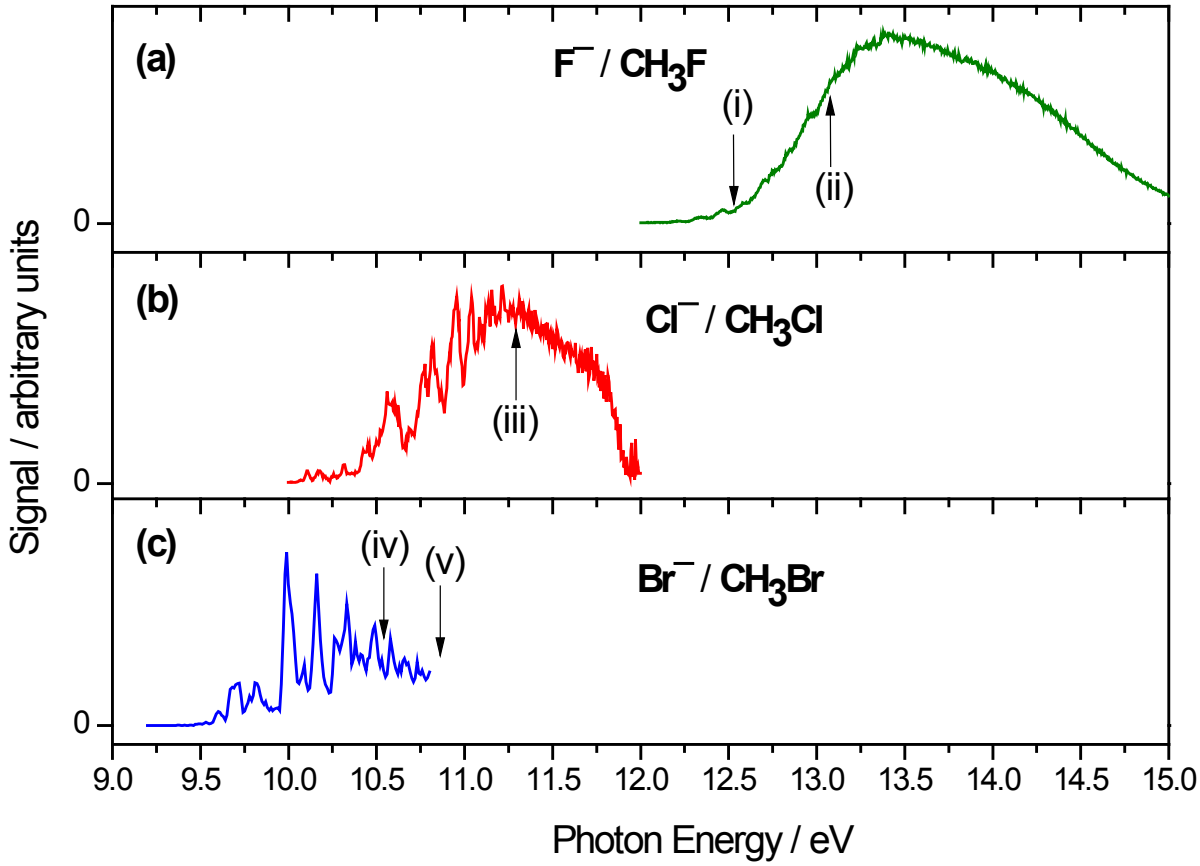
(a)
F⁻ / CH3F
(i)
(ii)
(b)
Cl⁻ / CH3Cl
(iii)
(c)
(iv)
(v)
Br⁻ / CH3Br
0
0
0
Signal / arbitrary units
9.0
9.5
10.0
10.5
11.0
11.5
12.0
12.5
13.0
13.5
14.0
14.5
15.0
Photon Energy / eV

Figure 19

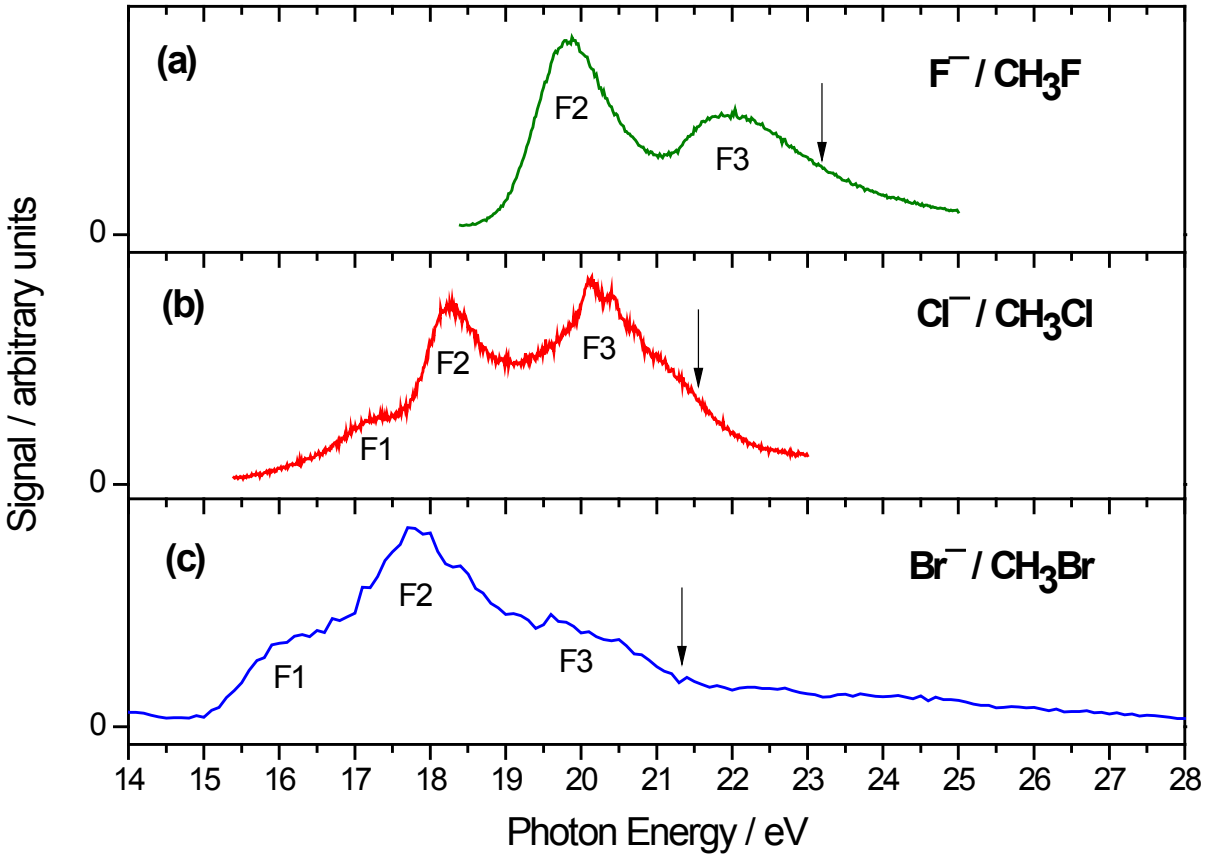
(a)
F2
F3
F⁻ / CH3F
0
(b)
F1
F2
F3
Cl⁻ / CH3Cl
0
(c)
F1
F2
F3
Br⁻ / CH3Br
0
Signal / arbitrary units
14
15
16
17
18
19
20
21
22
23
24
25
26
27
28
Photon Energy / eV

Figure 20

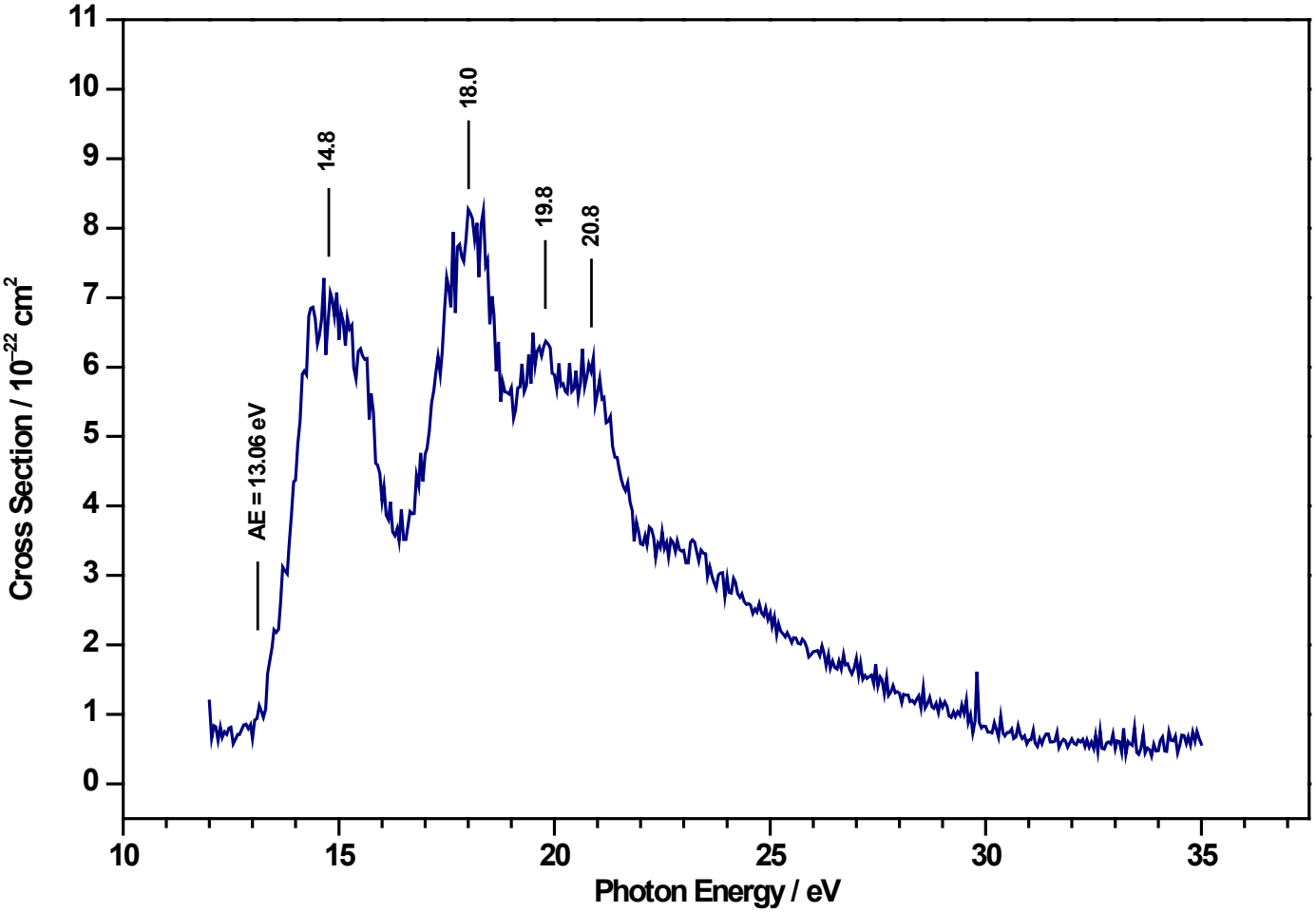
Cross Section / 10^{-22} cm^2
Photon Energy / eV
AE = 13.06 eV
14.8
18.0
19.8
20.8
0
1
2
3
4
5
6
7
8
9
10
11
10
15
20
25
30
35

Figure 21

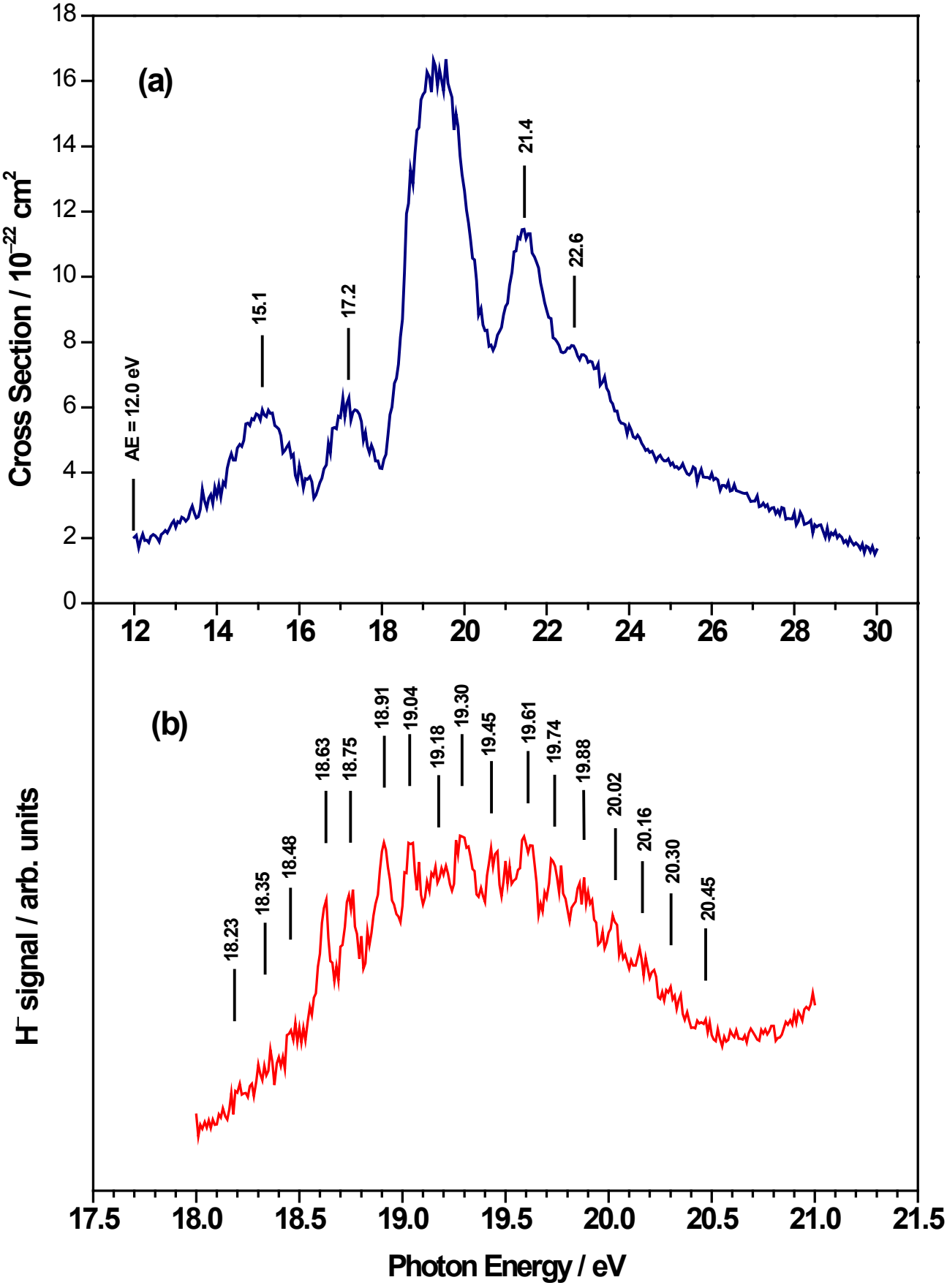
(a)
Cross Section / 10^{-22} cm^2
AE = 12.0 eV
15.1
17.2
21.4
22.6
(b)
H$^-$ signal / arb. units
18.23
18.35
18.48
18.63
18.75
18.91
19.04
19.18
19.30
19.45
19.61
19.74
19.88
20.02
20.16
20.30
20.45
Photon Energy / eV

Figure 22

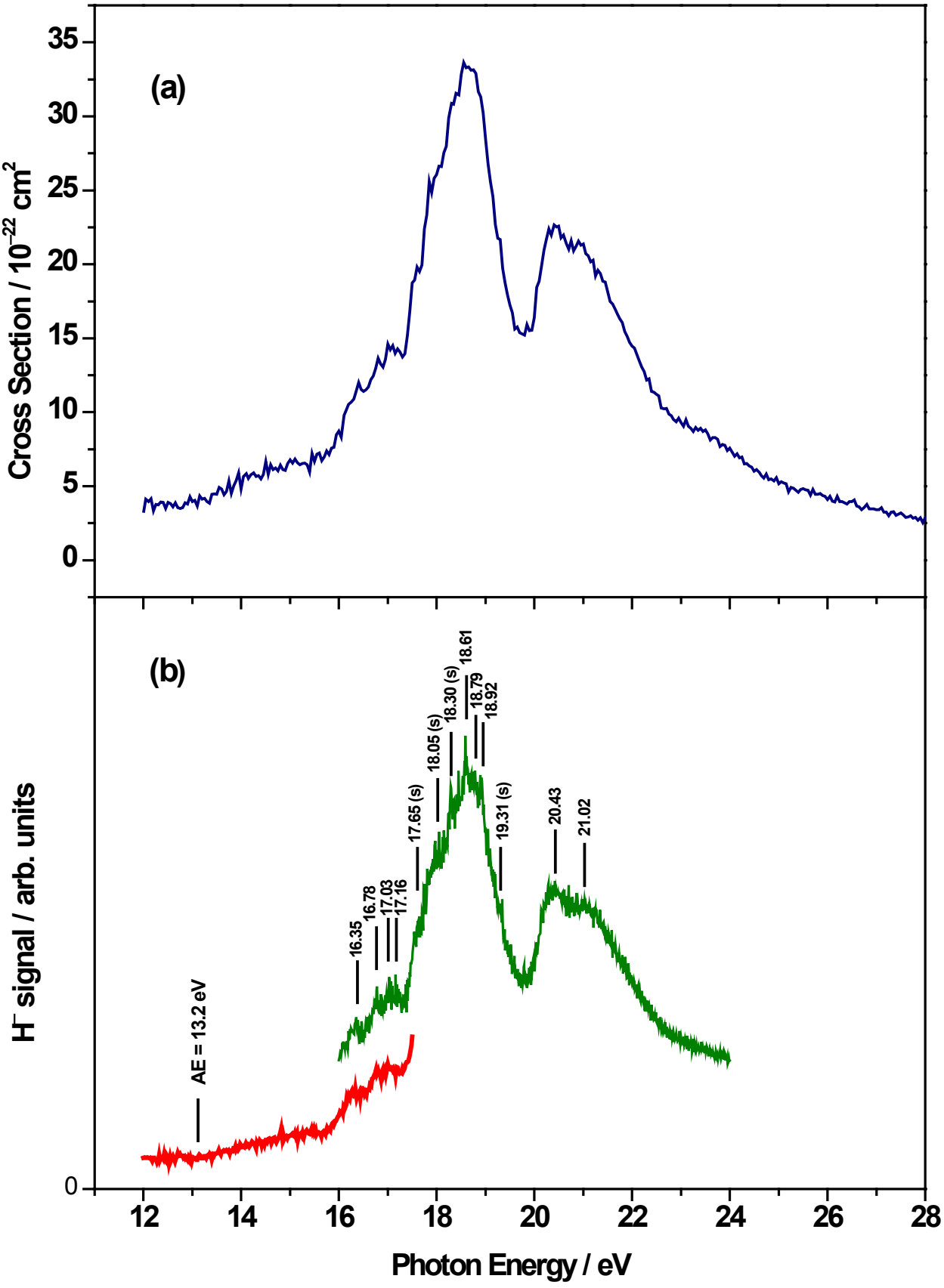
(a)
Cross Section / 10^{-22} cm^2
35
30
25
20
15
10
5
0
(b)
H$^-$ signal / arb. units
AE = 13.2 eV
16.35
16.78
17.03
17.16
17.65 (s)
18.05 (s)
18.30 (s)
18.61
18.79
18.92
19.31 (s)
20.43
21.02
0
12
14
16
18
20
22
24
26
28
Photon Energy / eV

Figure 23

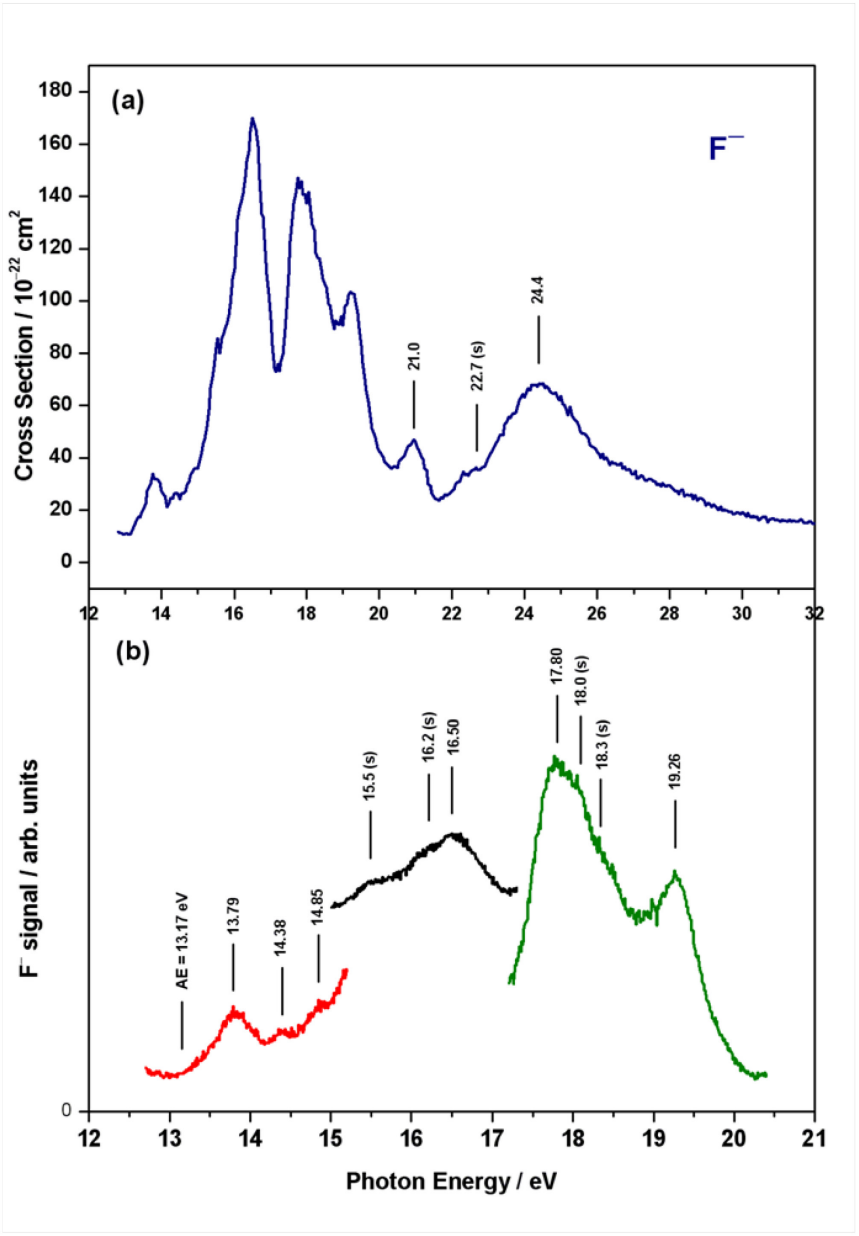
(a)
F⁻
Cross Section / 10⁻²² cm²
21.0
22.7 (s)
24.4
(b)
F⁻ signal / arb. units
AE = 13.17 eV
13.79
14.38
14.85
15.5 (s)
16.2 (s)
16.50
17.80
18.0 (s)
18.3 (s)
19.26
Photon Energy / eV
(c)
CF⁻
AE = 22.4 eV
25.1
27.5
Cross Section / 10⁻²² cm²
Photon Energy / eV

Figure 24

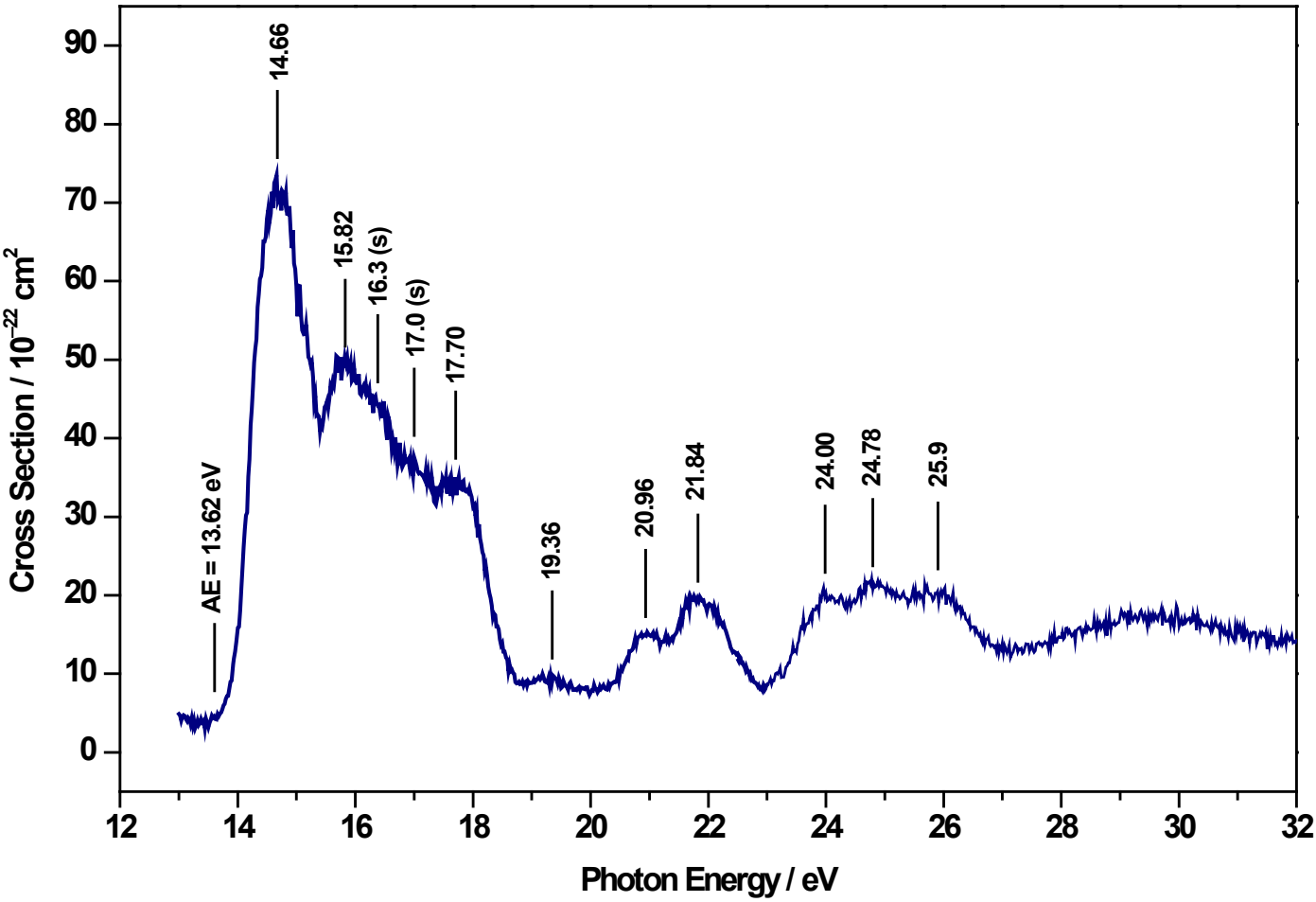
Cross Section / 10^{-22} cm^2
Photon Energy / eV
AE = 13.62 eV
14.66
15.82
16.3 (s)
17.0 (s)
17.70
19.36
20.96
21.84
24.00
24.78
25.9
0
10
20
30
40
50
60
70
80
90
12
14
16
18
20
22
24
26
28
30
32

Figure 25

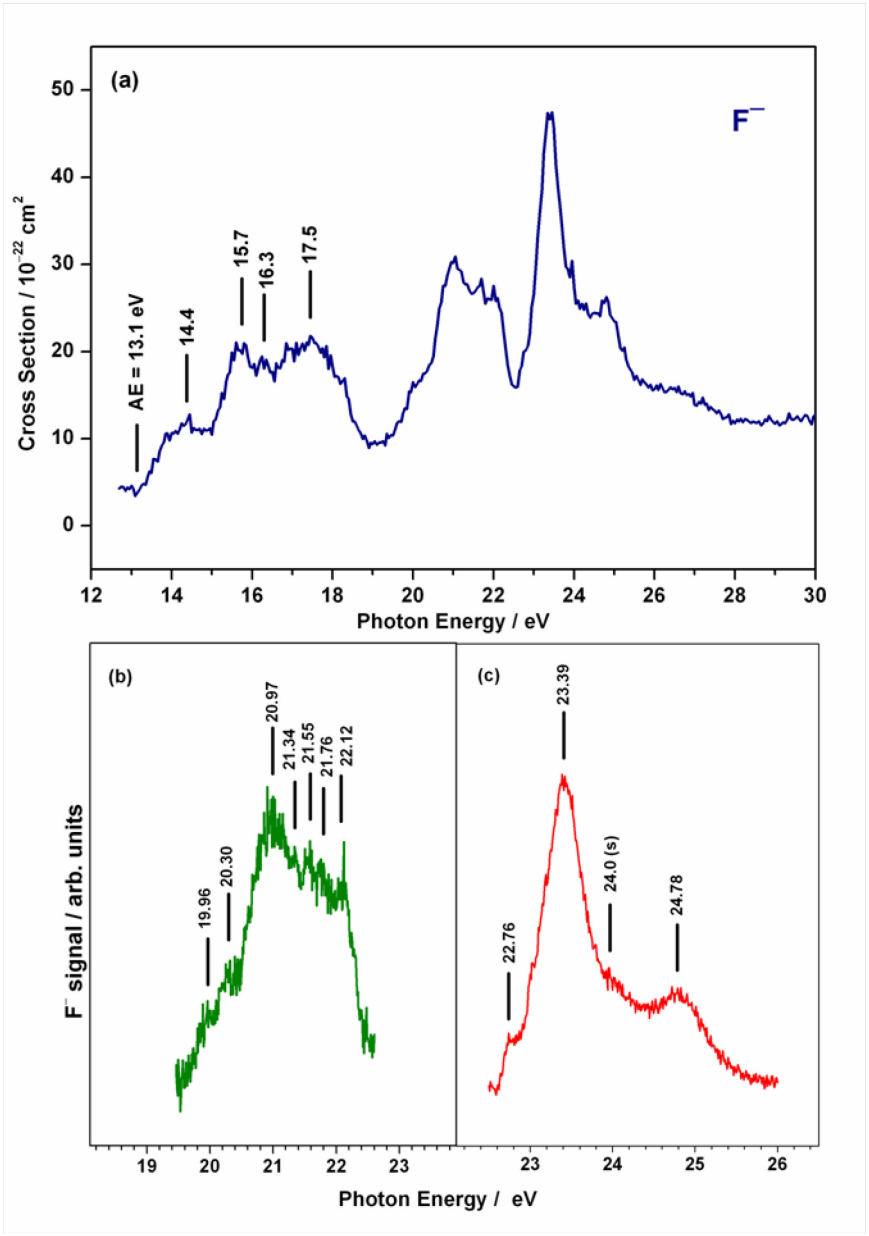
(a)
F⁻
Cross Section / 10⁻²² cm²
AE = 13.1 eV
14.4
15.7
16.3
17.5
Photon Energy / eV
(b)
F⁻ signal / arb. units
19.96
20.30
20.97
21.34
21.55
21.76
22.12
(c)
22.76
23.39
24.0 (s)
24.78
Photon Energy / eV
(d)
CF₂⁻
Cross Section / 10⁻²² cm²
AE = 20.4 eV
21.8
23.7
Photon Energy / eV

Figure 26

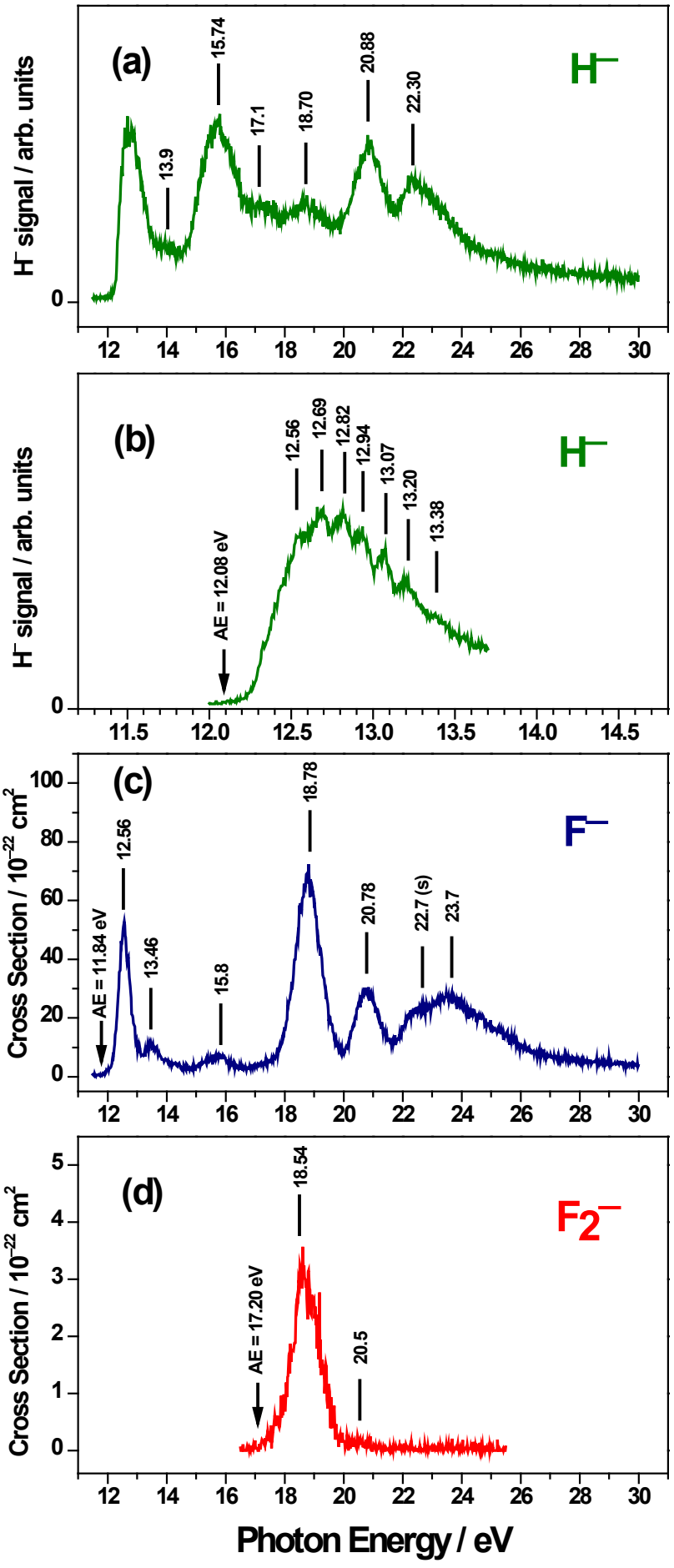
(a)
H⁻
15.74
13.9
17.1
18.70
20.88
22.30
H⁻ signal / arb. units
(b)
H⁻
12.56
12.69
12.82
12.94
13.07
13.20
13.38
AE = 12.08 eV
H⁻ signal / arb. units
(c)
F⁻
18.78
12.56
AE = 11.84 eV
13.46
15.8
20.78
22.7 (s)
23.7
Cross Section / 10⁻²² cm²
(d)
F2⁻
18.54
AE = 17.20 eV
20.5
Cross Section / 10⁻²² cm²
Photon Energy / eV

Figure 27

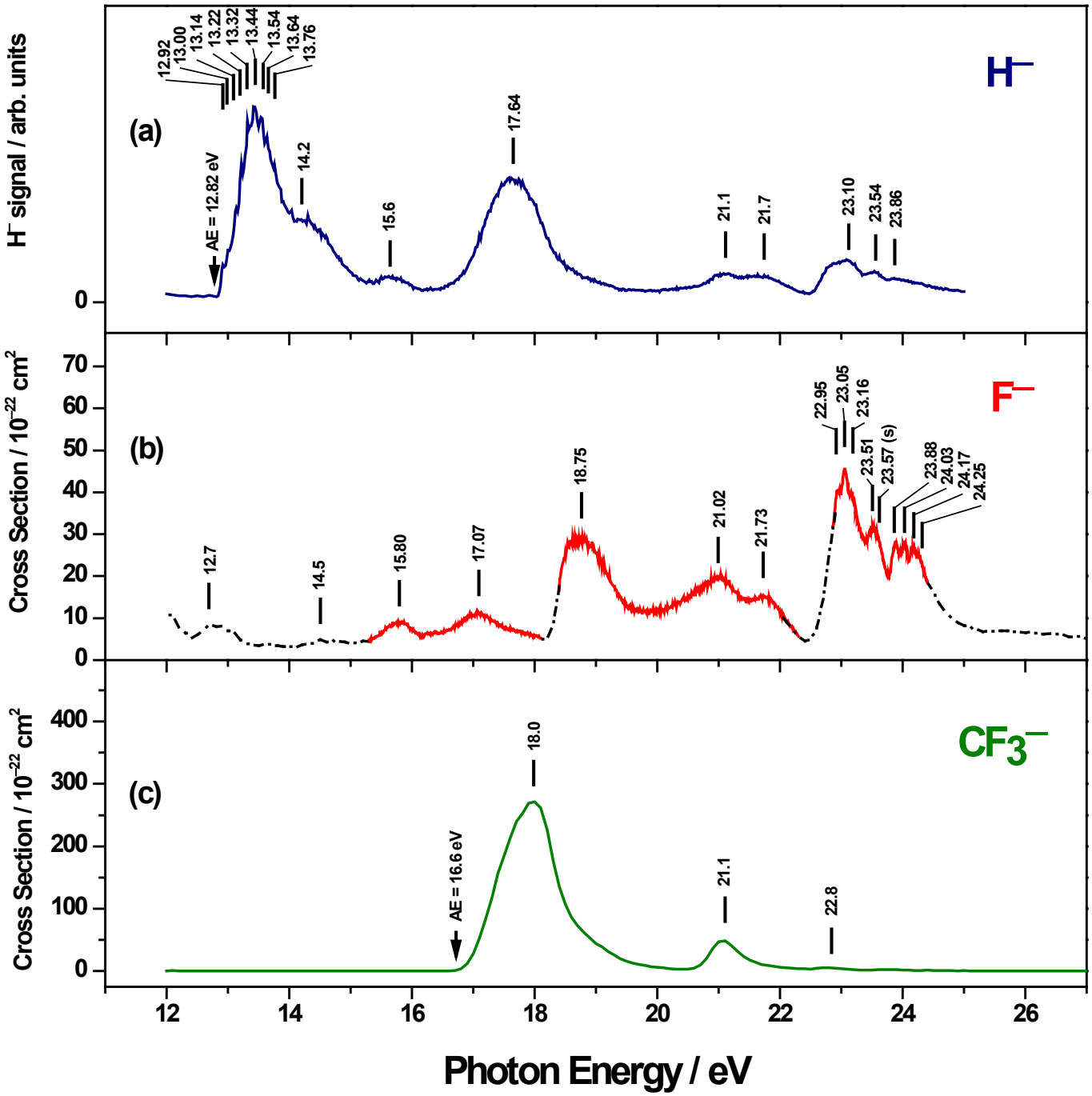
H⁻ signal / arb. units
(a)
H⁻
12.92
13.00
13.14
13.22
13.32
13.44
13.54
13.64
13.76
AE = 12.82 eV
14.2
15.6
17.64
21.1
21.7
23.10
23.54
23.86
Cross Section / 10⁻²² cm²
(b)
F⁻
12.7
14.5
15.80
17.07
18.75
21.02
21.73
22.95
23.05
23.16
23.51
23.57 (s)
23.88
24.03
24.17
24.25
Cross Section / 10⁻²² cm²
(c)
CF3⁻
AE = 16.6 eV
18.0
21.1
22.8
Photon Energy / eV

Figure 28

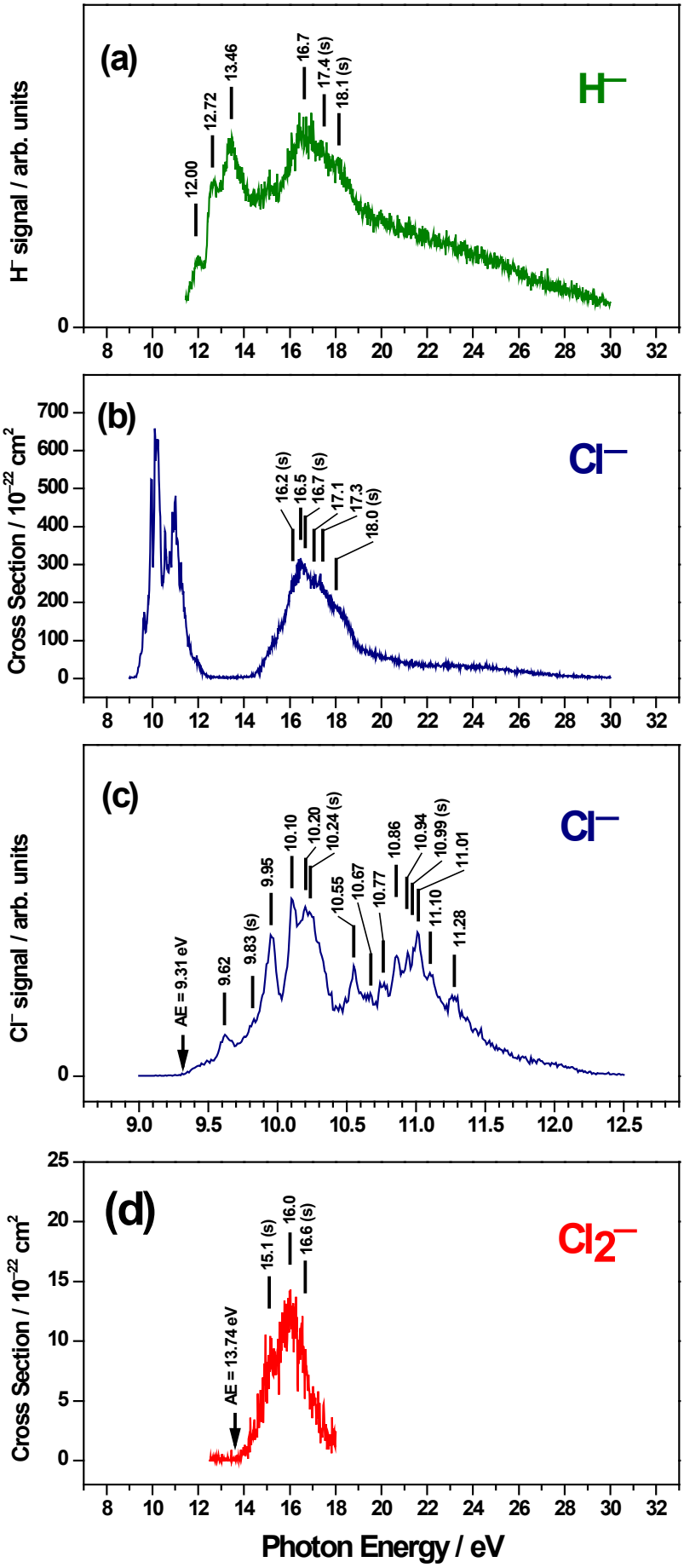
(a)
H⁻
H⁻ signal / arb. units
12.00
12.72
13.46
16.7
17.4 (s)
18.1 (s)
(b)
Cl⁻
Cross Section / 10⁻²² cm²
16.2 (s)
16.5
16.7 (s)
17.1
17.3
18.0 (s)
(c)
Cl⁻
Cl⁻ signal / arb. units
AE = 9.31 eV
9.62
9.83 (s)
9.95
10.10
10.20
10.24 (s)
10.55
10.67
10.77
10.86
10.94
10.99 (s)
11.01
11.10
11.28
(d)
Cl2⁻
Cross Section / 10⁻²² cm²
AE = 13.74 eV
15.1 (s)
16.0
16.6 (s)
Photon Energy / eV

Figure 29

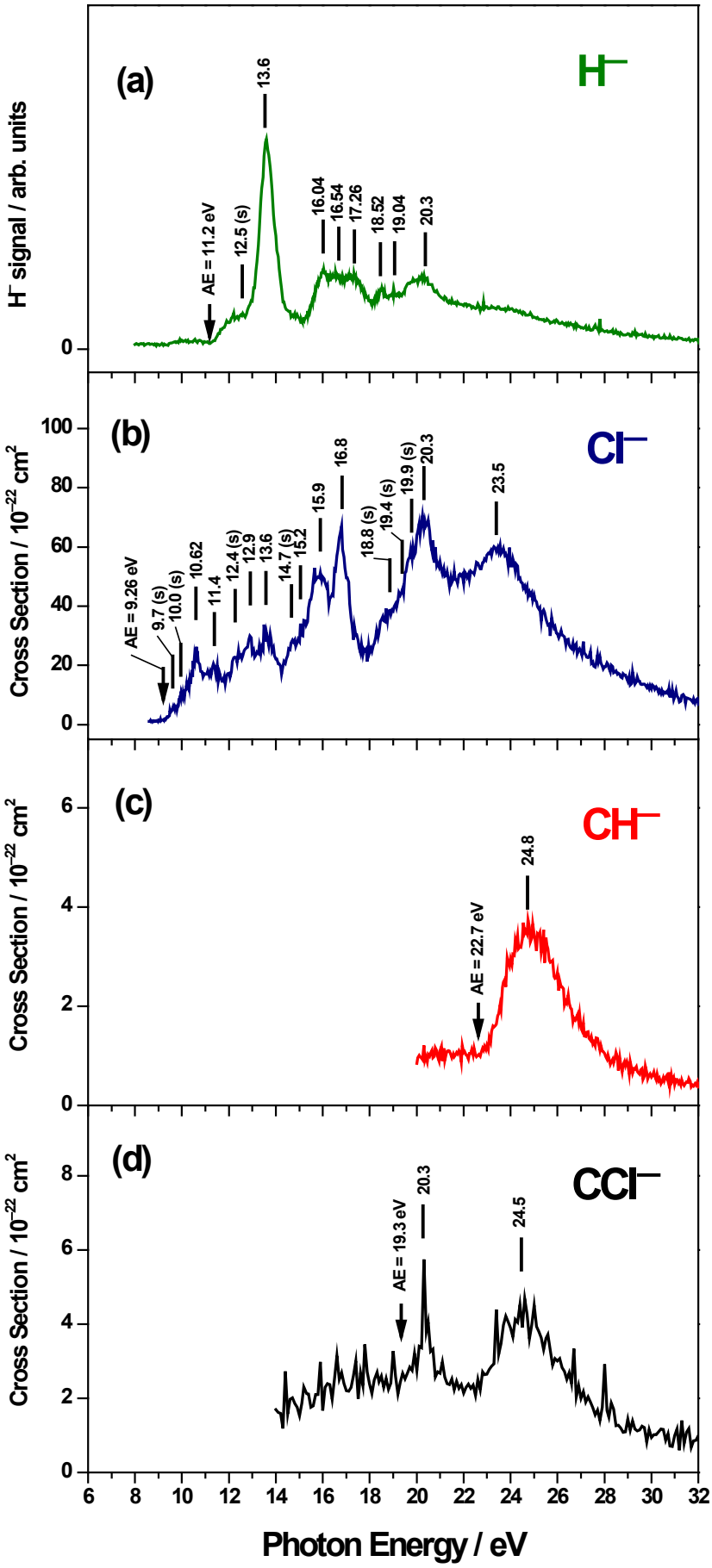
(a)
H⁻
H⁻ signal / arb. units
AE = 11.2 eV
12.5 (s)
13.6
16.04
16.54
17.26
18.52
19.04
20.3
(b)
Cl⁻
Cross Section / 10⁻²² cm²
AE = 9.26 eV
9.7 (s)
10.0 (s)
10.62
11.4
12.4 (s)
12.9
13.6
14.7 (s)
15.2
15.9
16.8
18.8 (s)
19.4 (s)
19.9 (s)
20.3
23.5
(c)
CH⁻
AE = 22.7 eV
24.8
(d)
CCl⁻
AE = 19.3 eV
20.3
24.5
Photon Energy / eV

Figure 30

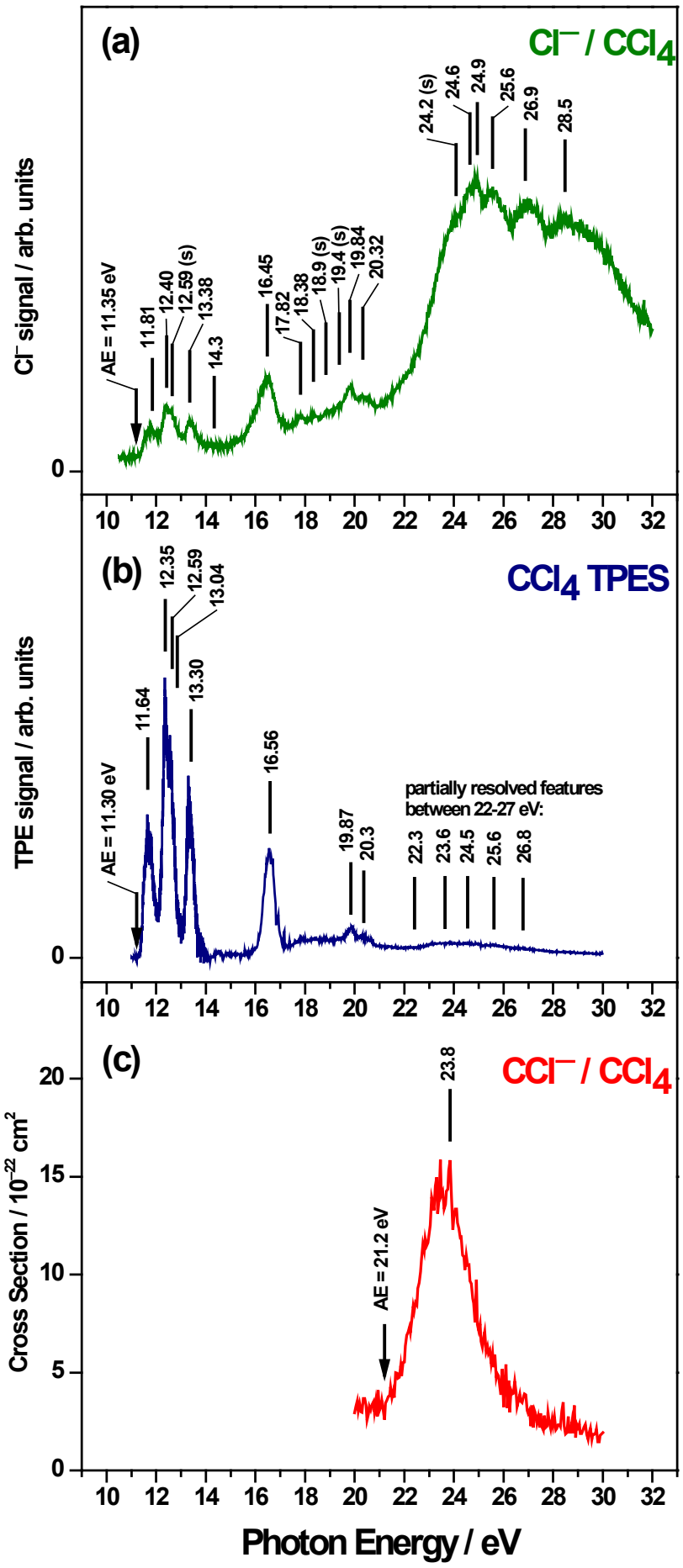
(a)
Cl⁻ / CCl4
Cl⁻ signal / arb. units
AE = 11.35 eV
11.81
12.40
12.59 (s)
13.38
14.3
16.45
17.82
18.38
18.9 (s)
19.4 (s)
19.84
20.32
24.2 (s)
24.6
24.9
25.6
26.9
28.5
(b)
CCl4 TPES
TPE signal / arb. units
AE = 11.30 eV
11.64
12.35
12.59
13.04
13.30
16.56
19.87
20.3
partially resolved features
between 22-27 eV:
22.3
23.6
24.5
25.6
26.8
(c)
CCl⁻ / CCl4
Cross Section / 10⁻²² cm²
AE = 21.2 eV
23.8
Photon Energy / eV

Figure 31

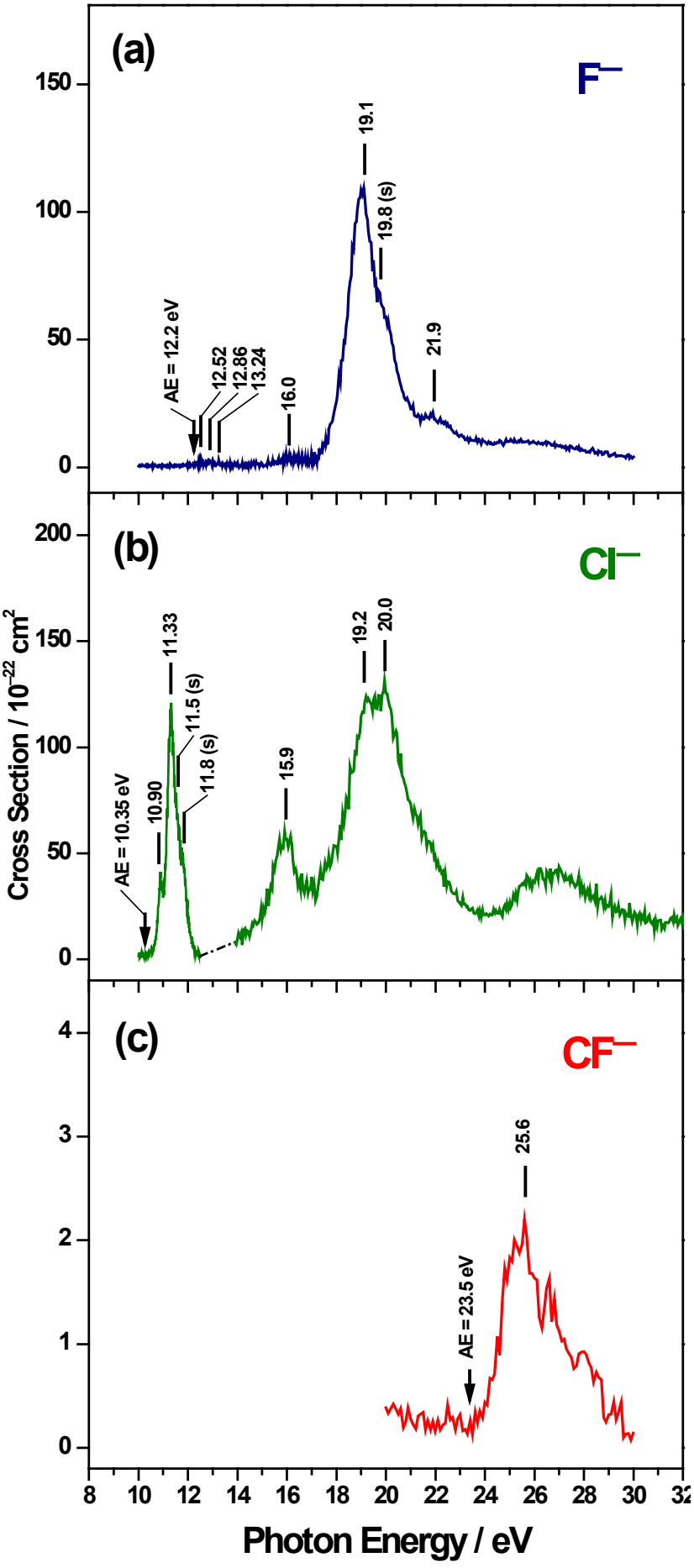
(a)
F⁻
AE = 12.2 eV
12.52
12.86
13.24
16.0
19.1
19.8 (s)
21.9
(b)
Cl⁻
AE = 10.35 eV
10.90
11.33
11.5 (s)
11.8 (s)
15.9
19.2
20.0
(c)
CF⁻
AE = 23.5 eV
25.6
Cross Section / 10⁻²² cm²
Photon Energy / eV

Figure 32

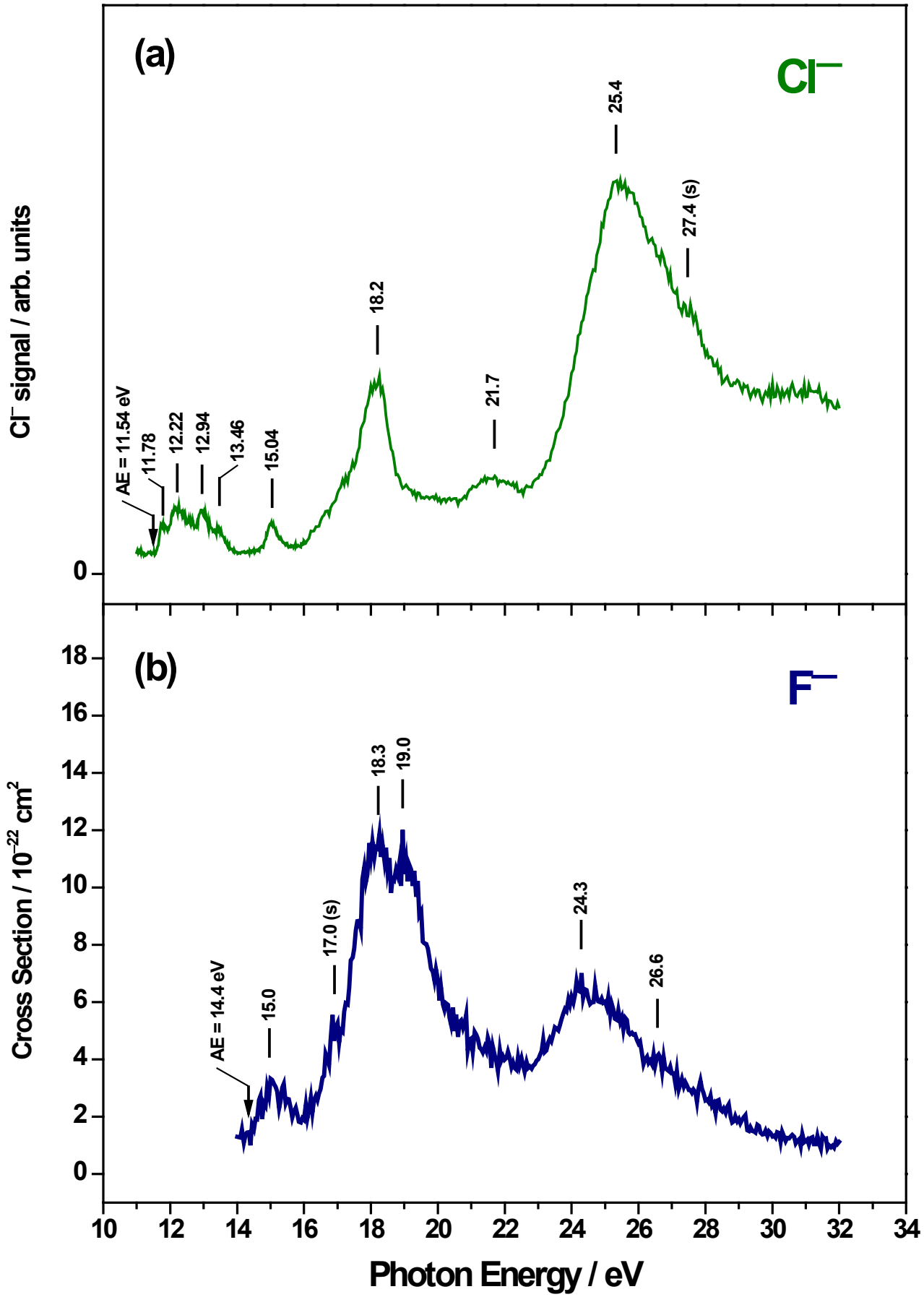
(a)
Cl⁻
25.4
27.4 (s)
18.2
21.7
AE = 11.54 eV
11.78
12.22
12.94
13.46
15.04
Cl⁻ signal / arb. units
0
(b)
F⁻
18.3
19.0
17.0 (s)
24.3
26.6
AE = 14.4 eV
15.0
Cross Section / 10⁻²² cm²
0
2
4
6
8
10
12
14
16
18
10
12
14
16
18
20
22
24
26
28
30
32
34
Photon Energy / eV

Figure 33

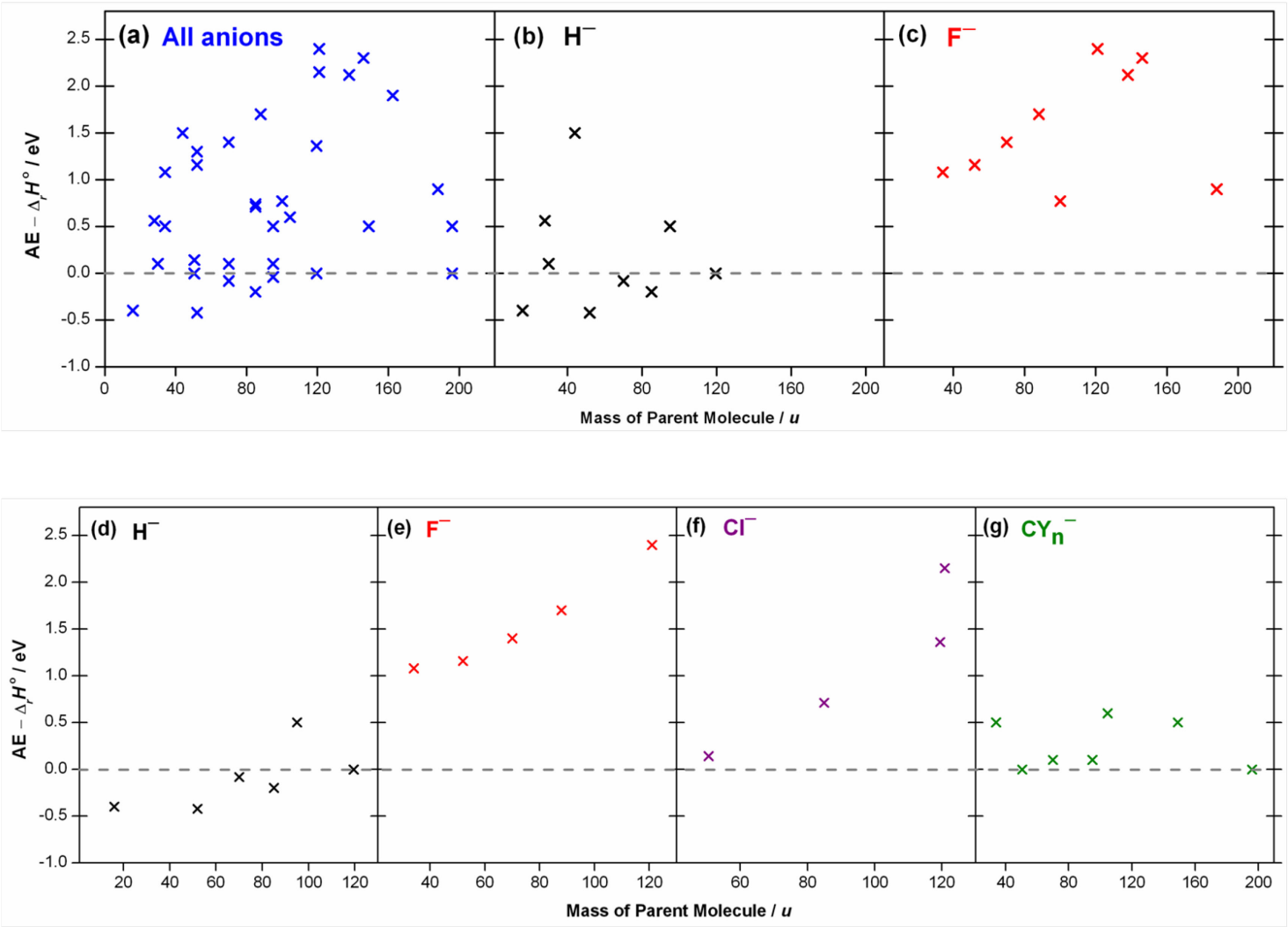
(a) All anions
(b) H⁻
(c) F⁻
(d) H⁻
(e) F⁻
(f) Cl⁻
(g) CYn⁻
AE − ΔrH° / eV
Mass of Parent Molecule / u

Figure 34

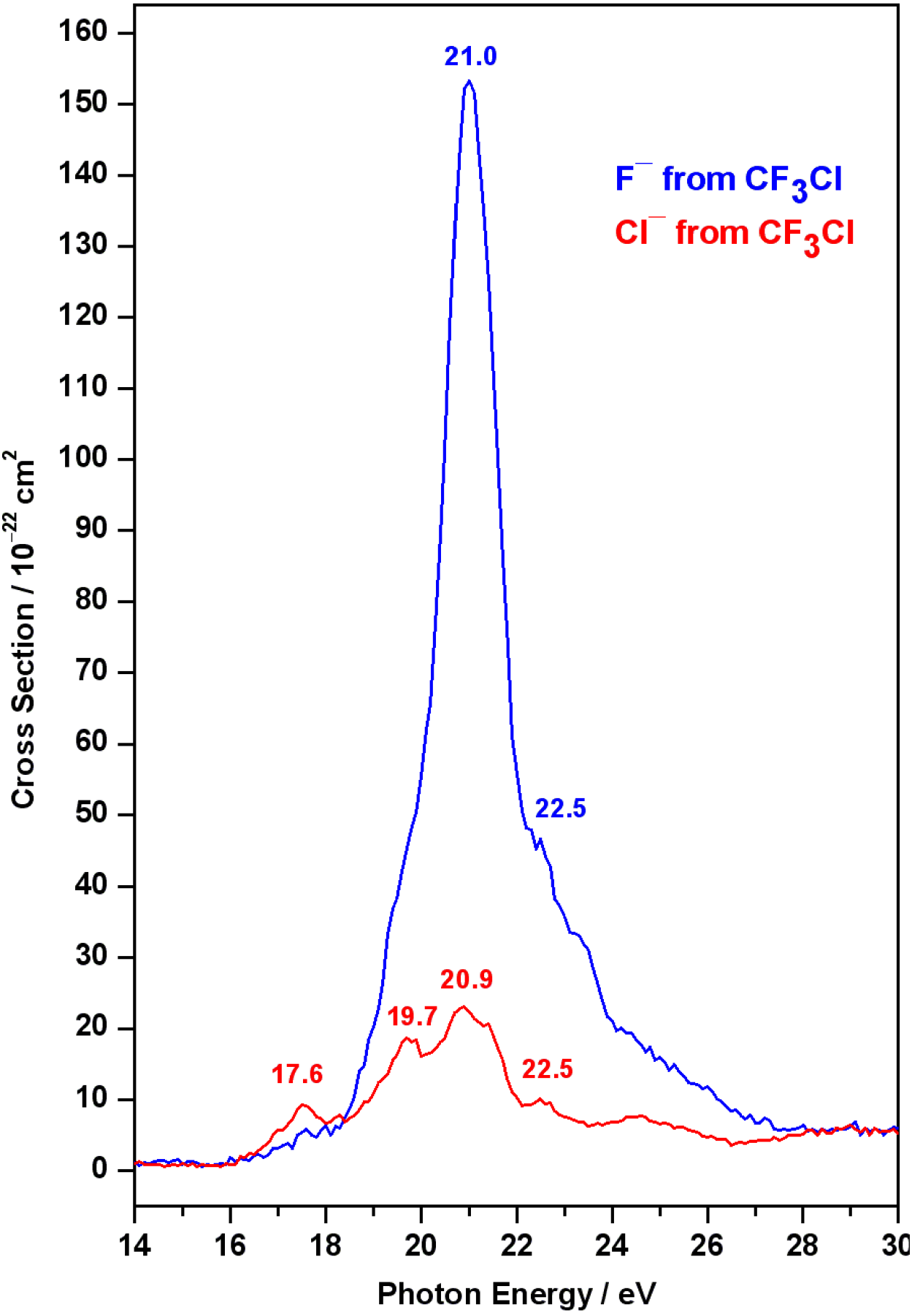
21.0
F⁻ from CF3Cl
Cl⁻ from CF3Cl
22.5
20.9
19.7
17.6
22.5
Cross Section / 10⁻²² cm²
Photon Energy / eV
0
10
20
30
40
50
60
70
80
90
100
110
120
130
140
150
160
14
16
18
20
22
24
26
28
30